Predicting colloid transport through saturated porous media: A critical review

AGU PUBLICATIONS

Water Resources Research

REVIEW ARTICLE
10.1002/2015WR017318

Special Section:
The 50th Anniversary of Water Resources Research

Key Points:
- Review of colloid transport in porous media
- Discussion of recent advances in understanding of colloid transport
- Current colloid transport research needs

Correspondence to:
D. M. O'Carroll,
docarroll@eng.uwo.ca

Citation:
Molnar, I. L., W. P. Johnson, J. I. Gerhard, C. S. Willson, and D. M. O'Carroll (2015), Predicting colloid transport through saturated porous media: A critical review, *Water Resour. Res.*, *51*, 6804–6845, doi:10.1002/2015WR017318.

Received 31 MAR 2015
Accepted 3 JUL 2015
Accepted article online 14 JUL 2015
Published online 2 SEP 2015

Predicting colloid transport through saturated porous media: A critical review

Ian L. Molnar[1], William P. Johnson[2], Jason I. Gerhard[1], Clinton S. Willson[3], and Denis M. O'Carroll[1,4]

[1]Department of Civil and Environmental Engineering, University of Western Ontario, London, Ontario, Canada, [2]Department of Geology and Geophysics, University of Utah, Salt Lake City, Utah, USA, [3]Department of Civil and Environmental Engineering, Louisiana State University, Baton Rouge, Louisiana, USA, [4]School of Civil and Environmental Engineering, Connected Water Initiative, University of New South Wales, Manly Vale, New South Wales, Australia

Abstract Understanding and predicting colloid transport and retention in water-saturated porous media is important for the protection of human and ecological health. Early applications of colloid transport research before the 1990s included the removal of pathogens in granular drinking water filters. Since then, interest has expanded significantly to include such areas as source zone protection of drinking water systems and injection of nanometals for contaminated site remediation. This review summarizes predictive tools for colloid transport from the pore to field scales. First, we review experimental breakthrough and retention of colloids under favorable and unfavorable colloid/collector interactions (i.e., no significant and significant colloid-surface repulsion, respectively). Second, we review the continuum-scale modeling strategies used to describe observed transport behavior. Third, we review the following two components of colloid filtration theory: (i) mechanistic force/torque balance models of pore-scale colloid trajectories and (ii) approximating correlation equations used to predict colloid retention. The successes and limitations of these approaches for favorable conditions are summarized, as are recent developments to predict colloid retention under the unfavorable conditions particularly relevant to environmental applications. Fourth, we summarize the influences of physical and chemical heterogeneities on colloid transport and avenues for their prediction. Fifth, we review the upscaling of mechanistic model results to rate constants for use in continuum models of colloid behavior at the column and field scales. Overall, this paper clarifies the foundation for existing knowledge of colloid transport and retention, features recent advances in the field, critically assesses where existing approaches are successful and the limits of their application, and highlights outstanding challenges and future research opportunities. These challenges and opportunities include improving mechanistic descriptions, and subsequent correlation equations, for nanoparticle (i.e., Brownian particle) transport through soil, developing mechanistic descriptions of colloid retention in so-called "unfavorable" conditions via methods such as the "discrete heterogeneity" approach, and employing imaging techniques such as X-ray tomography to develop realistic expressions for grain topology and mineral distribution that can aid the development of these mechanistic approaches.

1. Introduction

The introduction of colloid filtration theory (CFT) [*Yao et al.*, 1971] sparked four decades of research at the pore, macroscopic, and field scales to develop predictive capabilities for colloid transport and retention in porous media. Significant strides have been made in the development of mechanistic models and their upscaling that link pore-scale colloid transport processes to predictions of field-scale behavior. The fiftieth anniversary of *Water Resources Research* represents an ideal opportunity to review the major contributions in this evolving, highly relevant field. It is also an opportunity to critically reflect on how the accuracy of field-scale predictions may be constrained by the simplifying assumptions built into mechanistic models, correlation equations, and their relationship to our growing understanding of actual, pore-scale colloid behavior.

Prediction of colloid transport through the subsurface is important for a wide range of environmental and human-health-related risk scenarios. For example, predictive colloid transport models are necessary to assess and minimize the risk of pathogen transport in groundwater. Among numerous examples is the Walkerton Ontario, Canada tragedy [*O'Connor*, 2002] in which the town's drinking water supply well was

contaminated by *E. coli* transported in groundwater flow through the subsurface. Colloid transport from septic systems, agricultural runoff, and other sources through near-shore soils may lead to elevated concentrations of pathogenic colloids in beach sands [e.g., *Lipp et al*., 2001] and transport across the groundwater/surface water interface may be the cause of frequent beach closures [e.g., *Russell et al*., 2012]. A wide array of research into pathogen transport has been undertaken including virus transport [*Ryan et al*., 1999; *Schijven et al*., 1999; *Jin and Flury*, 2002] and column-scale bacteria transport [e.g., *Albinger et al*., 1994; *Baygents et al*., 1998; *Simoni et al*., 1998; *Torkzaban et al*., 2008], bacteria transport in the field [*Bales et al*., 1989; *Powelson et al*., 1993; *Harvey et al*., 1995; *DeBorde et al*., 1999; *Ryan et al*., 1999; *Schijven et al*., 1999; *Zhang et al*., 2001a; *Ryan et al*., 2002; *Blanford et al*., 2005; *van der Wielen et al*., 2008; *Scheibe et al*., 2011], and phage persistence in soils [e.g., *Yates et al*., 1985] among many others; numerous reviews of pathogen transport in groundwater are available [*Bitton and Harvey*, 1992; *Harvey*, 1997; *Taylor et al*., 2004; *Sen*, 2011].

Engineered nanoparticles (ENPs), another class of colloids, are of significant interest for their transport in porous media. On the one hand, ENPs are an emerging environmental contaminant. Industrial production of engineered nanoparticles, such as carbon nanotubes and nanosilver, has increased significantly in recent years [*Wiesner et al*., 2006; *Nowack and Bucheli*, 2007; *Christian et al*., 2008; *Majestic et al*., 2010; *Marambio-Jones and Hoek*, 2010; *Petersen et al*., 2011; *Gao et al*., 2013] and it is expected that their presence in the environment will increase. This can occur through diffuse ENP release [*Mueller and Nowack*, 2008], including ENP dispersal in aerosols, in exhaust emissions, and in land application of wastewater sludge containing nanoparticles originating in consumer products. Point sources of ENPs include leakage from landfills and accidental industrial releases. Prediction of ENP transport in porous media is important for assessing the risk from ENP migration in aquifers and the contamination of wells used for drinking water supply. ENP studies have involved modeling [*Cullen et al*., 2010; *Bai and Li*, 2012; *Taghavy et al*., 2013], pore-scale experiments [*Dunphy Guzman et al*., 2006; *May et al*., 2012; *May and Li*, 2013; *Molnar et al*., 2014], and column experiments [*Lecoanet et al*., 2004; *Wang et al*., 2008; *Jaisi and Elimelech*, 2009; *X. Y. Liu et al*., 2009; *Torkzaban et al*., 2010; *Uyusur et al*., 2010; *Lin et al*., 2011; *Zhang et al*., 2012; *Liang et al*., 2013; *Ren and Smith*, 2013; *Neukum et al*., 2014]. Numerous review papers exist, including *Petersen et al*. [2011] who present a review of the transport and environmental risks of carbon nanotubes.

ENPs are also being considered as a remediation strategy for sites contaminated with industrial organic liquids. For example, nano-zero-valent iron (nZVI) particles are injected into the subsurface at contaminated sites for the in situ reduction of chlorinated solvents in groundwater [*Johnson et al*., 2013; *O'Carroll et al*., 2013; *Tosco et al*., 2014a]. This novel approach has been evaluated at both the laboratory [e.g., *Berge and Ramsburg*, 2009; *Phenrat et al*., 2009; *Raychoudhury et al*., 2010; *Kocur et al*., 2013] and pilot field scales [*Johnson et al*., 2013; *Kocur et al*., 2014]. Recent advances include the tailored design and synthesis of novel ENPs including bimetallic composites and polymer coatings [*He and Zhao*, 2008; *Bennett et al*., 2010; *Sakulchaicharoen et al*., 2010; *Gastone et al*., 2014; *Tosco et al*., 2014b], which can influence surface charge, fluid viscosity, and other properties atypical of traditional colloid suspensions. The design and optimization of these ENP-based remediation schemes require accurate predictive models of ENP transport in porous media, and users of existing CFT need to understand how and where it is possible to change parameters appropriately for nontraditional suspensions.

Colloids can also enhance the transport of dissolved contaminants in groundwater via their sorption onto colloid surfaces. Colloid-facilitated transport has been studied for a wide range of contaminants including radionuclides [e.g., *Kersting et al*., 1999; *Novikov et al*., 2006], hydrocarbons [e.g., *Qi et al*., 2014], and pesticides [e.g., *de Jonge et al*., 1998; *Sprague et al*., 2000]. Research in this area includes modeling the reduction in contaminant retardation [*Corapcioglu and Jiang*, 1993; *Johnson et al*., 1995a; *Flury and Qiu*, 2008]. Several reviews and special journal sections have provided reviews of colloid-associated contaminant transport [*McCarthy and Zachara*, 1989; *Ouyang et al*., 1996; *Ryan and Elimelech*, 1996; *de Jonge et al*., 2004; *Sen and Khilar*, 2006]. Further understanding of colloid transport mechanisms are required to predict the risk posed by colloid-enhanced transport mechanisms.

The predictive tools developed to explore column and field-scale colloid transport phenomena are primarily continuum-based numerical models that solve the advection-dispersion equation for solute transport in porous media. Terms employing rate coefficients to drive colloid mass transfer to the stationary (solid) phase and back are used to describe the macroscopically observed transport behavior of colloids as described by breakthrough-elution concentration histories and profiles of retained concentration as a function of distance. Rate constants for colloid transfer to the stationary phase may be independently determined using upscaled

predictions from mechanistic models that employ relevant force and torque balances to determine colloid trajectories in flow fields corresponding to representative pore (collector) geometries. Relevant forces include fluid drag, diffusion, gravity, as well as colloid-surface forces including van der Waals and electric double layer as described by DLVO theory [*Derjaguin and Landau*, 1941; *Verwey and Overbeek*, 1948] and its derivatives. The upscaled mechanistic predictions provide good prediction of colloid transport at the continuum scale for spheroidal colloids in uniform media when colloid-collector repulsion is absent (so-called "favorable" conditions), as is typically the case for oppositely charged surfaces [e.g., *Elimelech*, 1991].

In the environment, however, the typical condition is that both colloids and collector surfaces carry negative charge. Colloids exhibiting net negatively charged surfaces under environmental pH conditions include bacteria [e.g., *McClaine and Ford*, 2002; *Bradford et al*., 2006b; *Foppen and Schijven*, 2006], protozoa [e.g., *Ruohola et al*., 2012; *Y. Liu et al*., 2009], viruses [e.g., *Ryan et al*., 1999; *Mondal and Sleep*, 2013], and engineered nanoparticles [e.g., *Torkzaban et al*., 2010; *Jiang et al*., 2012a; *Liang et al*., 2013; *Kocur et al*., 2014; *Molnar et al*., 2014]. Common minerals exhibiting negatively charged surfaces at typical pH include quartz, silica, feldspars, mica, and certain clays [*Molnar et al*., 2011, Table 1]. The combination of both colloids and collectors carrying a negative charge leads to electric double layer repulsion (as well as steric repulsion from surface macromolecules), thereby yielding "unfavorable" conditions for attachment.

Repulsion between colloids and porous media collectors results in complex transport behavior that is mediated by the topology of the pore domain and the flow field, via such features as low-flow (diffusion-limited) zones that may be generated in nonspheroidal or nonuniform media, such as many environmental sediments and soils. In recognition of these complexities, mechanistic models have been adapted to address more complex scenarios [*Long and Hilpert*, 2009; *Ma et al*., 2009; *Long et al*., 2010; *Ma and Johnson*, 2010; *Ma et al*., 2011, 2013; *Pazmino et al*., 2014b]. However, upscaling of these types of models for implementation into advection-dispersion or other transport equations represents an important ongoing research opportunity.

Whereas mechanistic predictions regarding the above complexities are not yet readily implemented into continuum-scale transport models, advances have occurred in descriptive continuum-scale colloid transport models describing these complexities [e.g., *Tufenkji and Elimelech*, 2004a, 2005b, 2005a; *Šimůnek and van Genuchten*, 2008; *Bradford et al*., 2009, 2011b; *Leij and Bradford*, 2013; *Katzourakis and Chrysikopoulos*, 2014]. These models employ parameters fitted to column-scale breakthrough-elution concentration histories and provide a method to infer potential pore-scale mechanisms driving complex transport behavior. There is clearly an important ongoing research opportunity associated with obtaining high resolution, pore-scale information on the behavior of colloids and its generalization into continuum-scale models in order to further improve predictive approaches to incorporating colloid interaction with soil and flow heterogeneity.

This paper provides a critical review of colloid transport literature with a specific focus on linking pore-scale processes to column-scale and field-scale observations as well as continuum-scale transport models across a range of relevant subsurface scenarios. This review exclusively discusses colloid transport through water-saturated media and aims to help distinguish and clarify the roles of different pore-scale and continuum-scale modeling approaches, focusing on post-1990 colloid transport work. The paper is structured so as to (i) provide an introduction to the fundamentals and review existing knowledge and knowledge gaps for those who are relatively new to the field and (ii) provide a more detailed, critical assessment of the state of the art. In section 2, a brief review is provided of mean-field DLVO interactions and experimentally observed colloid transport phenomena, focusing on the contrasting transport behaviors observed under favorable versus unfavorable conditions for attachment. Section 3 describes strategies by which kinetic parameters have been used in continuum models to infer mechanisms from experimental observations. Section 4 reviews the current and emerging ability of mechanistic approaches to independently predict kinetic parameters used in continuum models (e.g., retention coefficients) in both favorable and unfavorable conditions. Section 5 examines upscaling of mechanistic predictions to rate constants, explores the role of topology in upscaling strategies, and highlights opportunities for future research.

2. Mean-Field DLVO Interactions and Experimental Observations

2.1. Mean-Field DLVO Forces

As mentioned, the mechanistic models that underpin predictive tools for colloid transport depend upon DLVO interactions. Classic DLVO theory [*Derjaguin and Landau*, 1941; *Verwey and Overbeek*, 1948] attempts

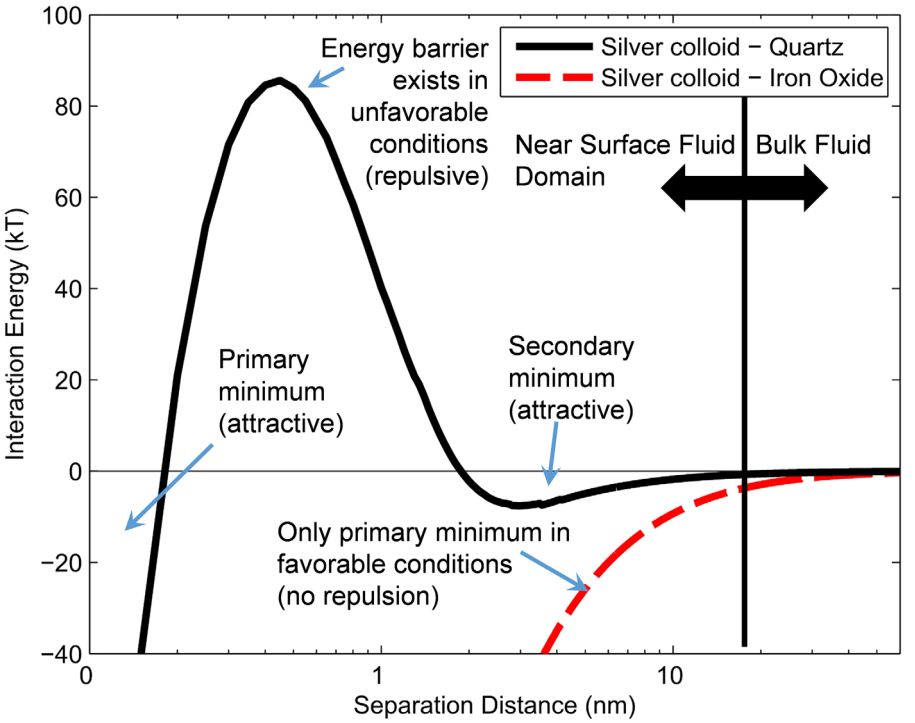

Figure 1. Two examples of classic DLVO interaction profiles for favorable conditions (dashed red line) and unfavorable conditions (solid black line) for a 0.3 μm diameter silver colloid interacting with an iron oxide surface and quartz surface respectively in a 300 m*M* ionic strength solution. The calculation was performed using the sphere-plate Surface Element Integration technique [*Bhattacharjee et al*., 2000] with representative literature values for zeta potentials (silver colloids: −28 mV (Molnar et al., submitted manuscript, 2015), quartz: −55 mV [*Liang et al*., 2013], and iron oxide: −25 mV (Molnar et al., submitted manuscript, 2015)) and Hamaker constants (silver colloids: 15×10^{-20} J [*Pinchuk*, 2012], quartz: 7.93×10^{-20} J [*Ross and Morrison*, 1988], and iron oxide: 23.2×10^{-20} J [*Faure et al*., 2011].

to describe the colloid-collector interactions in terms of adhesive and repulsive forces. By summing the adhesive (negative) and repulsive (positive) energies between a colloid and collector over a range of separation distances, an interaction energy profile—the net energy versus separation distance—is constructed. Figure 1 presents two typical, classic DLVO interaction energy profiles for favorable (silver colloid-iron oxide) and unfavorable interaction conditions (silver colloid-quartz). The figure illustrates a number of distinct features or regions that are typical of colloid-surface interaction profiles. In unfavorable conditions, a repulsive barrier exists that either limits colloid attachment to the surface (experimental observations) or prevents attachment (for energy barriers exceeding several kT in mechanistic simulations).

Outward from this repulsive barrier exists a small region of attraction where colloids may accumulate in a secondary minimum at separation distances tens of nm from the collector surface. In situations where colloids either possesses enough energy to overcome the barrier or where no barrier exists (i.e., favorable conditions), they can enter the primary minimum (Figure 1) and physically attach to the surface.

The "near-surface fluid domain" is defined, for the purposes of this review, as the region between the collector surface and the distance over which van der Waals attraction is significant, i.e., secondary minimum and closer (see Figure 1). The "bulk fluid domain" is defined as the area beyond the near-surface fluid domain beyond which colloid-collector DLVO interactions are insignificant. For typical colloid-collector systems, the interface between the bulk fluid domain and the near-surface domain occurs in the range of several to hundreds of nm [e.g., *Johnson and Hilpert*, 2013].

It is worthwhile mentioning that the energy barrier also influences colloid detachment from the primary minimum. In classic DLVO theory, the primary minimum is an infinitely deep well and the height of the energy barrier is inconsequential to colloids entrapped within the minimum. However, short-range forces such as Born repulsion serve to limit the depth of the well to finite values [*Ruckenstein and Prieve*, 1976]. In this finite-depth scenario, the energy barrier now contributes to the effective depth of the energy well and acts as a barrier to both colloid attachment and detachment [*Ryan and Elimelech*, 1996]. Increasing the

height of the energy barrier via perturbations in solution chemistry will deepen the energy well holding the colloid on the surface of the collector [*Hahn et al*., 2004].

The forces acting on the colloids are the derivative of the energies with respect to separation distance, such that both energy and force profiles exhibit the same features: primary minimum, repulsive barrier, and secondary minimum. Using this sign convention, attractive forces are negative and repulsive forces are positive. The separation distances of these features differ slightly between the force and energy profiles, but this is not important to this discussion. This review refers to the features illustrated in Figure 1 without distinguishing specifically between force and energy. Traditional mechanistic colloid transport and retention models describe colloid-collector interactions (i.e., repulsion, physical contact, and retention in the secondary minimum) by considering the above-described DLVO theory. A shortcoming of this theory (as presented above) is that it considers the surfaces to be monolithic (homogeneous). It is worthwhile emphasizing that this monolithic DLVO approach does not represent a "mean interaction energy" of colloids, but rather it is an interaction calculated from the bulk surface properties of colloids and collectors. This so-called mean-field DLVO approach is an overgeneralization of the surface characteristics of colloids and collectors, since it does not account for microscale to nanoscale heterogeneity that is expected to exist on real surfaces (as discussed in section 4). Hence, while we review below the great utility of mean-field DLVO interactions for interpreting the transport behavior of colloids in porous media, we also discuss in subsequent sections the emerging opportunities offered by the incorporation of heterogeneity into colloid-surface DLVO interactions.

2.2. Experimental Observations: Influence of Favorable Versus Unfavorable Conditions

While DLVO forces are significant over small (nanoscale) separation distances (see near-surface fluid domain in Figure 1), the presence or absence of a repulsive energy barrier controls the transport and retention of colloids at column and field scales. A large number of column-scale transport experiments have demonstrated the implications of these small-scale interactions that yield field-scale consequences, as described below.

A note on terminology: "attachment" is herein defined as the immobilization, via physical contact, of the colloid onto the collector surface within the primary energy well. As continuum-scale experiments typically cannot distinguish attachment from other retention mechanisms (such as occupancy in the secondary energy minimum), the term "retention" will be employed to describe colloids that do not exit the system during the term of the experiment. Likewise, continuum-scale experiments that observe delayed exit of colloids from the experiment typically cannot distinguish between colloids that detached from a collector surface or colloids that were temporarily retained without attachment. Thus, the term "reentrainment" will be employed to avoid attributing a particular mechanism to the colloids' delayed exit during these experiments. To be clear, the processes of attachment versus retention and detachment versus reentrainment are indeed distinguishable in many pore-scale direct observation experiments, as well as in pore-scale mechanistic simulations (they must be distinguished in the latter). In those contexts, we will refer specifically to attachment and detachment as appropriate.

Column experiments conducted under favorable conditions typically exhibit relatively simple colloid transport behavior: as seen in Figure 2 (right-most column), colloid breakthrough during injection reaches a steady state (i.e., temporally constant) plateau [*Elimelech et al*., 2000; *Li et al*., 2004; *Tufenkji and Elimelech*, 2004a; *Li et al*., 2005; *Tufenkji and Elimelech*, 2005a].

During the elution phase in favorable conditions, the concentration of colloids exiting the column decreases sharply with time indicating that there is negligible reentrainment of previously retained colloids [*Li et al*., 2004; *Tufenkji and Elimelech*, 2004a, 2005a]. The corresponding profiles of retained colloid concentrations with column length show a classic log linear decrease under favorable conditions (Figure 2, right column), as predicted by analytical solutions of the advective-dispersive-colloid transport equation (discussed in section 3) [*Li et al*., 2004; *Tufenkji and Elimelech*, 2004a, 2005a; *Han et al*., 2014]. These simple, well defined column-scale behaviors are due to the straightforward colloid-collector interactions at the pore scale under favorable conditions. Colloids that approach the collector experience no repulsion and come into physical contact with the collector surface (immobilize) [*Kuznar and Elimelech*, 2007; *Johnson et al*., 2010]. These colloids do not typically detach, since the strong attractive forces exceed fluid drag forces [*Bergendahl and Grasso*, 2000].

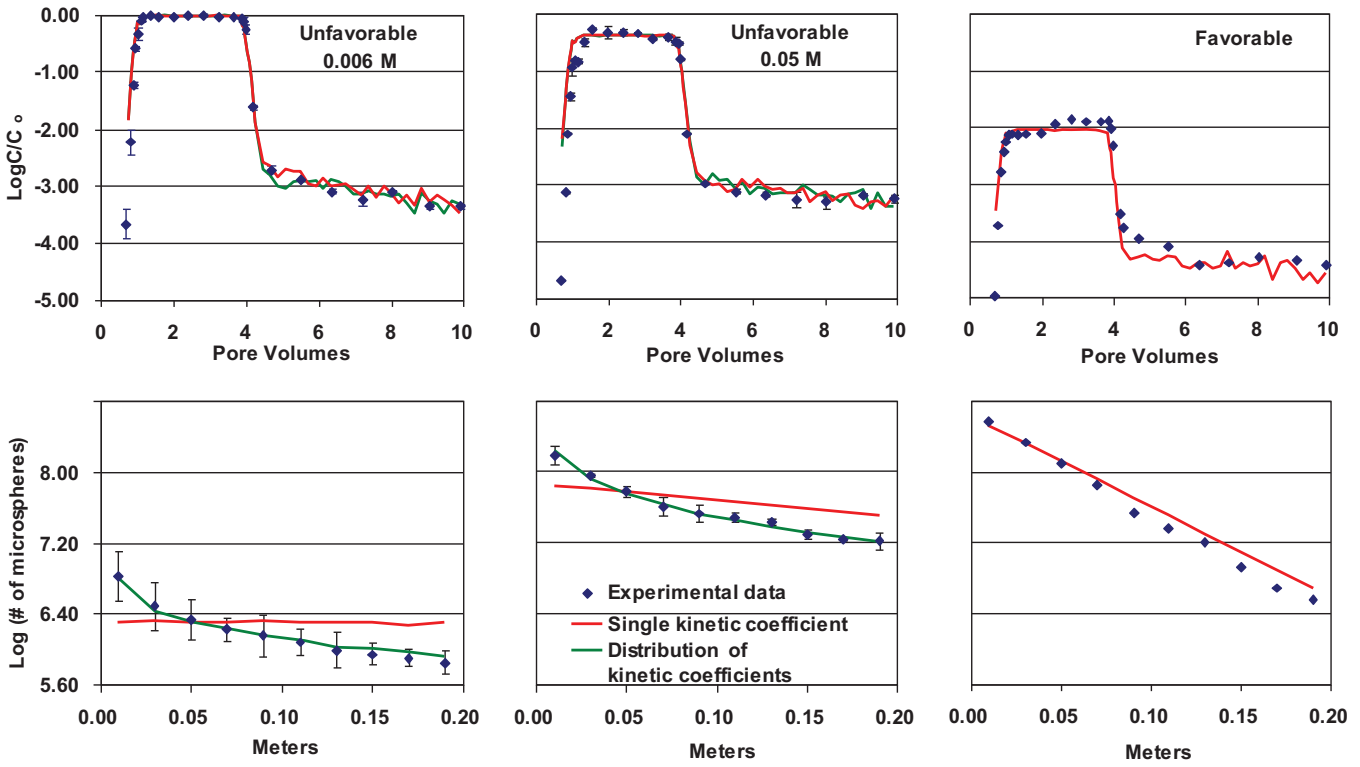

Figure 2. Experimental data (symbols) for the breakthrough-elution behavior (top row) and retained profiles (bottom row) of polystyrene latex microspheres in quartz sand in unfavorable and favorable conditions described in *Li and Johnson* [2005]. Lines are continuum model descriptions with a single deposition rate coefficient. The single deposition rate coefficient was used to generate a probabilistic deposition distribution. Adapted from *Li and Johnson* [2005].

Column experiments conducted under unfavorable conditions exhibit significantly different behavior from those conducted under favorable conditions (Figure 2, left and middle columns). Depending on the experimental conditions, unfavorable breakthrough behavior may also reach a steady state plateau (Figure 2, left and middle of top row) [*Elimelech et al.*, 2000; *Li et al.*, 2005; *Jiang et al.*, 2012a]. However, nonsteady state behavior may also occur. The effluent concentration may gradually increase over time, suggesting that a limited number of sites for colloid retention exist and are progressively filled (i.e., blocking) [*Johnson and Elimelech*, 1995; *Camesano et al.*, 1999; *X. Y. Liu et al.*, 2009; *Lin et al.*, 2011; *Mattison et al.*, 2011; *C. Wang et al.*, 2012; *Liang et al.*, 2013]. Decreasing concentration during breakthrough (called ripening) suggests that favorable colloid-colloid interactions allow already retained colloids (presumably due to inferred "favorable" heterogeneity as described in section 4) to serve as additional sites for further colloid retention [*Tong et al.*, 2008; *Jiang et al.*, 2012a].

Extended tailing may occur during the elution phase of unfavorable experiments (Figure 2, left and middle top row). Tailing is defined by the slow release of colloids from the column (illustrated in Figure 2) and is indicative of significant reentrainment, as observed for microbes in the laboratory [*Fontes et al.*, 1991; *Hornberger et al.*, 1992; *Lindqvist et al.*, 1994; *McCaulou et al.*, 1994; *Johnson et al.*, 1995b; *McCaulou et al.*, 1995; *Hendry et al.*, 1997, 1999; *Harter et al.*, 2000; *Li and Johnson*, 2005; *Li et al.*, 2005], field [*Scholl and Harvey*, 1992; *Harvey et al.*, 1995; *DeBorde et al.*, 1999; *Ryan et al.*, 1999; *Schijven et al.*, 1999], and nonbiological colloids [*Li et al.*, 2004; *Tufenkji et al.*, 2004; *Li et al.*, 2005; *Tong et al.*, 2005; *Johnson et al.*, 2007b]. The reentrainment behavior under unfavorable conditions is sensitive to solution chemistry and fluid flow as shown for reentrainment with perturbations, including variation in ionic strength [*Ryan et al.*, 1999; *Tufenkji and Elimelech*, 2004a, 2005a; *Shen et al.*, 2007; *Mattison et al.*, 2011; *Jiang et al.*, 2012a; *Shen et al.*, 2012], variation in pH [*Ryan et al.*, 1999; *Tufenkji and Elimelech*, 2004a, 2005a], and variation in fluid velocity [*Shang et al.*, 2008; *Pazmino et al.*, 2014a]. Traditionally, such release has been attributed to colloids that were retained in secondary minima, although more recent mechanistic simulations incorporating heterogeneity indicate that detachment from primary minima may contribute as well (as described in section 4).

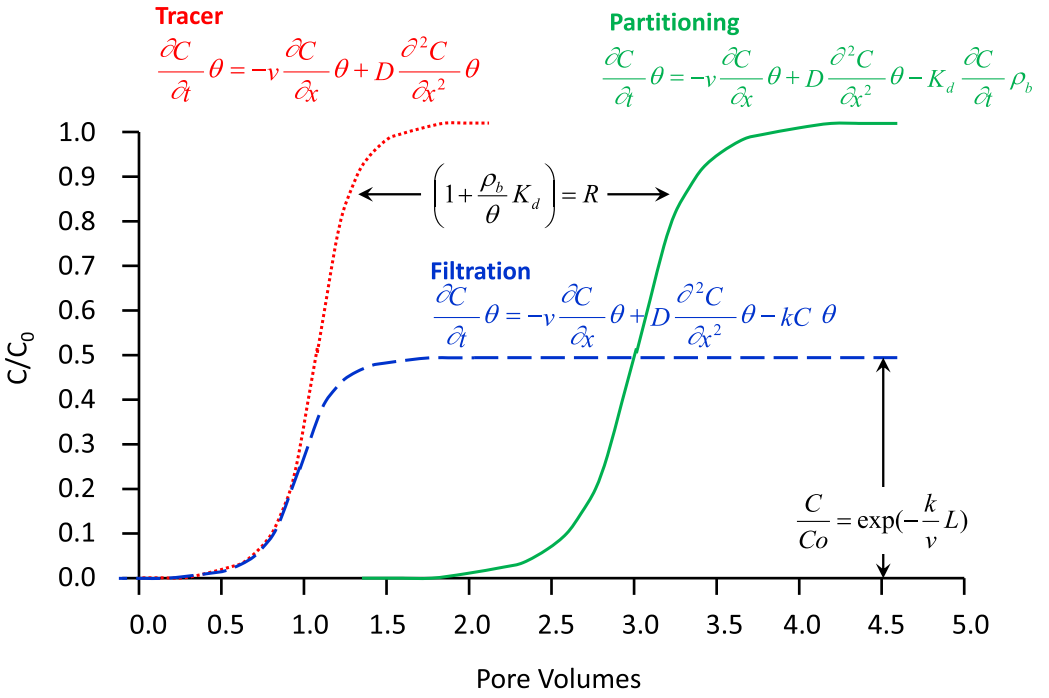

Figure 3. Typical breakthrough curve profiles that illustrate how equilibrium partitioning (i.e., retardation) (solid green line) and filtration (i.e., kinetic removal) (dashed blue line) impact breakthrough behavior relative to a conservative tracer (dotted red line). The variables in the equations are defined as C, effluent concentration; v, advective velocity; t, time; x, position; θ, porosity; D, dispersivity; K_d, partitioning coefficient; ρ_b, bulk density; R, retardation coefficient; k, kinetic retention coefficient; C_o, initial (injection) concentration; and L, travel length.

The resulting retention profiles from unfavorable condition experiments (Figure 2, left and middle bottom row) have shown nonlog linear (e.g., nonmonotonic or hyperexponential) decreases in concentration as function of distance [*Li et al*., 2004; *Tufenkji and Elimelech*, 2004a; *Tufenkji et al*., 2004; *Tufenkji and Elimelech*, 2005a,b; *Tong and Johnson*, 2007; *Liang et al*., 2013]. Hyperexponential and nonmonotonic profiles have also recently been described for engineered nanomaterials [*Liang et al*., 2013; *D. Wang et al*., 2014].

Column-scale experiments have been described using continuum-scale models employing rate constants and other parameters. Trends in these parameters as a function of fluid velocity, solution ionic strength (IS), among others, allow inference of the mechanisms responsible for observed differences in colloid transport and retention in favorable versus unfavorable conditions, as described in the following section.

3. Continuum-Scale Models: Inferring Mechanisms From Kinetic Coefficients

Continuum-scale models of the transport of species in groundwater solve mass balance equations at the macroscopic scale. At this scale, microscopic properties are averaged over a representative elementary volume (REV) and the averaged property (e.g., porosity, fluid pressure, and colloid concentration) is treated as a value that represents the property throughout the REV [*Bear and Cheng*, 2010]. Continuum models necessarily blur microscopic details and employ simplifying assumptions in the averaging process. The result is partial differential equations that describe spatial and temporal rate of change of key macroscopic properties (e.g., fluid velocity and colloid concentration) at a practical scale. These equations are typically discretized and solved on a numerical grid that correlates REVs to nodes. The advection-dispersion equation (ADE), which describes the transport of a nonreactive solute tracer in groundwater, is a typical example (see Figure 3, tracer equation). Additional continuum-scale (averaged) terms are incorporated as additional mechanisms, processes, and reactions and are necessary to describe the behavior of a solute or colloid at this scale (e.g., partitioning to surfaces, filtration, degradation; examples for colloids provided in Figure 3 and further discussed below). The values (or functions) assigned to the coefficients of these terms depend on the specific solute/colloid-soil-groundwater conditions being considered and are often determined through batch studies (e.g., for sorption) or model fitting to experimental column effluent results (e.g., colloid retention).

The treatment of colloid retention in continuum-scale models differs significantly from that of solutes due to their interactions with the surface being kinetic (colloids) rather than equilibrium (solutes) [*Schijven and Hassanizadeh*, 2000; *Tufenkji*, 2007]. However, it is worth noting that solute adsorption is not always strictly equilibrium based as there is evidence that adsorption can, in some circumstances, also be a kinetic process [*Bahr and Rubin*, 1987; *Fujikawa and Fukui*, 1991; *Cvetkovic and Dagan*, 1994; *van Kooten*, 1996; *Espinoza and Valocchi*, 1997; *Zhang and Selim*, 2006; *Dusek et al*., 2015]. In many scenarios, the high diffusion rates of solutes allow them to reach surfaces (adsorb) and leave (desorb) readily, at rates that are typically high relative to groundwater fluid velocities (i.e., low Peclet numbers). Thus, solute-surface interactions can be represented as a local equilibrium process that can often be represented using a linear proportionality (partition constant). Partition constants are empirical (experimentally measured), independently determined from continuum-scale experiments, and the one representing distribution of solute between water and sediment is often referred to as K_d (defined as $C_s = K_d \times C_w$ where C_s is the solid-phase concentration and C_w is the aqueous phase concentration).

In contrast, colloids exhibit relatively low diffusion, which limits their ability to reach surfaces (but also makes the likelihood of colloids reaching surfaces mechanistically predictable as described in section 4). Colloid transfer to surfaces (filtration) is therefore described using kinetic retention coefficients [*Harvey and Garabedian*, 1991; *Schijven and Hassanizadeh*, 2000; *Tufenkji*, 2007]. The resulting breakthrough behaviors of solutes versus colloids are quite distinct (Figure 3) in that partitioning (specifically the proportionality between concentrations in water and sediment) retards transient breakthrough of the solute relative to a conservative tracer and yields complete steady state breakthrough (effluent and influent concentrations equivalent, $C = C_0$). In contrast, filtration (and other predominantly one-way processes such as degradation) yields reduced steady state breakthrough ($C < C_0$), and transient breakthrough is not generally retarded relative to a conservative tracer (Figure 3) [e.g., *Foppen and Schijven*, 2006]. It is noted that transient breakthrough of colloids may occur earlier than for tracers if Taylor dispersion (intrapore fluid velocity variation), or size exclusion of colloids from small pores (interpore fluid velocity variation), yields enhanced advection of colloids relative to solutes [e.g., *Bales et al*., 1989; *Powelson et al*., 1993; *Zhang et al*., 2001b; *Keller et al*., 2004; *Chrysikopoulos and Syngouna*, 2014].

The classic ADE for a nonreactive solute tracer (see Figure 3, tracer equation) is commonly modified for solute partitioning behavior (see Figure 3, partitioning equation) as well as colloid transport (see Figure 3, filtration equation). The modified-ADE commonly employed for colloid transport incorporates a single kinetic retention coefficient for colloid retention. The single-rate description of colloid transport yields continuum-scale behavior that, in the absence of colloid aggregation, generally provides an excellent match to the colloid transport and retention behavior discussed in section 2 for favorable conditions (Figure 2) [e.g., *Li et al*., 2004; *Tufenkji and Elimelech*, 2004a, 2005a].

In unfavorable conditions, the single-rate description of colloid transport often fails to capture experimentally observed breakthrough and retention behavior (the nonsteady state breakthrough and nonlog linear retention profiles described in section 2; see Figure 2). The hyperexponential retention profiles often observed in unfavorable conditions suggest that there is a high deposition rate near the porous medium inlet followed by a region with low deposition rates. A number of studies have inferred that this depth-dependent retention rate is due to a distribution of retention rates that are present within the experimental system [*Schijven and Hassanizadeh*, 2000; *Schijven and Šimůnek*, 2002; *Tufenkji et al*., 2003; *Li et al*., 2004; *Tufenkji and Elimelech*, 2004a, 2005b, 2005a; *Foppen and Schijven*, 2006; *Foppen et al*., 2007; *Tong and Johnson*, 2007; *Chatterjee et al*., 2011]. To describe this observation, a second, additional kinetic retention coefficient is often employed—termed "dual-deposition" or "two-site" models—to better fit the experimental retention profiles (discussed in section 2). The two kinetic retention coefficients represent (a) a "fast" kinetic retention coefficient to describe the early, sharp decrease in retained concentration and (b) a "slow" kinetic retention coefficient to describe the later, more gradual decline in retained concentration [*Schijven and Šimůnek*, 2002; *Tufenkji and Elimelech*, 2004a, 2005b, 2005a; *Chatterjee et al*., 2011; *Mattison et al*., 2011; *Mondal and Sleep*, 2013]. This results in an improved model fit to experimental hyperexponential profiles (Figure 2).

The hyperexponential profiles (initially observed for bacteria and protozoa) were attributed to heterogeneity among the bacterial population such that "stickier" individuals were retained upgradient of "less sticky" individuals [*Albinger et al*., 1994; *Harvey et al*., 1995; *Hendry et al*., 1997; *Baygents et al*., 1998; *Simoni et al*.,

1998; *Bolster et al*., 1999; *Schijven et al*., 1999; *Bolster et al*., 2000]. Distributions in colloid size, surface charge, coatings, and hydrophobicity have been inferred to yield heterogeneity among colloid populations, and hyperexponential retention profiles as illustrated in Figure 2 [*Simoni et al*., 1998; *Schijven and Hassanizadeh*, 2000; *Schijven and Šimůnek*, 2002; *Tufenkji et al*., 2003; *Li et al*., 2004; *Foppen et al*., 2007; *Tong and Johnson*, 2007; *Chatterjee et al*., 2011].

Other studies have attributed the inferred "fast" and "slow" dual-deposition behavior to differences in interactions energies between colloids and collectors emanating partially from localized soil heterogeneities as well as deep secondary energy minima, the latter yielding "fast" retention, and the former yielding "slow" retention [*Tufenkji and Elimelech*, 2004a, 2005b, 2005a] on the basis that the former mechanism requires overcoming the repulsive energy barrier prior to retention. Additional studies have also suggested that soil heterogeneities, such as heterogeneities of attractive iron oxyhydroxide situated within bulk repulsive silica, can create "fast" and "slow" deposition rates in the favorable and unfavorable regions [*Schijven and Hassanizadeh*, 2000, 2002].

Whereas the above studies implicate soil heterogeneity in generating fast versus slow retention rates, they do not articulate how this would generate preferential upgradient versus downgradient retention (hyperexponential profiles) [*Johnson and Li*, 2005]. Assuming that inferred heterogeneity is distributed throughout the column (not predominantly located near the column inlet), then the kinetic retention coefficient across the column would be uniformly increased or decreased across the column by the presence of heterogeneity. Based on similar reasoning, a number of studies have concluded that soil heterogeneity alone is likely not the primary cause of this behavior [*Schijven and Šimůnek*, 2002; *Li et al*., 2004; *Foppen et al*., 2007; *Tong and Johnson*, 2007].

The above review demonstrates the utility of continuum-scale models for inferring colloid transport, retention, and reentrainment mechanisms; however, it should be noted that the kinetic parameters used in these models tend to be descriptive rather than predictive. For example, currently only the filtration rate constant under favorable conditions can be independently predicted (for spheroidal uniform colloids and media). No independently derived mechanistic basis currently exists for predicting "fast" and "slow" rate coefficients present in these dual-deposition models; rather, they require fitting to experimental breakthrough and retention profile data. Thus, dual-deposition rate models cannot be used to predict colloid transport without conducting detailed experiments a priori. The corollary is that, while this dual-deposition approach successfully produces hyperexponential profiles, the underlying mechanism(s) can only be inferred, and are not proven by a fit to data. For example, the observed decrease in attachment rate coefficient with increasing transport distance has been attributed to both (1) straining [*Bradford et al*., 2002, 2003, 2004, 2006a] and (2) heterogeneity among the colloid population [e.g., *Tong and Johnson*, 2007] which are very different mechanisms for achieving this phenomenon.

Another common example of mechanisms inferred from fitting to continuum-scale data are the dual-region or multiporosity models. The classic ADE for a one-dimensional system employs a single average pore water velocity. This single-velocity approach relies on the assumption that the velocity distribution within the porous medium can be approximated by a single, or volume-averaged, velocity term that predicts, in the absence of retardation, a classic breakthrough curve with $C/C_o = 0.5$ at the location of the advective front. It also predicts a symmetrically sharp decrease in concentration during the elution phase of the experiment. As discussed in section 2, this approach provides an excellent description of colloid transport through uniform, homogeneous and simple (i.e., glass bead) porous media in favorable deposition conditions.

However, the anomalous early breakthrough and extended tailing behavior discussed in section 2 suggests that this average-velocity approach may not be appropriate for a wide range of water-saturated soils in both favorable and unfavorable conditions. These behaviors have been modeled at the continuum-scale by employing a distribution of permeabilities (e.g., dual-porosity or dual-permeability models). While these models are commonly employed for solute transport behavior in the presence of preferential pathways/low permeability regions and fractures/rock matrix [e.g., *Haggerty and Gorelick*, 1995; *Haggerty et al*., 2000; *Šimůnek et al*., 2003; *Rotter et al*., 2008; *Šimůnek and van Genuchten*, 2008], they have also been adapted for use in colloid transport, although to a relatively limited extent. Specifically, these studies have suggested that early-time colloid breakthrough and bimodal breakthrough curves may be linked to preferential flow [*Leij and Bradford*, 2013; *Subramanian et al*., 2013] which may occur in both physically heterogeneous [e.g.,

Zheng and Gorelick, 2003; *Y. Wang et al.*, 2014a] and uniform media [e.g., *Berkowitz et al.*, 2006; *Scheibe et al.*, 2013] and also due to size exclusion effects discussed in section 2.

Continuum-scale solute modeling studies have suggested that extended tailing is linked to the presence of low permeability zones and is described via dual-porosity (i.e., dual-region) or multiporosity models [e.g., *Haggerty and Gorelick*, 1995; *Haggerty et al.*, 2000]. Colloid transport models typically describe tailing by assuming that a fraction of colloids are temporarily (i.e., reversibly) retained [*Johnson et al.*, 1995b; *Zhang et al.*, 2001a; *Schijven and Hassanizadeh*, 2002; *Schijven and Šimůnek*, 2002; *Landkamer et al.*, 2013; *Mondal and Sleep*, 2013]. Conceptually, this treatment is similar to dual-region models to describe solute tailing as the retention still occurs in regions with below-average velocity, although for colloid transport in uniform media this is typically assumed to be the near-surface zone [*Johnson and Hilpert*, 2013]. Attribution of temporary colloid retention to residence in the near-surface fluid domain (i.e., secondary minima) can be inferred but is not proven by the match of continuum-scale models to column experiment observations. Notably, recent pore-scale modeling studies have suggested that below-average velocity regions in the bulk pore space may also temporarily retain colloids [*Cardenas*, 2008; *Torkzaban et al.*, 2008; *X. Q. Li et al.*, 2010; *Z. Li et al.*, 2010; *Li et al.*, 2012] suggesting that the near-surface fluid zone may not be the only contributor to extended tailing.

Mass transfer coefficients used in continuum models are often fitted parameters, determined by inverse modeling of experimental data [*Köhne et al.*, 2009a, 2009b; *Y. Wang et al.*, 2014b]. Results from these continuum models are powerful tools for identifying potential mechanisms and demonstrating the influence of physical heterogeneity (mobile versus immobile zones) and solution chemistry (e.g., favorable versus unfavorable attachment conditions). For example, trends in kinetic parameters describing colloid retention and reentrainment show qualitative agreement with DLVO predictions (barrier height and secondary minimum depth) as a function of ionic strength [e.g., *Elimelech and O'Melia*, 1990a, 1990b; *Elimelech*, 1991; *Petosa et al.*, 2010]. Although quantification of rate constants through experimentation is useful, a priori determination of mechanisms, and independent derivation of rate constants, would enable prediction of colloid transport in a range of scenarios but requires mechanistic modeling as will be discussed in the next section.

4. Mechanistic Prediction of Retention in Favorable and Unfavorable Conditions

Differences between molecular (e.g., solute) and colloidal transport processes in porous media drive differing modeling approaches to describe their transport. Specifically, solutes exhibit much greater random motion and lack a deterministic trajectory so their likelihood of reaching a surface is determined empirically by laboratory analyses (e.g., batch equilibration tests). By contrast, colloids exhibit relatively limited diffusive (i.e., Brownian) motion and possess largely deterministic trajectories, enabling mechanistically based prediction of the likelihood of colloids reaching surfaces. Although for nanosized colloids, the distinction between deterministic colloidal trajectories and random diffusive solute behavior is blurred as these colloids exhibit a large degree of Brownian motion. The simulation of deterministic trajectories as well as quantification of the likelihood of colloids reaching surfaces is encompassed in CFT.

Most CFT approaches have two major components: (i) a mechanistic force/torque model that describes colloid trajectory and attachment (described in section 4.1) and (ii) correlation equations that approximate the results of the mechanistic models (described in section 4.2). A typical predicted model parameter, be it from a mechanistic model or correlation equation, is the "collector contact efficiency," η, defined as the fraction of colloids entering the mechanistic model geometry that contacts the collector. Both mechanistic models and the resultant correlation equations have largely been successful in predicting η for micron-sized colloids in "favorable" conditions [e.g., *Yao et al.*, 1971; *Rajagopalan and Tien*, 1976; *Tufenkji and Elimelech*, 2004b]. It is also important to note that these approaches are subject to error arising separately at the mechanistic model and correlation equation level. In the case of mechanistic models, errors may result from employing incorrect physicochemical parameters and numerical approximations. In the case of correlation equations, errors may be due to the extent to which they are able to approximate mechanistic model results. Mechanistic models and correlation equations for unfavorable conditions, the subject of considerable recent research, are discussed in section 4.3. The following section will discuss model assumptions and their implications for the prediction of colloid and nanoparticle transport. For a conceptual and

mathematical summary of the major mechanistic models discussed, including all of the relevant force/torque equations employed by each model, the reader is referred to Tables (A1–A6) in Appendix A.

4.1. Mechanistic Simulations: Favorable Conditions

There are more than 10 different CFT mechanistic models, each employing different environmental conditions, model geometries, or force/torque mechanisms [*Yao et al*., 1971; *Payatakes et al*., 1974a, 1974b; *Rajagopalan and Tien*, 1976; *Paraskeva et al*., 1991; *Burganos et al*., 1992, 1994; *Cushing and Lawler*, 1998; *Tufenkji and Elimelech*, 2004b; *Long and Hilpert*, 2009; *Ma et al*., 2009; *Nelson and Ginn*, 2011]. Each of these mechanistic models is associated with one or more approximating correlation equations. Given the large number of mechanistic models and correlation equations, some of which are simple extensions or variations of previous models and correlation equations (discussed below), there may be some confusion related to which mechanistic model or correlation equation is applicable in a given scenario.

4.1.1. The Geometry of Mechanistic Models

The first CFT model proposed by *Yao et al*. [1971] considered colloids approaching a single, isolated collector that was perfectly spherical and surrounded by an infinite fluid. This approach, as noted by *Yao et al*. [1971], produced velocity distributions that were likely poor representations of realistic porous media. The isolated-sphere approach was subsequently modified to employ a Happel sphere-in-cell geometry [*Happel*, 1958] that included porosity, as well as constricted tube geometry [*Payatakes et al*., 1974a, 1974b; *Paraskeva et al*., 1991; *Burganos et al*., 1992, 1994]. The most popular, the Happel sphere-in-cell approach, considers the collector, otherwise isolated from the influence of other collectors and perfectly spherical, to be surrounded by an envelope of fluid that is associated with the collector. Tables A1 and A2 in Appendix A illustrate some of the model geometries that are employed in the most popular mechanistic models. This CFT-Happel approach was first employed by *Rajagopalan and Tien* [1976] and has been employed in more recent CFT models [*Tufenkji and Elimelech*, 2004b; *Nelson and Ginn*, 2011] as it is conceptually straightforward and simple to upscale the results. Figure 4, adapted from I. L. Molnar et al. (The impact of immobile zones on the transport and retention of nanoparticles in porous media, submitted to *Water Resources Research*, 2015), illustrates the Happel sphere-in-cell geometry along with the boundary conditions that would be employed by Eulerian mechanistic models [e.g., *Tufenkji and Elimelech*, 2004b]. The flow field around the collector is assumed to be equivalent to Stokes (i.e., creeping) flow around a sphere and undisturbed by the presence of nearby collectors (approximate velocity vectors are illustrated in the figure). v_o and C_o are the fluid velocity and colloid concentration upstream of the collector, respectively, and are considered uniform over the projected area upstream of the collector (A_1 in the figure).

Because an actual porous medium includes grain-grain contacts, it may yield flow phenomena inconsistent with Stokes flow around a Happel collector, including recirculation/vortex zones [*Cardenas*, 2008; *Torkzaban et al*., 2008; *Z. Li et al*., 2010] and low-flow zones [*X. Q. Li et al*., 2010; *Li et al*., 2012]. While Stokes flow incorporates low fluid velocities adjacent to the collector's surface, the low/recirculating flow phenomena induced by grain-grain contacts likely extends this characteristic further outward. Thus, the flow field illustrated in Figure 4 and used in many mechanistic models is simplified relative to the expected actual flow field within a porous medium. It is important to understand the conditions under which this simplification is acceptable and when it may result in poor predictions of the rate at which colloids contact the surface.

Predictions from mechanistic models for medium-to-larger sized colloids (e.g., $>$100 nm) are generally in excellent agreement with experiments performed for favorable conditions [*Yao et al*., 1971; *Rajagopalan and Tien*, 1976; *Tufenkji and Elimelech*, 2004b; *Tong and Johnson*, 2006; *Nelson and Ginn*, 2011]. However, there is evidence that smaller colloids (e.g., $<$100 nm, including viruses and engineered nanoparticles) are potentially impacted by grain-grain contact flow phenomena in even favorable conditions [*Long and Hilpert*, 2009; *Boccardo et al*., 2014]. Mechanistic single-collector models have been observed to overpredict η for Brownian particle transport experiments in favorable conditions [e.g., *Elimelech and O'Melia*, 1990a; *Tong and Johnson*, 2006; *Long and Hilpert*, 2009; *Nelson and Ginn*, 2011]. Hypothesizing that this is due to the simplified geometries employed by single-collector CFT models, *Long and Hilpert* [2009] and *Long et al*. [2010] explicitly incorporated the impact of grain-to-grain contacts by performing Lattice Boltzman (LBM) colloid transport and retention simulations in randomly generated collector packings. The *Long and Hilpert* [2009] mechanistic model produced η predictions for Brownian particles that were in better agreement with experimental results relative to single-collector models [*Nelson and Ginn*, 2011]. This improved prediction may

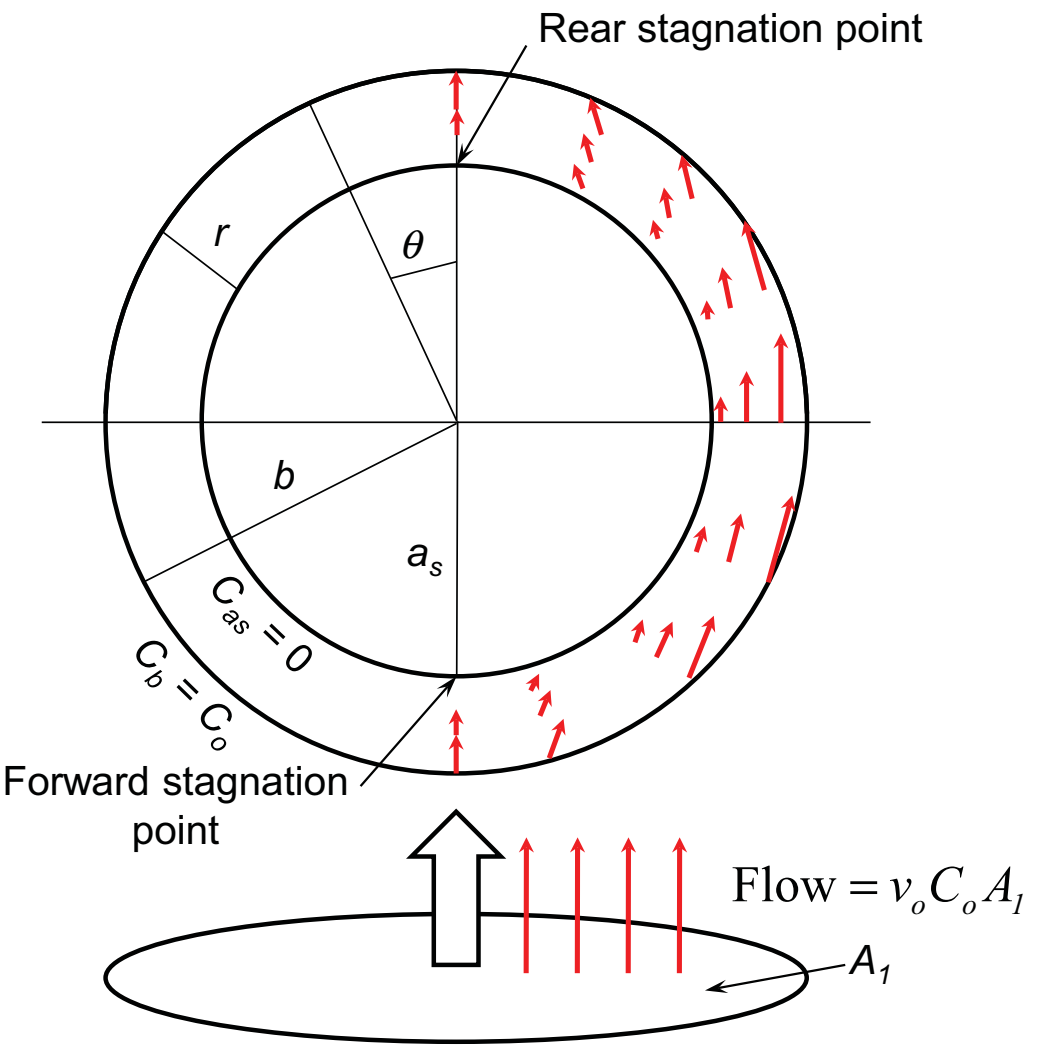

Figure 4. Illustration of a typical CFT model employing a Happel sphere-in-cell model with boundary conditions (only applicable to Eulerian models). The geometry of the model is defined by a_s, the radius of the collector, b, the radius of the Happel cell, and r, the thickness of the fluid envelope. The red arrows on the right-hand side of the model represent approximate flow vectors around the sphere. C_b and C_{as} represent the Eulerian constant concentration boundary conditions at the edge of the fluid envelope and collector surface where C_o represents the concentration of approaching colloids. Adapted from Molnar et al. (submitted manuscript, 2015).

result from including grain-to-grain contacts and the resulting low-flow or recirculation/vortex zones that increase the distance particles must diffuse to reach certain surfaces.

The mechanistic model that incorporates grain-to-grain contact using a hemisphere-in-cell approach [*Ma et al*., 2009; *Ma and Johnson*, 2010] does still somewhat overpredict η [*Nelson and Ginn*, 2011]. This may be due to the orientation of the contacting grains. In the hemisphere-in-cell model, the flow direction is always perpendicular to the line connecting adjoining grain centers (see Figure 4). In a randomly packed porous medium, the flow direction occurs at many orientations relative to the line connecting adjoining grain centers, which is expected to yield a significantly larger low-flow/recirculation zone [*Torkzaban et al*., 2008].

Nelson and Ginn [2011] employed a Happel sphere mechanistic model to achieve a similarly good match to experiments for Brownian particles. This was likely due to an improved correlation equation (discussed in section 4.2) that better approximated the mechanistic model, notably in the low fluid velocity (i.e., diffusive) regime, as opposed to employing a better mechanistic model. Noting the improved prediction accuracy, *Ma et al*. [2013] subsequently adjusted their correlation equation to extend to the diffusion-dominated velocity regime.

4.1.2. Modeling Diffusion in Mechanistic Models

Complexities associated with describing, or predicting, colloid trajectories that exhibit significant Brownian motion are also likely a contributing factor to overprediction of η by mechanistic models. The size of small nanoparticles (e.g., 5–50 nm) and the mechanisms governing their transport fall between that of molecules and larger nanoparticles (e.g., $>$50 nm); thus, they exhibit large Brownian motion relative to colloids but possess trajectories that are more deterministic than solutes. While the trajectories of larger, non-Brownian, colloids have been adequately described since the early numerical description by *Rajagopalan and Tien* [1976], the treatment of Brownian motion has varied considerably. *Yao et al*. [1971] solved for diffusive flux by employing the *Levich* [1962] solution of the convective-diffusive equation for an isolated sphere in an infinite fluid. The *Levich* [1962] solution is a simplified description of diffusion as it does not incorporate mechanisms such as anisotropic diffusion. Anisotropic diffusion describes the decrease in colloid diffusivity that occurs within several particle diameters of the surface. As such, Brownian motion perpendicular to the surface becomes small relative to the tangential motion [*Eral et al*., 2010]. Mechanistic models that ignore diffusive mechanisms such as anisotropic diffusion or hydrodynamic retardation (defined as the decrease in colloid velocity near the collector surface due to resistance from the near-surface fluid) could also yield overestimates of η for Brownian particles as the models cannot account for the decrease in particle velocity that occurs near collector surfaces.

Rajagopalan and Tien [1976], despite using a numerical solution to solve for the trajectories of large colloids (i.e., a Lagrangian approach), solved diffusion by employing an analytical method similar to that of *Yao et al*. [1971] but specific to the Happel sphere-in-cell geometry [*Cookson*, 1970] which ignores anisotropic diffusion. *Tufenkji and Elimelech* [2004b] employed the Eulerian numerical model of *Elimelech* [1994] which solves the advective diffusive equation and included anisotropic diffusion and hydrodynamic retardation. *Long and Hilpert* [2009] similarly solved diffusion numerically via the ADE but did not include anisotropic diffusion. *Nelson and Ginn* [2011] added a scaled randomly oriented translation of the colloid to mimic Brownian motion. *Ma et al*. [2009] employed a scaled Brownian force so that diffusive movement was subjected to the effects of hydrodynamic retardation equivalent to other governing forces. Tables A1–A6 in Appendix A present the equations employed to describe Brownian motion in the most commonly used mechanistic models.

4.1.3. Eulerian and Langrangian Numerical Solution Frameworks

Strategies to numerically solve the mechanistic models fall broadly into two categories: Eulerian and Lagrangian frameworks. The exception is the *Rajagopalan and Tien* [1976] model which employed both approaches, depending on whether the trajectory of the colloid was mostly deterministic (Lagrangian approach) or Brownian (Eulerian approach). Early models tended to be Eulerian [*Elimelech*, 1992; *Tufenkji and Elimelech*, 2004b], and with increased computational power, Lagrangian mechanistic models have been adopted [*Ma et al*., 2009; *Ma and Johnson*, 2010; *Nelson and Ginn*, 2011; *Ma et al*., 2013].

While both categories of mechanistic models have successfully described colloid transport and attachment in certain scenarios, Eulerian mechanistic models have limitations, especially within the Happel sphere geometry. For Happel sphere mechanistic models employing an Eulerian or analytical framework [*Rajagopalan and Tien*, 1976—diffusion only; *Tufenkji and Elimelech*, 2004b], a constant concentration boundary condition is specified at the outer fluid envelope surrounding the collector. The concentration at this boundary is assumed to be the concentration within the bulk fluid upstream of the collector (i.e., $C_b = C_o$, Figure 4). This constant concentration boundary condition represents the distance at which the collector ceases to exert an influence on colloid distribution in the pore space.

For Brownian colloid systems with very high removal rates and low Peclet numbers, the constant concentration boundary condition on the downstream half of the Happel fluid envelope may be inappropriate [*Song and Elimelech*, 1992; *Nelson and Ginn*, 2011]. In these circumstances, the colloid concentration at the downstream boundary would be lower than that of the upstream boundary. As a result, there would be an implicit discrepancy between the mechanistic model and what would occur in reality. This would result in overestimates of η for Brownian colloids [*Song and Elimelech*, 1992].

The concentration boundary conditions also implicitly assume a concentration gradient of $\frac{C_b - C_{as}}{r}$ (see Figure 4) which describes diffusive flux toward the collector surface. The gradient imposed by these boundary conditions may not be representative of the actual concentration gradient within a realistic porous medium as

C_b might not be equivalent to C_o. The pore-scale flow phenomena resulting from grain-to-grain contacts (discussed earlier) may yield larger low velocity zones than predicted by Stokes flow. This extended low-flow zone may yield distances between the collector surface and boundary $C = C_o$ that are larger than the thickness of the Happel sphere fluid envelope. If the distance is larger in reality than in the Happel sphere model, the resulting concentration gradient would be smaller than is predicted. As such the diffusive flux toward the collector surface may be lower than predicted by Eulerian mechanistic models.

With Lagrangian mechanistic models, issues related to boundary conditions are largely avoided by introducing individual particles on the upstream outer fluid envelope boundary. The trajectories of the individual colloids (i.e., attachment or exiting the system) are determined without imposing a concentration at the downstream boundary of the fluid envelope.

4.1.4. Stokes Flow in Mechanistic Simulations

As discussed above, mechanistic CFT models assume that the flow regime around a collector can be modeled by assuming Stokes, or creeping, flow [*Yao et al*., 1971; *Rajagopalan and Tien*, 1976; *Tufenkji and Elimelech*, 2004b; *Nelson and Ginn*, 2011] (Tables A1 and A2 in Appendix A detail the governing flow equations for the most commonly used models). Stokes flow occurs at very low Reynolds numbers (Re $<<$ 1) where inertial forces become insignificant relative to viscous forces. This assumption is likely appropriate at the low flow rates typically associated with filtration and ambient groundwater (i.e., no pumping) in nonfractured systems.

The application of Stokes flow results in streamlines that are mirrored on the forward and rear flow sides of the collector. At low flow rates, this results in downstream velocity distributions that are approximately similar to the upstream flow distribution (uniform v_o over area A_1 in Figure 4). However, in situations of high flow where Re $>$ 1 [*Potter and Wiggert*, 2002], the flow is no longer strictly within the Stokes regime. Under these conditions, the point at which flow separates from the rear side of the collector will change (i.e., it will produce a wake) and the rear flow stagnation point will widen relative to the forward flow stagnation point [*Potter and Wiggert*, 2002]. This could yield discrepancies between experimental results and mechanistic simulations of colloid transport and retention.

Non-Stokes flow is likely in laboratory experiments conducted at high flow rates. Surveying the literature, and assuming reasonable parameters when values were not available (i.e., viscosity $= 1 \times 10^{-3}$ Pa s, $T = 293$ K), suggests that many experiments were conducted with Re close to or exceeding 1 [e.g., *Yao et al*., 1971; *Elimelech and O'Melia*, 1990a; *Elimelech*, 1991; *Lecoanet et al*., 2004; *Lecoanet and Wiesner*, 2004; *Phenrat et al*., 2007, 2010a]. Given this finding, conclusions derived from studies where a CFT conceptual model was adopted, but Re was also high, need to be considered with caution.nZVI experiments typically employ high flow rates with the justification that velocities near the injection well may be very large [*Kocur et al*., 2013]. Given that non-Stokes flow may occur near the injection well, CFT mechanistic models and correlation equations for prediction of nZVI transport must be used with caution. Overall, this suggests that careful consideration of Reynolds numbers and flow regime is required when designing column-scale transport experiments, interpreting model fits to the data, or modeling field-scale nZVI injection.

4.2. Correlation Equations Derived Under Favorable Conditions

The above discussion focuses on the mechanistic models underlying CFT. However, these models are time consuming to run, and so require approximation via phenomenological expressions to allow easy implementation. To this end, mechanistic models are run under a range of environmental conditions (see Table 1). Results from simulations conducted using the mechanistic models are then fit to a phenomenological expression composed of dimensionless groups of relevant physicochemical parameters. This expression serves as a correlation equation thereby serving as a simple predictor for η. Such correlation equations currently exist only for favorable attachment scenarios since the underlying mean-field mechanistic models predict no attachment in unfavorable scenarios; attempts to adapt mechanistic models for unfavorable conditions are discussed in section 4.3.

The correlation equations divide colloid transport to the surface into three distinct dimensionless numbers representing interrelated mechanisms: interception via fluid drag interactions alone, diffusion-enhanced interception, and sedimentation-enhanced interception. A separate contribution to the overall η is determined for each dimensionless number (i.e., η_I, η_D, and η_G, respectively), such that the overall collector efficiency is described as $\eta = \eta_I + \eta_D + \eta_G$. In the absence of diffusion or sedimentation, η_I is greater for larger colloids,

Table 1. Range of Parameter Values Employed to Derive Recent η Correlation Equations[a]

	Particle Diameter, d_p (μm)	Collector Diameter, d_c (μm)	Approach Velocity, U (m/s)	Hamaker Constant, A (J)	Particle Density, ρ_p (g/cm^3)	Fluid Temperature, T (K)	Porosity, θ	Fluid Viscosity, μ (Pa s)
TE 2004	0.01–10	50–500	7×10^{-6} to 2×10^{-3}	3×10^{-21} to 4×10^{-20}	1–1.8	298	0.36	0.8×10^{-3}
LH 2009	0.1–1	20–450	10^{-7} to 10^{-5}	10^{-20}	1.05	298	0.3–0.42	0.8×10^{-3}
Long et al. [2010]	0.02–1	3600	2.5×10^{-8} to 10^{-6}		1.055	298	0.38	
MPFJ 2009	0.05–10	510	1.7×10^{-5}	3.84×10^{-21}	1.055	298	0.37	0.998×10^{-3}
MHJ 2013	0.01–10	510	1.15×10^{-7} to 1.7×10^{-5}	3.84×10^{-21}	1.055, 4	298	0.25, 0.37	0.998×10^{-3}
NG 2011	0.01–10	10–1200	10^{-7} to 2×10^{-3}	3×10^{-21} to 4×10^{-20}	1–1.8	278–303	0.26–0.48	0.798×10^{-3} to 1.518×10^{-3}

[a]η correlation equations: TE 2004, *Tufenkji and Elimelech* [2004b]; LH 2009, *Long and Hilpert* [2009]; *Long et al.* [2010]; MPFJ 2009, *Ma et al.* [2009]; MHJ 2013 *Ma et al.* [2013]; NG 2011, *Nelson and Ginn* [2011].

since the number of streamlines that approach the surface to within one colloid radius increases as the colloid size increases. Diffusion enhances interception since it allows colloids to move across streamlines and come into contact with the collector. Because Brownian motion is greater for smaller colloids, η_D is greater for smaller colloids. Because settling allows colloids to move across the streamlines and come into contact with the collector, η_G is greater for larger colloids. The superimposed contributions from these interrelated mechanisms yield a trend of η with colloid size that matches mechanistic simulations and experimental observations wherein a minimum value of η occurs corresponding to colloid diameters of $\sim$1 μm, due to smaller colloids undergoing greater diffusion, and larger colloids undergoing greater settling. As an example, the correlation equation of *Rajagopalan and Tien* [1976] is (corrected version presented in *Logan et al.* [1995])

$$\eta \approx \gamma^2\left[4A_s{}^{1/3}N_{Pe}^{-2/3}+A_sN_{LO}^{1/8}N_R^{15/8}+0.00338A_sN_G^{1.2}N_R^{-0.4}\right] \tag{1}$$

where the dimensionless parameters (i.e., N_R, N_{PE}, N_{LO}, and N_G) are defined in Table 2, and A_s is a porosity-dependent parameter defined as

$$A_s=\frac{2(1-\gamma^5)}{2-3\gamma+3\gamma^5-2\gamma^6} \tag{2}$$

where $\gamma=(1-\theta)^{1/3}$. A_s accounts for the influence of neighboring collectors on the fluid flow field in the Happel sphere-in-cell geometry and θ represents the porosity of the porous medium. Tables A1 and A2 in Appendix A list the correlation equations for the six most commonly used models.

Figure 5 illustrates how well the correlation equations listed in Table 1 predict the experimental kinetic retention coefficient *k*. Figure 5 compares experimental and predicted values of k (the upscaled η) since the definition of η differs among the different collector geometries (Appendix A, Tables A1 and A2 provide the equation for k for each model). As can be seen, the currently existing correlation equations generally provide very good predictions of η for micron-sized colloids in the range of conditions for which the correlations were developed [e.g., *Tong and Johnson*, 2006; *Nelson and Ginn*, 2011]. However, they generally overpredict η for Brownian particles (Figure 5, the "nanoparticles" region). While a number of possible causes for this overprediction were identified in the discussion related to mechanistic models, another possible source of error may be the approximating correlation equations themselves. Many of the flow and transport scenarios for Brownian particles involve parameter values that are outside the limited range of conditions employed to derive the correlations [e.g., *Quinn et al.*, 2005; *Kocur et al.*, 2013; *Krol et al.*, 2013; *O'Carroll et al.*, 2013; *Gastone et al.*, 2014; *Kocur et al.*, 2014; *Tosco et al.*, 2014b].

Table 2. List of Dimensionless Parameters in Predicting Colloid Filtration

Parameter	Definition[a]	Description
N_R	a_p/a_s	Aspect ratio
N_{PE}	Ud_c/D_{BM}	Peclet number
N_{LO}	$H/\left(9\pi\mu a_p^2U\right)$	London number
N_G	$2a_p^2(\rho_p-\rho_f)g/(9\mu U)$	Gravity number

[a]a_p and a_s are the colloid and collector radii; d_c is the collector diameter, U is the approach velocity; D_{BM} is the bulk diffusion coefficient (described by Stokes-Einstein equation); μ is the fluid viscosity, ρ_f and ρ_g are the fluid and colloid densities, respectively; g is the gravitational acceleration constant.

This is often the case for the prediction of engineered nanoparticle transport. For example a limited range of viscosities, similar to water, have been used in mechanistic model simulations used in the development of correlation

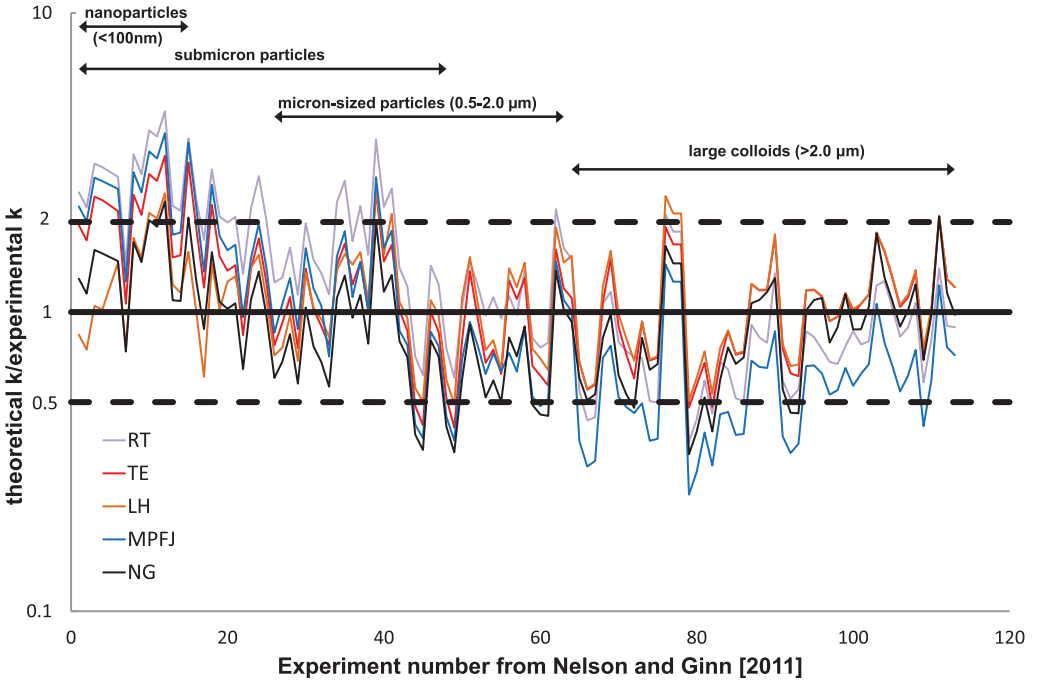

Figure 5. A comparison of experimentally determined retention rate coefficients versus correlation equation predicted retention rate coefficients (k) for a number of different correlation equations on a semilog plot. While correlation equations predict η, these values have been converted to k to allow comparisons between different model geometries. The experiment numbers on the *x* axis are taken from *Nelson and Ginn* [2011]. As indicated on the chart, low experiment numbers correspond to smaller colloids. The solid horizontal line at y = 1 represents an exact match between correlation equation predictions and experimental observations. The dashed horizontal lines at y = 0.5 and y = 2 represent factor of two differences (i.e., where the correlation equation predication is half as large and twice as large as the experimental observation). RT: *Rajagopalan and Tien* [1976], TE: *Tufenkji and Elimelech* [2004b], LH: *Long and Hilpert* [2009] and *Ma and Johnson* [2009], and NH: *Nelson and Ginn* [2011]. Adapted from *Nelson and Ginn* [2011].

equations (Table 1). *Long and Hilpert* [2009] and *Tufenkji and Elimelech* [2004b] derived their η correlation equation using a single value of water kinematic viscosity at 25°C (0.8×10^{-6} m^2/s) and *Nelson and Ginn* [2011] employ a range of viscosities, but for a range of water temperatures from 5 to 30°C. However, ENPs are often stabilized in a polymer solution to prevent aggregation and settling [e.g., *Hotze et al*., 2010; *Phenrat et al*., 2010b, 2010c; *Kocur et al*., 2013]. These stabilized ENP solutions tend to be much more viscous than water: 2×10^{-3} to 1.3×10^{-2} Pa s [*Krol et al*., 2013], 7×10^{-3} Pa s [*Kocur et al*., 2014], 6×10^{-3} Pa s [*Sakulchaicharoen et al*., 2010], 1.2×10^{-2} to 8.8×10^{-2} Pa s [*Gastone et al*., 2014; *Tosco et al*., 2014b] and upward of 1.942 Pa s [*Quinn et al*., 2005]. Since current η correlation equations were not derived for this range of viscosities, caution should be used in applying existing correlations to engineered nanoparticle subsurface applications. Extending CFT models to include a wider range of viscosities should be considered for future research.

Similarly, η correlation equations, with the exception of *Ma et al*. [2013], were derived for a relatively small range of colloid densities (i.e., 1–1.8 g/cm^3) (Table 1). While viruses, bacteria, and protozoa likely fall within this near-neutrally buoyant range, aggregates of metallic ENPs may have significantly higher densities. No correlation equation has been derived using a mechanistic CFT model that explicitly considers high-density colloids such as aggregates of metallic ENPs. Nor have existing correlation equations been experimentally validated for high-density colloids.

4.3. Mechanistic Simulations: Unfavorable Conditions

Mechanistic force/torque balance simulations that use mean-field DLVO interactions predict zero attachment even under conditions of modest repulsion (e.g., interaction energy > several kT, see Figure 1) between colloids and grain surfaces [*Elimelech and O'Melia*, 1990b]. Yet as discussed earlier, unfavorable conditions are observed in numerous environmental scenarios. As a result, we have until recently lacked mechanistic theory to predict colloid attachment and transport in environmental contexts, and there as yet exists no easily implemented approximating correlation equation for mechanistically based prediction of colloid attachment under unfavorable conditions.

The inability of mean-field force/torque balances to predict colloid attachment in unfavorable conditions has driven the development of semiempirical expressions to predict attachment [*Elimelech*, 1992; *Bai and Tien*, 1996, 1999; *Chang et al*., 2009]. Like the approximating correlation equations for favorable conditions described above, these semiempirical correlations are composed of dimensionless groups of relevant physicochemical parameters that were fit via coefficients and powers. An example correlation from *Elimelech* [1992] is provided:

$$\eta_{unf} = 0.0257 (N_{col})^{1.19} \eta_{fav} \tag{3}$$

where η_{unf} and η_{fav} are the collector efficiencies in the presence and absence of repulsion, respectively, and N_{col} represents the ratio of attractive to repulsive colloid-collector interactions and is defined as follows:

$$N_{col} = \frac{A_{132}}{\varepsilon_0 \varepsilon_r \xi_p \xi_c \kappa^{-1}} \tag{4}$$

where A_{132} is the combined Hamaker constant for the colloid, water, and porous media, ε_o and ε_r are the absolute and relative permittivities in vacuum and water, respectively. The parameters ζ_p and ζ_c are the mean-field potentials of the colloid and collector surfaces, and κ^{-1} is the inverse Debye length. The reported fitted coefficient (0.0257) and power (1.19) correspond to the general set of experiments reported by *Elimelech* [1992]. Please note that throughout this document, we do not use subscripting of η to denote whether it represents favorable versus unfavorable conditions, except in circumstances where direct comparison of these two conditions is required.

Semiempirical correlation coefficients and powers were fit directly to experimental data rather than to mechanistic simulations. They are therefore limited to the experimental conditions from which they were developed, and their relative performance across a larger range of conditions is generally poor when applied outside the experimental conditions under which they were developed. In contrast, the approximating correlation equations for favorable conditions typically show relative errors less than a factor of three (i.e., the error is less than 3X the estimated η) [*Nelson and Ginn*, 2011; *Ma et al*., 2013]. The relatively greater success of correlation equations developed for favorable conditions may reflect their having been fit to mechanistic simulations, which ideally extends their utility to a larger range of conditions, but may also reflect the greater complexity of colloid transport under unfavorable conditions.

The ratio (η_{unf}/η_{fav}) provides a measure of the effect of repulsion and is called the collision or attachment efficiency (α). The value of α should therefore range from 0 to unity. Investigators can obtain α by comparing experiments conducted under unfavorable versus favorable conditions, or as more often is the case, by substituting favorable condition correlation equation predictions of η_{fav}. Whereas the latter approach yields reasonable estimates of α for many conditions, it may yield values of $\alpha > 1$ for less unfavorable (nearly favorable) conditions. This reflects the fact that, as described above, the approximating correlation equations for favorable conditions are just that, approximations of the underlying mechanistic models, and so they may introduce error via the approximation. Furthermore, even the underlying mechanistic models may introduce error if the experimental conditions "violate" assumptions in the underlying mechanistic models (e.g., uniformity, spheroidal colloids, and collectors) as is also true for predictions under favorable conditions.

4.3.1. Secondary Minimum Association

Whereas mean-field mechanistic models do not predict immobilization (attachment) of colloids in the presence of significant repulsion, they do predict the accumulation of colloids in the near-surface fluid domain due to secondary minimum attraction under unfavorable conditions [e.g., *Johnson et al*., 2007a]. The experimentally observed "skimming" behavior of colloids in the near-surface fluid domain under unfavorable conditions [e.g., *Johnson et al*., 2010] is predicted by mean-field mechanistic models, for example, in dense and simple cubic packing structures [e.g., *Johnson et al*., 2007a] and impinging jet systems where flow is directed normal to a planar surface and spreads radially from the flow stagnation axis [*Johnson and Hilpert*, 2013].

The influence of secondary minimum interactions is accounted for in mean-field force/torque models underlying CFT but this has received limited attention. The reason being that these models (often

performed in the Happel unit cell) were usually run under favorable conditions (absence of repulsive barrier yields absence of secondary minimum) but would need to be run under unfavorable conditions in order for the influence of the secondary minimum to be observed. Furthermore, when these models were run under unfavorable conditions, the primary purpose was to demonstrate lack of immobilization (lack of attachment) for significant repulsion [e.g., *Elimelech and O'Melia*, 1990b].

The possibility that experimentally inferred colloid retention at the column scale may include secondary minimum-associated colloids prompted the development of easily adopted approaches to predict potential colloid retention via this mechanism. Foremost among these is the Maxwell approach [*Franchi and O'Melia*, 2003; *Hahn and O'Melia*, 2004; *Shen et al*., 2007; *Tosco et al*., 2009; *Sang et al*., 2013], which determines the kinetic energy distribution among the colloid population from the Maxwell frequency distribution of their velocities. Retained colloids are those with insufficient kinetic energy to escape from the secondary energy minimum into the bulk fluid domain. The Maxwell approach is a simplified version of CFT in that it does not account for fluid flow, collector geometry, or mechanistic force/torque balance, such that the subsequent fate (e.g., exit from the collector) of colloids associated with the surface via secondary minimum interactions is not actually determined.

The utility of the Maxwell approach lies in its relative ease of application relative to a full force/torque balance. It must be stressed that although both the Maxwell or mean-field mechanistic force/torque balance approaches predict accumulation in the secondary energy minima, they predict no colloid attachment to (i.e., immobilization on) surfaces (except for energy barriers less than several kT).

4.3.2. Immobilization

As mentioned above, mean-field mechanistic models do not predict the experimentally observed immobilization of a significant fraction of near-surface colloids [e.g., *Johnson et al*., 2010] on bulk repulsive surfaces. Instead, as stated above, colloids are predicted to skim (spin and translate) outboard of the energy barrier in the near-surface fluid domain. As such, the challenge in prediction of colloid attachment (immobilization) is how to achieve physical contact with the surface when mean-field prediction indicates that it is prevented by the repulsive barrier. A number of strategies have been recently employed to mechanistically predict this immobilization. These strategies can be categorized as (1) macroscopic heterogeneity, (2) implied physical heterogeneity, and (3) representative discrete heterogeneity.

Heterogeneity has, for at least 20 years, been acknowledged as a potential explanation for the discrepancy between mechanistic predictions and experimental observations in environmental (unfavorable) conditions [*Ryan and Elimelech*, 1996]. Since then, research has confirmed the potential role of heterogeneity in colloid retention in environmental conditions. While our understanding of the processes governing colloid-heterogeneity interactions has evolved considerably, there remain a number of questions regarding the role and significance of heterogeneity at macroscopic and microscopic scales as described below.

4.3.2.1. Macroscopic and Implied Physical Heterogeneity

Macroscopic surface heterogeneity (i.e., readily measured surface properties) arises from, for example, the presence of multiple mineral surfaces with different isoelectric points such that some surfaces are positively charged, and some are negatively charged (e.g., iron oxyhydroxides versus silica) at circum-neutral pH. For porous media having macroscopic geochemical heterogeneity, the unfavorable fraction of the surface can be approximated as having $\alpha = 0$, and the favorable fraction of surface can be approximated as having $\alpha = 1$. This approach is successful in that a simple linear combination of the binary α values weighted by the corresponding fractions of favorable versus unfavorable surfaces in the porous media yields reasonable prediction of observed retention in macroscopically heterogeneous media [*Song et al*., 1994; *Johnson et al*., 1996; *Chen et al*., 2001; *Loveland et al*., 2003].

The primary limitation of this approach is that while macroscopic surface heterogeneities are widespread in environmental porous media, there is significant evidence that these heterogeneities may only minimally influence colloid transport in soils. Natural organic matter (NOM) has been shown to sorb strongly to positively charged (i.e., favorable) mineral surfaces such as ferric and aluminum oxyhydroxides and switch their surface charges from positive to negative [*Amirbahman and Olson*, 1993; *Gu et al*., 1995; *Johnson and Logan*, 1996; *Pieper et al*., 1997; *Mosley et al*., 2003; *Mylon et al*., 2004; *Foppen et al*., 2008; *Y. Liu et al*., 2009; *Abudalo et al*., 2010; *D. Wang et al*., 2012]. The sorption of NOM to surfaces that are favorable for colloid attachment

will potentially yield unfavorable attachment conditions. Given the widespread prevalence of NOM throughout environmental media, many macroscopic heterogeneities may be coated by organics that yield unfavorable conditions thereby limiting the relevance of macroscopic heterogeneities in environmental media. A large number of colloid transport studies have demonstrated this NOM "masking effect" in which the presence of organic matter can increase colloid transport [*Amirbahman and Olson*, 1993; *Johnson and Logan*, 1996; *Pieper et al*., 1997; *Mylon et al*., 2004; *Foppen et al*., 2008; *Pelley and Tufenkji*, 2008; *Abudalo et al*., 2010; *Morales et al*., 2011; *Jiang et al*., 2012b; *D. Wang et al*., 2012].

Environmental media coated with NOM cannot be represented by this "patchwise" linear approximation since the entire media would be represented by $\alpha = 0$; whereas significant colloid retention is experimentally observed in such media [*Elimelech and O'Melia*, 1990b; *Li et al*., 2004; *Tong and Johnson*, 2006; *Johnson et al*., 2010]. The discrepancy suggests the presence of microscale to nanoscale heterogeneity (i.e., not readily measurable surface properties) on the bulk repulsive surface, which may allow attachment to occur [e.g., *Elimelech and O'Melia*, 1990b] as described below in section 4.3.2.2.

The inferred presence of microscale to nanoscale heterogeneity on surfaces has spurred the development of a variety of mechanistic approaches to account for nanoscale to microscale physical and chemical heterogeneity. One approach that not only capitalizes on the predicted accumulation of colloids in secondary minima but also provides a mechanism to immobilize a subset of these secondary minimum-associated colloids is herein called the "implied physical heterogeneity approach" [*Torkzaban et al*., 2008]. The approach extends surface friction, which is traditionally considered to act at the primary minimum [e.g., *Johnson et al*., 1971; *Bergendahl and Grasso*, 2000], out to the secondary minimum, which is traditionally considered "non contact" such that the relevant friction in the secondary minimum arises from fluid viscosity [e.g., *Rajagopalan and Tien*, 1976]. Extending surface friction to the secondary minimum replaces the traditionally assumed relatively weak friction from fluid viscosity with stronger surface friction that immobilizes colloids in zones of low fluid drag (e.g., low velocity or recirculation zones). The approach effectively treats the near-surface fluid domain (see Figure 1) as a highly viscous fluid yielding a friction coefficient equal to that of the surfaces in contact. This method is justified on the basis that there can exist roughness, macromolecules, etc. that may effectively extend surface friction to the attractive secondary well [*Johnson et al*., 2009].

The approach is successful in that it identifies zones on the surface where colloids can be immobilized due to drag forces being less than the extended friction force. However, an important limitation of the approach is that it has not been reconciled with existing work that considers secondary minimum interactions as noncontact forces [*Israelachvili*, 2011], and it does not build on the formal approach provided by the previously existing body of work accounting for steric forces associated with water structure, roughness, and macromolecules in the near-surface domain [*Israelachvili*, 2011].

With respect to predictions, the implied physical heterogeneity approach predicts attachment only in zones of low fluid drag [*Torkzaban et al*., 2007, 2008; *Bradford et al*., 2011a]; whereas experiments demonstrate colloid deposition in high fluid drag zones such as forward flow stagnation zones [*Johnson et al*., 2010; *Pazmino et al*., 2014b] under unfavorable conditions. Forward flow stagnation zones are regions where flow impinging normal to the collector surface is converted to tangential flow. Tangential flow is zero on the forward flow stagnation axis that is defined as the center of the impinging flow. Normal flow on this axis decays with decreasing separation distance from the surface to a minimum (taken to be zero) at the forward flow stagnation point on the collector surface. Adjacent to the collector surface outside the forward flow stagnation point, tangential flow and tangential drag force on colloids rapidly increase. As a result, the forward flow stagnation zones are not zones of low fluid drag except at the forward flow stagnation point (identified in Figure 4). The same principle applies to the rear flow stagnation zone and point, where tangential flow converging on the flow stagnation axis is converted to normal flow away from the grain surface. Simulations utilizing implied physical heterogeneity also predict that colloids will immobilize (attach) at long distances (e.g., multiple tens of nm) from the surface, in which case detachment will occur in response to very slight increases in fluid drag [*Pazmino et al*., 2014a]. In contrast, direct observation experiments show that detachment requires fluid velocity perturbations significantly higher than the loading velocity [*Pazmino et al*., 2014a], as further described below.

4.3.2.2. Microscale to Nanoscale Heterogeneity

The existence of microscale to nanoscale heterogeneity (herein called discrete heterogeneity) on bulk repulsive surfaces is inferred from the observed attachment of colloids under unfavorable conditions lacking

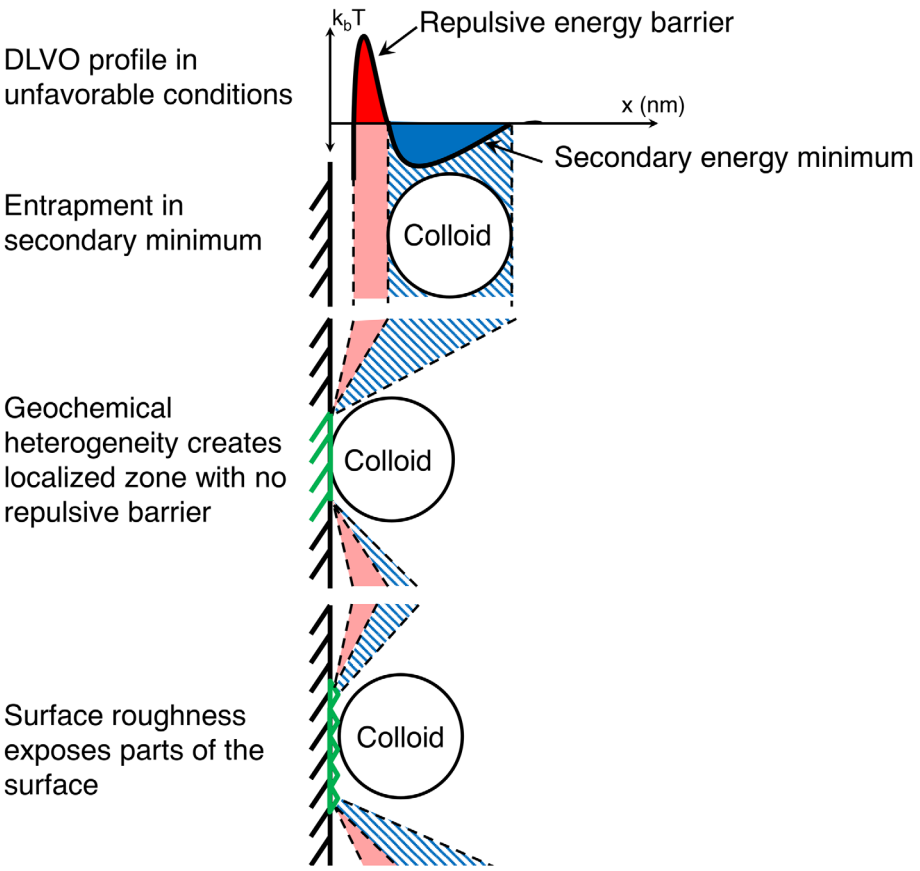

Figure 6. The different attachment/retention interactions that may occur when the colloid is near the collector surface. The representative DLVO profile is an approximation of unfavorable deposition conditions with both an electrostatic repulsive energy barrier (red) and an attractive secondary energy minimum (blue). For ease of interpretation, the size of the primary energy barrier is on the same order as the depth of the secondary minimum but there are scenarios where the primary energy barrier may be much larger than what is pictured. In addition, for ease of interpretation the colloids are depicted as being the same size as the heterodomain features they are interacting with; this is not necessarily the case as the size of these features may range from the microscale to nanoscale while colloids may be up to 10 μm in diameter.

macroscopic heterogeneity. The rationale for this inference is that repulsion experienced by colloids from a bulk like-charged surface may be locally eliminated or reduced by the presence of physical asperities (protrusions associated with roughness) and charge heterogeneity [*Bhattacharjee et al*., 1998; *Hoek and Agarwal*, 2006]. As illustrated in Figure 6, physical asperities reduce repulsion because interaction forces scale directly with radius of curvature [*Israelachvili*, 2011], and the asperity reduces (locally) the radius of curvature associated with colloid-surface interaction. Charge heterogeneity creates local zones of opposite charge (attraction) that scales with the size of these zones, as illustrated in Figure 6.

Whereas macroscopic heterogeneity (e.g., metal oxyhydroxide coatings on silica) may be removed via acid-base cleaning, nanoscale to microscale heterogeneity from roughness and cation substitution in the mineral matrix are not removed, and in fact may be enhanced, by cleaning approaches [*Litton and Olson*, 1993; *Johnson et al*., 1996; *Tong and Johnson*, 2006; *X. Y. Liu et al*., 2009; *DiCarlo et al*., 2010; *Molnar et al*., 2011; *Jiang et al*., 2012a]. The sometimes-invoked assumption that colloid retention on cleaned surfaces must occur via straining (due to presumed absence of heterogeneity) has been discussed [*Johnson et al*., 2011] (see section 5.3 for a discussion on successes and opportunities in straining research).

4.3.2.3. Representative Discrete Heterogeneity

Another approach to achieve physical contact between the colloid and the collector surface in spite of significant repulsion between the bulk surfaces is to replace the mean-field colloid-collector interactions with interactions that explicitly recognize the existence of discrete nanoscale to microscale physical and chemical heterogeneity on the collector (or potentially colloid) surface where colloid-collector repulsion is locally reduced or eliminated (herein referred to as heterodomains) [e.g., *Duffadar and Davis*, 2007; *Bendersky and*

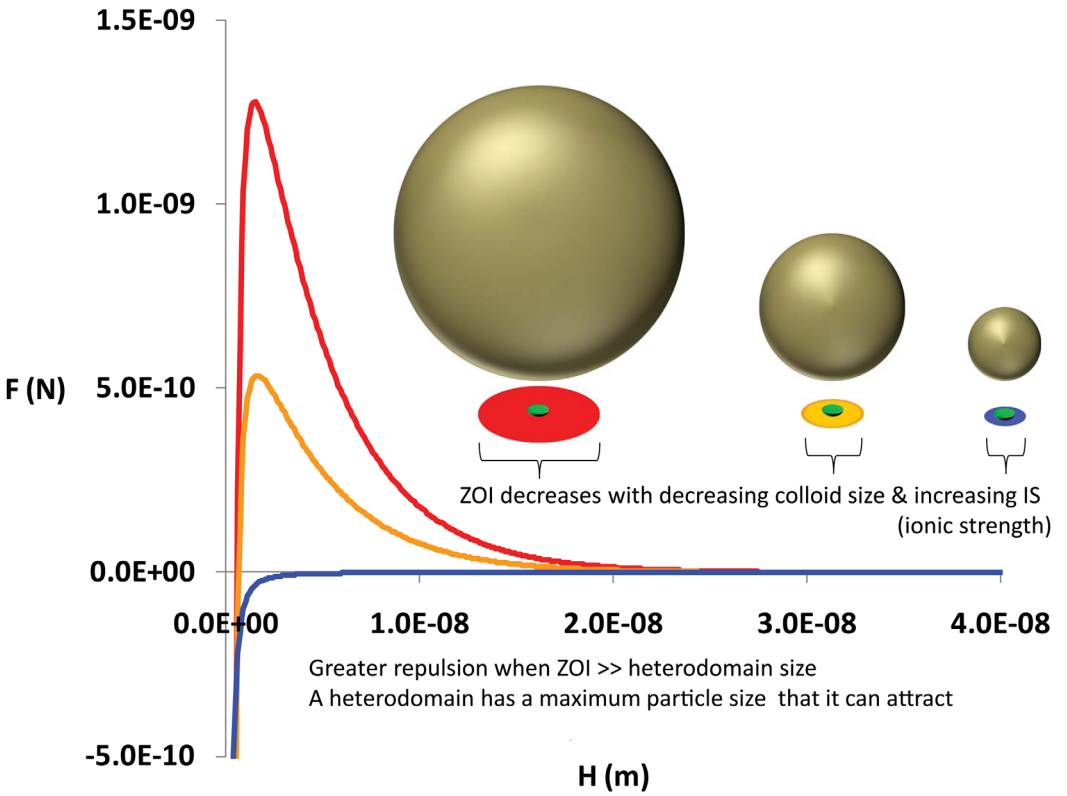

Figure 7. Colloidal force profiles as a function of colloid-collector separation distance (H) for 1.95, 1.1, and 0.25 μm colloids. The height of the energy barrier corresponds to the size of the colloid. The largest colloid—1.95 μm—has the largest energy barrier, the medium colloid—1.1 μm—has the smaller energy barrier, and the smallest colloid—0.25 μm—has no energy barrier. The projected colored circle represents the ZOI, the inner circle represents an 80 nm radius heterodomain. The ZOI color corresponds to the force profile. The repulsive force is greatest for the lowest ZOI coverage by heterodomain(s). Varied heterodomain size relative to ZOI would have the same effect, as would varied IS for a given colloid and heterodomain size (increased IS yields decreased radius of ZOI). Adapted from *Pazmino et al.* [2014b].

Davis, 2011; *Shen et al.*, 2013]. Heterodomains differ from the previously discussed macroscopic surface heterogeneities as they are not readily measurable surface properties. These heterodomains, illustrated in Figure 6, can bring colloids into physical (e.g., primary minimum) contact with the surface, where surface friction is more generally accepted to be applicable [*Johnson et al.*, 1971; *Bergendahl and Grasso*, 2000], as described in detail in *Pazmino et al.* [2014b].

Discrete heterogeneity on a collector surface yields different net interactions (attractive versus repulsive) for different colloid sizes [*Pazmino et al.*, 2014b]. Due to curvature of the colloid surface and the rapid decay of colloid-collector interactions with increasing separation distance, the zone of significant colloid-collector interaction (ZOI) is a fraction of the projected area of the colloid. The ZOI area decreases with increasing ionic strength [*Duffadar et al.*, 2009; *Pazmino et al.*, 2014b]. The net colloid-collector interaction is determined by the combination of attractive and repulsive interactions across the ZOI, which is determined by the fraction of the ZOI that is occupied by heterodomain(s) [*Pazmino et al.*, 2014b, 2014a]. Hence, the net colloid-collector interaction (attractive versus repulsive) depends on the interplay of colloid size, heterodomain size, and ionic strength, as shown in Figure 7 adapted from *Pazmino et al.* [2014b]. In the figure, a given heterodomain size and ionic strength condition yield a net interaction force that depends directly on colloid size, as shown by the force curves in Figure 7, where blue yields no repulsion and red yields the largest repulsion. This occurs because the radius of the ZOI (R_{ZOI}) increases with colloid size, as shown by spheres in Figure 7. The fractional coverage (of ZOI) by heterodomains decreases as the colloid size increases relative to a given heterodomain size, leading to net attractive interaction at all separation distances for the smallest (blue) colloid, and net strong repulsion at intermediate distances (repulsive barrier) for the largest (red) colloid.

Successes of the discrete heterogeneity approach, referring to the incorporation of nanoscale zones of attraction in the DLVO interaction, include (i) colloid attachment on the open surface and (ii) wedging in

grain-to-grain contacts for larger colloids both emerge from the force/torque simulations that incorporate discrete nanoscale heterogeneity [*Ma et al.*, 2011]. Quantitative prediction of experimentally observed attachment of colloids on silica emerges from incorporation of representative discrete nanoscale heterogeneity into mechanistic force/torque balance [*Pazmino et al.*, 2014b]. The approach also predicts the experimentally observed detachment of colloids (i.e., a fractional release of the attached population) in response to perturbations in ionic strength or fluid velocity. Notably, both the observed and simulated colloid detachment in response to fluid velocity perturbations required perturbations to be significantly greater than the loading velocity. This resulted from colloid immobilization (attachment) in the primary minimum where van der Waals attraction generated strong adhesion [*Pazmino et al.*, 2014a]. This is an important contrast to the implied physical heterogeneity approach, which immobilizes colloids multiple tens of nm from the surface in the secondary minimum, as described above.

The discrete heterogeneity approach represents (to the knowledge of the authors) the first report of an ability to predict attachment quantitatively and detachment (from physical contact) qualitatively, using the same set of fundamental parameters in force/torque simulations for both predictions [*Pazmino et al.*, 2014b, 2014a]. However, there are still challenges to be addressed in the discrete heterogeneity approach; to date discrete heterogeneity cannot be independently measured in ways directly relevant to colloid-surface interaction. For example, zeta potentials are too insensitive to reflect nanoscale to microscale heterogeneity [*Elimelech et al.*, 2000], atomic force microscopy has limited resolution [*Shellenberger and Logan*, 2002; *Taboada-Serrano et al.*, 2005; *Drelich and Wang*, 2011], and surface spectroscopic techniques do not yield information directly applicable to colloid-surface interaction. Whereas there are many opportunities to explore application of the above techniques, at present the discrete heterogeneity approach requires empirical determination of a representative heterogeneity on surfaces. Currently, the published literature reflects representative discrete heterogeneity on silica surfaces only [*Pazmino et al.*, 2014b]. Although silica is an important primary target surface (i.e., the vast majority of colloid transport experiments utilize silica porous media), the approach needs to be extended to other surfaces and conditions to test its general applicability.

The outcomes that emerge from the force/torque simulations utilizing discrete heterogeneity match experimental observations across an array of colloid sizes, fluid velocities, and ionic strength values. The discrete heterogeneity approach, by developing a representative heterogeneity for a surface, provides a mechanism to represent differences in heterogeneity among different mineral types and different pH conditions. These changes are not captured by mean-field parameters such as bulk surface zeta potential [*Elimelech et al.*, 2000].

Representative discrete heterogeneity provides a potential platform for mechanistic representation of blocking or ripening, both of which begin with a limited number of colloid attachment sites. Heterodomains (representative heterogeneity) would serve as these initial attachment sites, with subsequent decrease (blocking) or increase (ripening) in the number of attachment sites with increased colloid attachment, depending on whether colloid-colloid interactions are repulsive or attractive, respectively.

As explained above, for a given heterogeneous surface, the net interaction (attractive versus repulsive) depends on colloid size and surface properties. As such, slight differences in colloid size and/or surface properties may generate effective heterogeneity in "stickiness" among the colloid population. Demonstrating this effect may yield a mechanistic explanation for the apparent heterogeneity in retention rate coefficients among apparently uniform populations, which is thought to drive the observed nonlog linear profiles of retained colloids observed under unfavorable conditions [*Albinger et al.*, 1994; *Harvey et al.*, 1995; *Hendry et al.*, 1997; *Baygents et al.*, 1998; *Simoni et al.*, 1998; *Bolster et al.*, 1999; *Schijven et al.*, 1999; *Bolster et al.*, 2000; *Li et al.*, 2004; *Tufenkji and Elimelech*, 2004a; *Tufenkji et al.*, 2004; *Tufenkji and Elimelech*, 2005a,b; *Tong and Johnson*, 2007; *Liang et al.*, 2013; *D. Wang et al.*, 2014].

5. Upscaling From Pore to Continuum Scale

The parameter η describes the efficiency of colloid delivery to the surface (favorable conditions) or the near-surface fluid domain (unfavorable conditions) at the pore scale. Its implementation into continuum-scale models (upscaling) is performed under the simple assumption that the control volume considered in the continuum model is represented by a collection of identical pore-scale collectors comprising the same volume and having the same porosity as the control volume [*Logan et al.*, 1995; *Nelson and Ginn*, 2011;

Johnson and Hilpert, 2013]. Under this assumption, the equation expressing η as a rate constant (k) for the Happel sphere-in-cell geometry is

$$k = -\frac{3(1-\theta)^{1/3}}{2d_c}\ln(1-\eta)v \tag{5}$$

where d_c is the average collector diameter, v is velocity, and θ is porosity. The functional form of k is not the same for all η correlations, it is a function of the conceptual model employed; the hemisphere-in-cell [*Ma et al*., 2009] and constricted tube [*Paraskeva et al*., 1991] geometries have different relationships for k.

5.1. Opportunities in Secondary Minimum Interactions

The k-η relationship (equation (5)) describes colloid delivery to the near-surface fluid, which under favorable conditions is practically equivalent to attachment. Under unfavorable conditions, the fate of near-surface colloids is less straightforward. While a fraction of near-surface (secondary minimum-associated) colloids may attach in response to local attraction emanating from heterogeneity, the complement may translate across the surface until they return to the bulk fluid.

While equation (5) is specifically for porous media, it is worthwhile mentioning that it is possible to link the observed deposition rates in impinging jet systems to mechanistically predicted collector efficiencies in pore-scale models [*Pazmino et al*., 2014b]. In contrast, comparison of k between these systems requires relating the flow fields between them, and this likely requires incorporating discrete heterogeneity representations into Happel sphere-in-cell geometry.

Additionally, the presence of secondary minima in unfavorable conditions may yield an indefinite residence time of colloids in the near-surface fluid domain. Secondary minimum interactions will influence the average velocity of the colloid population to an extent depending on η as well as the depth of the secondary minimum, since velocity in the near-surface fluid is far lower than the average pore water velocity. Furthermore, secondary minimum-associated colloids may be effectively retained in the control volume (e.g., packed column in experiments) if elution does not occur prior to termination of the observation. Currently, there exists no relationship to quantitatively account for the influence of secondary minimum association on the concentration and timing of colloid elution. Developing such a relationship will require identifying the frequency with which colloids transfer between the bulk and near-surface fluid domains, as discussed below.

5.2. Opportunities in the Role of Topology

The fact that mechanistic simulations and upscaling provide good prediction at the continuum scale under favorable conditions suggests that mixing of near surface and bulk fluid must occur between subsequent collectors (grains) in the control volume [*Johnson and Hilpert*, 2013]. This is inferred on the basis that under favorable conditions in the absence of mixing, the near-surface fluid would become depleted of colloids, increasingly so with each subsequent collector, yielding decreasing k with increased transport distance [*Johnson and Hilpert*, 2013]. The log linear profiles of retained colloids that are typically observed under favorable conditions indicate that k remains constant with transport distance. Hence, mixing of near-surface and bulk fluid between subsequent collectors is reasonably inferred. In contrast, absence of mixing between collectors under unfavorable conditions would yield increasing excess of colloids in the near-surface fluid (via secondary minimum attraction), increasingly so with each subsequent collector, such that k would increase with increased transport distance [*Johnson and Hilpert*, 2013]. Whereas k does vary with transport distance under unfavorable conditions (e.g., hyperexponential and nonmonotonic profiles of retained colloids), it does not strictly increase with transport distance.

Nevertheless, the association of distance-varying k and extended tailing with unfavorable conditions suggests a relationship with colloid accumulation in the near surface under unfavorable conditions. *Johnson and Hilpert* [2013] speculated that incomplete mixing of bulk and near-surface fluid between subsequent grains may at least partially drive the observed extended tailing (and nonlog linear retained profiles) under unfavorable conditions. This, in addition to the above-described potential influence of discrete heterogeneity on amplifying heterogeneity among the colloid population, provide potent mechanisms to potentially explain these critical phenomena observed under unfavorable conditions.

Since colloid transfer from the bulk to the near-surface fluid occurs at forward flow stagnation points, and colloid transfer from the near-surface to the bulk fluid occurs largely at rear flow stagnation zones (less so

for Brownian-dominated colloids) [*Johnson and Hilpert*, 2013], the degree of mixing between collectors is a topological issue that depends on the alignment of the local flow field with the grain-to-grain contacts [*Johnson and Hilpert*, 2013]. Whereas experimental evidence that topology (degree of alignment of flow field and grain-to-grain contacts) governs retention at the continuum scale has been provided [*Johnson and Hilpert*, 2013], the opportunity exists for many additional studies to explore experimentally and theoretically the relationship of observed profiles of retained colloids to topology (as governed by packing structure). Such information can guide development of upscaling techniques for nonuniform media.

An additional mechanism potentially driving extended tailing under unfavorable conditions is provided by recent pore-scale modeling studies that suggest the possibility of indefinite colloid retention under unfavorable conditions in low-flow/recirculation zones associated with grain-grain contacts (discussed in section 4.1.1) [*Cardenas*, 2008; *Torkzaban et al*., 2008; *X. Q. Li et al*., 2010; *Z. Li et al*., 2010; *Li et al*., 2012]. Temporary hydraulic retention of colloids in these regions could drive long-term tailing as colloids slowly exit the immobile zones via Brownian motion (Molnar et al., submitted manuscript, 2015). More generally, solute transport demonstrates diffusive mass transfer between advective and nonadvective zones [e.g., *Haggerty and Gorelick*, 1995; *Haggerty et al*., 2000; *Berkowitz et al*., 2006; *Scheibe et al*., 2013]. There is opportunity to distinguish the influence of near-surface residence from the influence of mass transfer between bulk advective versus nonadvective zones in colloid transport. This is particularly true for nanoparticles, for which it is not yet demonstrated whether their diffusivity will allow them to enter bulk nonadvective domains and whether this entry would require skimming along the secondary minima (as required by micron-sized colloids) or direct diffusive mass transfer that could occur in both favorable and unfavorable conditions.

5.3. Opportunities in Straining

Another critical aspect of nonuniformity of porous media is the expectation that a fraction of the pore throats will be too small for colloids to pass (i.e., straining) [*Bradford et al*., 2002, 2003, 2004; *Tufenkji et al*., 2004; *Bradford et al*., 2006a, 2006b; *Shen et al*., 2008; *Bradford et al*., 2013]. The process of straining is not included in CFT because, while both filtration and straining lead to attachment, straining has no dependence on diffusion, sedimentation, and limited dependence on colloid-surface interaction. Early work on straining [*Sakthivadivel*, 1966, 1969; *Herzig et al*., 1970; *McDowell-Boyer et al*., 1986] identified the ratio of mean particle:collector diameter (d_p/d_c) as the critical factor in determining straining. These early works presented a range of critical d_p/d_c ratios required for straining, such as $>5\%$ [*Sakthivadivel*, 1966, 1969] and $>18\%$ [*Matthess et al*., 1985]. These large critical ratios suggest that only the largest (i.e., $d_p \sim 10$ μm) colloids in fine textured soils would be strained. However, there has recently been a large volume of research published inferring (see section 3 for a discussion on the limitations of inferred transport behavior) colloid straining as a significant removal mechanism for a wide range of colloid and collector sizes [*Bradford et al*., 2002, 2003, 2004; *Tufenkji et al*., 2004; *Bradford et al*., 2005; *Foppen et al*., 2005; *Bradford et al*., 2006a, 2006b; *S. Xu et al*., 2006; *Gaillard et al*., 2007; *Shen et al*., 2008; *Xu et al*., 2008; *Xu and Saiers*, 2009; *Chowdhury et al*., 2011; *Porubcan and Xu*, 2011; *Sagee et al*., 2012; *Bradford et al*., 2013; *Du et al*., 2013; *Raychoudhury et al*., 2014]. These studies have inferred that d_p/d_c ratios can be much lower than originally reported (as low as 0.01%) [*Bradford et al*., 2002, 2003, 2004; *W. Xu et al*., 2006; *Shen et al*., 2008; *Xu et al*., 2008; *Tosco and Sethi*, 2010; *Raychoudhury et al*., 2014]. In addition, a number of studies have suggested that straining is not strictly a function of pore throat and colloid size by suggesting that flow velocity [*Bradford et al*., 2006b; *Du et al*., 2013], input concentration [*Bradford and Bettahar*, 2006], ionic strength [*Shen et al*., 2008], and colloid shape [*Xu et al*., 2008] can influence straining behavior. However, many of these studies base their evidence for straining on a priori assumptions that may not be correct (e.g., that acid washed sand possesses no macroscopic surface impurities ergo straining is predominant) [*Johnson et al*., 2011]. These a priori assumptions have led to, for instance, a number of studies suggesting that even nanosized colloids (with d_p/d_c ratios orders of magnitude lower than suggested in the early literature) can be strained out of solution [*Tosco and Sethi*, 2010; *Sagee et al*., 2012; *Raychoudhury et al*., 2014].

Many of the above investigators relate straining to wedging; however, wedging is a mode of filtration for larger colloids, whereas straining is entrapment in pore throats too small to pass. Wedging is a mode of attachment (filtration) that involves mass transfer from the bulk fluid to the near-surface fluid and eventual contact with two surfaces simultaneously in order to create the adhesive resisting torque that is needed to arrest larger colloids which experience a large drag torque [*Ma et al*., 2011]. Thus, wedged colloids can be much smaller than the pore throats through which they pass [*Johnson et al*., 2010], and wedging is subject to the same force/

torque balance governing colloid attachment to the open surface [*Johnson et al*., 2007a; *Ma et al*., 2011]. In contrast, straining is purely a matter of colloid size being larger than the pore throat, and as such does not concern the mass transfer of colloids from the bulk fluid to the near-surface fluid domain. Instead, straining is a process that cannot be investigated at the single pore scale and instead requires investigation at the assemblage scale where pore throat size distribution can be determined and compared to colloid size distribution.

While the models developed to incorporate straining at the continuum-scale can accurately reproduce colloid retention behavior when fit to experimental data [*Bradford et al*., 2003, 2004; *S. Xu et al*., 2006; *Flury and Qiu*, 2008; *Shen et al*., 2008], they are subject to the same limitations of inferred mechanisms discussed in section 3 and elsewhere in the literature [*Johnson et al*., 2011]. Developing mechanistic methods to predict colloid straining will require an understanding of the pore throat distributions and flow fields. Pore-scale visualization methods such as micromodels and X-ray computed tomography (XCT) are uniquely suited to this purpose.

5.4. Opportunities in Imaging and X-Ray Computed Microtomography

Flow and transport within porous media are governed by the pore size distribution and the topology; i.e., the way in which pores of different sizes are connected [*Vogel and Roth*, 2001]. Thus, while micromodels, Happel spheres, cubic packings, etc. are useful for studying fundamental colloid transport processes and mechanisms, the idealized or simple pore structures do not represent environmental media. Over the past two decades or so, X-ray computed tomography (XCT) has become a relatively standard approach for extracting grain and pore-scale features of unconsolidated porous media (see recent review by *Wildenschild and Sheppard* [2013]) due to its ability to "see inside" of three-dimensional opaque materials. XCT is a nondestructive, nonintrusive technique for acquiring 3-D data sets where the fundamental unit, the volume element (voxel), has a value that represents the average X-ray absorption of the material within the voxel. This X-ray absorption value is a function of density, atomic number, and the energy of incident X-rays. In this way, it is possible to differentiate between different materials. Therefore, the primary information is simply the voxel gray value (mass linear attenuation, which roughly corresponds to absorbance for SXCMT and CT# for conventional XCT). The major advantage of microtomography over conventional 2-D methods (e.g., thin sections, microscopy) is the level of quantitative information that can be derived from a full 3-D property map.

While the most common use of XCT in porous media characterization is the segmentation of the volume into solid and void space (which has come to mean the identification of discrete materials in an image; e.g., the binarization of an image into solid and void), XCT can be used to separate and identify more than two phases. Figure 8 (left) is a vertical cross section from a raw XCT image data set of a partially water-drained column packed with two types of glass beads (75% of the beads (by mass) contained some lead; the other 25% did not have any lead). The presence of lead increases the X-ray absorption of the voxels within those glass beads and makes them distinguishable from the glass beads without lead (note: the voxels with lead show up brighter due to the higher absorption values) and from the water. Figure 8 (right) is the identical cross section after the phases have been segmented; i.e., each voxel has been uniquely identified as glass bead with lead (white); glass bead without lead (light gray); water (dark gray); and air (black).

A significant amount of research has gone into quantifying the geometrical and topological properties from XCT data sets and relating those to flow and transport processes [*Vogel and Roth*, 2001; *Herring et al*., 2015] as well as extracting physically representative pore network structures, i.e., a direct mapping of the pore bodies, throats, and connectivity [*Lindquist et al*., 1996; *Bhattad et al*., 2011]. Two specific items to note here: (1) the topological properties of the pore space will have a strong influence on the flow and transport, thus impacting the spatial distribution of colloids as well as their trajectories toward and around collector surfaces and (2) the direct mapping of the pore structure (e.g., pore body and throat sizes as well as connectivity) provides quantitative data that can be used to determine whether or not certain colloid transport mechanisms (e.g., straining, discussed in section 5.3) might be relevant.

There has been some pore-scale visualization work on straining in both saturated and unsaturated conditions [*Crist et al*., 2004; *Auset and Keller*, 2006; *Bradford et al*., 2006b; *Han et al*., 2006; *Gaillard et al*., 2007]. However, straining studies have yet to fully incorporate the rich, quantitative data that can be extracted from these methods such as coupling real pore throat distributions with FEM/LBM modeling of the flow field (discussed in section 5.4). The type of quantitative data relevant to straining that can be obtained from XCT can be demonstrated using one of the data sets found in Molnar et al. (The impact of immobile zones on the transport and retention of nanoparticles in porous media, submitted to Water Resources

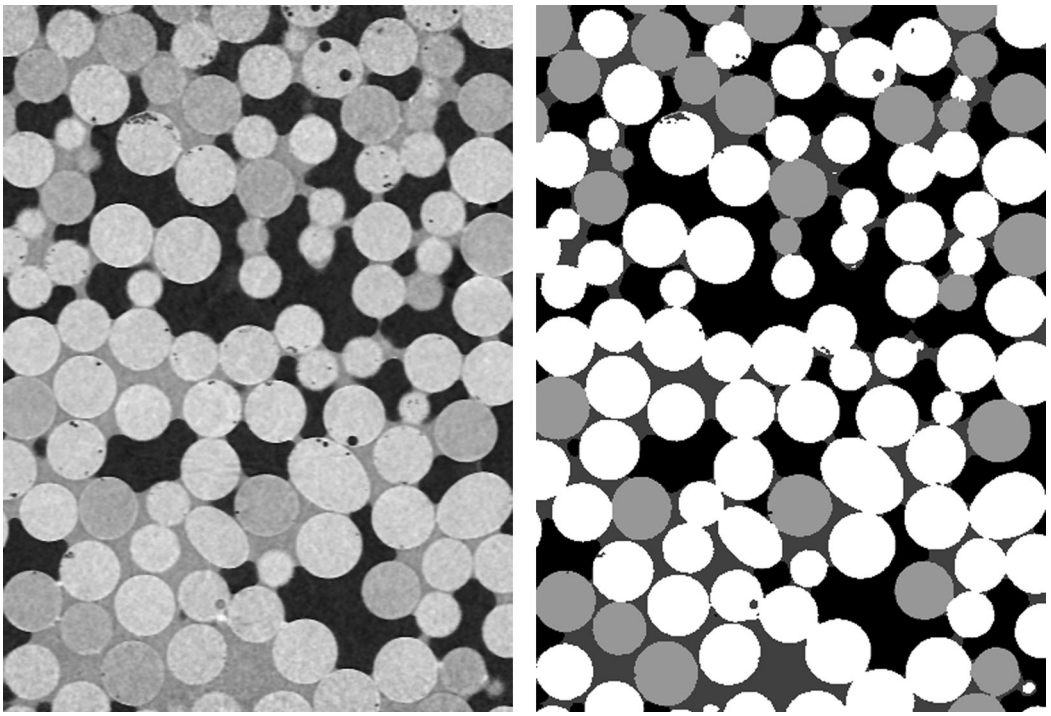

Figure 8. Fractionally wet unsaturated glass bead pack; (left) gray scale XCT cross section; (right) segmented cross section where the white represents glass beads containing some lead; light gray: glass beads without lead; dark gray: water; and black: air. Imaged at 10.08 μm/voxel. Dimensions: 5.24 mm (vertical) $\times$ 3.78 mm (horizontal).

Research, 2015). In a domain of 3.4 $\times$ 3.4 $\times$ 4.4 mm^3 imaged at a resolution of 9.87 μm/voxel, the methods described in *Thompson et al*. [2006] and *Bhattad et al*. [2011] were used to determine that there were 616 sand grains and the pore network structure consisted of 3422 unique pore bodies and 17,160 pore throats. The average size (and range) of pore bodies and throats were 62.4 (10.5–203) μm and 40.6 (9.87–156) μm, respectively. The sizes listed here are the pore and throat inscribed radii, which are defined as the radius of the largest spheres (pores) and circles (throats) that can be drawn within the identified geometries. In addition, the average pore coordination number was 5.1 with a range of 1–33 pore connections per pore.

The richness of the XCT data sets and the ability to resolve the pore space, combined with increases in computing power allows for the direct flow modeling at the pore scale in XCT-obtained domains of real pore networks using Finite Element Modeling (FEM), LBM, etc. In particular, the unstructured nature of the FEM allows one to capture the discontinuous and complex nature of the solid/void interface, highly relevant for capturing the near-surface flow field (within nm if necessary), low-flow/recirculating regions and stagnation points. While these simulation approaches are now at the point where detailed hydrodynamics and bulk flow properties (e.g., permeability) are representative, there are still challenges to obtaining representative bulk transport properties (e.g., breakthrough curves) due to the complex, time scale-dependent nature of the transport processes (e.g., diffusion (Brownian motion), surface-particle interactions, and gravity) and the number of particles that need to be simulated (thousands if not tens or hundreds of thousands). Nevertheless, the increasing sophistication of pore-level hydrodynamic modeling is providing critical insights into colloid transport through and around complex structures [*X. Q. Li et al*., 2010; *Z. Li et al*., 2010; *Li et al*., 2012].

XCT has been successfully used to examine some pore-scale colloid transport details, in particular the spatial location of retained colloids. *Gaillard et al*. [2007] and *Chen et al*. [2008] demonstrated the ability to identify the distribution of micrometer-sized colloids (of high X-ray attenuation) in a sandstone and *Iltis et al*. [2011] mapped the distribution of biofilm in porous media using silver microspheres. Both of these studies utilized micron-sized colloids and, due to their material properties, had high X-ray attenuation coefficients enabling relatively straightforward identification within the systems. *Molnar et al*.

[2014] developed a method that used absorption-edge XCT to extract silver nanoparticle concentrations within individual pores in static and quasi-dynamic (i.e., transport) systems. This approach was then used to assess how relatively immobile (e.g., low velocity) pore space regions near grain-grain contacts could yield deviations between experimentally observed and CFT-predicted retention rates (Molnar et al., submitted manuscript, 2015). While the large amount of spatial data of μm-scale nAg concentrations provides powerful statistical measures of the nAg distributions within the pore space, limitations due to X-ray diffraction across the grain/void interface prevents concentration measurements close to grain surfaces (termed "shadow zone" in *Molnar et al*. [2014] which, in the system studied, was $\sim$18 μm). The development and application of techniques for eliminating this shadow zone will allow for better estimates of near-surface concentrations and gradients and potentially of the impact of surface heterogeneities.

XCT has also been applied to extract granular properties such as particle size, shape, and angularity as well as geomechanically relevant structural properties such as grain-grain contacts (see review by *Moreno-Atanasio et al*. [2010]). As mentioned above, the ability to separate the system into void and solid phases allows for detailed hydrodynamic simulations that can be used to better understand the particle trajectories and proximity to the collector surface, locations of straining and wedging.

However, several factors currently limit the use of XCT for fundamental colloid transport studies including the spatial resolution, sample sizes below that necessary to obtain representative properties, and image contrast. The true spatial resolution of a CT instrument also depends on the sharpness of the imagery [*Ketcham and Carlson*, 2001; *Wildenschild et al*., 2002]. The spatial resolution of most XCT systems limits the ability to capture small structural/surface features (or heterogeneities) that can influence colloid-surface interactions and retention. While increases in the spatial resolution are possible through the use of higher-resolution XCT systems or other imaging techniques (e.g., SEM, thin sections), the quantitative details extracted may not be representative of the bulk sample and, if not collected directly with (or concurrently with) the XCT data, need to be mapped back to the image data [e.g., *Golab et al*., 2012]. Quantitative delineation of the mineral phases, which strongly influence the spatial distribution of favorable/unfavorable attachment sites depends on the X-ray attenuation properties of the minerals (as well as the spatial resolution). Fluid phase separation using doping agents is a common approach [e.g., *Al-Raoush and Willson*, 2005; *Schnaar and Brusseau*, 2005; *Prodanović et al*., 2007; *Porter and Wildenschild*, 2010; *Porter et al*., 2010]; however, much less work has been done on the spatial distribution of mineralogy. See the recent review paper by *Kyle and Ketcham* [2015] that discusses the approaches and limitations to mineral identification and quantification (while they focus primarily on ores, this is a very good overview). An interesting but intensive approach that uses the 2-D-3-D registration of SEM and XCT was developed by a group at the Australian National University [*Golab et al*., 2012; *Sheppard et al*., 2014]. In addition to providing additional submicron level structural details, this technique allows for the coupling of mineralogy (from the SEM) with the XCT data.

A major limitation of an XCT-based imaging approach is the inability to identify coatings/films on solid surfaces that are thinner than several microns and/or have X-ray absorption values that are similar to the grain. This may limit or prevent direct mapping of transport-relevant heterogeneities onto the grain surface, resulting in the need for indirect "mapping" of chemical heterogeneities.

While XCT is allowing for more detailed pore-level and grain-level characterization and the increases in computing power are pushing the simulation details to higher levels, there are still a number challenges/opportunities that can have a major impact on our understanding of colloid transport such as developing robust techniques to, directly or indirectly, extract and map submicron heterogeneities. In addition, improvements in the spatial resolution are needed to ensure that the pore structure/topology and mineralogy distribution is representatively captured in complex, environmental media. These features, when combined with improved techniques in quantitatively mapping colloid concentrations and in the modeling of complex pore-level hydrodynamics and colloid transport mechanisms (such as mineral specific surface-particle forces), will greatly improve our understanding of colloid transport in natural systems.

6. Conclusions

In this paper, we have presented the many advances in our understanding of colloid transport in porous media in the past 25 years. There is an increasingly sophisticated understanding of the applications of

employing short-range DLVO forces to describe colloid transport through porous media. The favorable and unfavorable deposition conditions that arise from DLVO interactions yield significantly different experimental transport and retention behaviors. However, the experimentally observed behaviors often differ from mean-field DLVO predictions; this is especially true for colloid retention in unfavorable conditions. A large amount of recent research has successfully elucidated a number of causes for these discrepancies such as grain and colloid-heterogeneity, secondary minimum interactions, and site blocking. A large portion of our understanding of these mechanisms has arisen from column-scale transport experiments coupled with continuum-scale models that, by fitting various rate parameters, can successfully describe experimental transport behavior.

There have also been significant advances in colloid filtration theory, a two-component method for predicting the colloid attachment rate parameter, k. The first component, a detailed mechanistic model of colloid transport and attachment onto a unit-cell collector by way of a force-torque balance, has become increasingly advanced with modern computational power. Particularly, successes have occurred with describing Brownian motion and moving toward a mechanistic approach to predicting colloid retention (and detachment) in unfavorable conditions, the prevailing condition in the environment. The second component of CFT, correlation equations that summarize the results of the detailed mechanistic models have also improved significantly and can, for the most part, accurately predict retention of larger colloids in favorable conditions.

Despite the large number of advances and successes, there remain many gaps in our current understanding, limiting our ability to predict colloid transport in a range of porous media systems. Many of the mechanisms invoked to describe discrepancies between DLVO-predicted colloid transport behavior and experimental observations arise from the use of fitted kinetic retention parameters in continuum-scale models. However, fitted parameters can only infer mechanisms, not prove those mechanisms are responsible for the fit. As such, many of the mechanisms attributed to colloid transport and retention behavior remain inferred. There are substantial opportunities available to develop mechanistic approaches to validating, and predicting, the influence of these mechanisms. Relatively new tools, such as XCT, will prove invaluable in this as they are capable of quantitatively extracting pore and grain details (i.e., pore body/throat sizes and distributions, void topologies and grain shapes, and mineralogy) as well as directly observing colloid distribution in the pore space and coupling with high-fidelity simulations of the flow fields.

Mechanistic CFT models and their respective correlation equations still struggle to predict nanoparticle transport and retention. It is still unclear if the unit-cell CFT approach is valid for highly diffusive materials. While fitting the α parameter effectively overcomes the discrepancy between theoretical predictions and experimental observations for nanoparticle transport, true prediction of nanoparticle transport and retention will require accurate mechanistic models and correlation equations. Likewise, existing correlation equations are only derived for a limited range of environmental conditions that are not applicable to many nanoparticle scenarios such as a viscous solution of nano-zero-valent iron stabilized with polymer.

Finally, while mechanistic models are now able to quantitatively predict colloid attachment and qualitatively predict detachment under unfavorable conditions, these are limited to idealized systems involving carboxylate modified polystyrene latex microspheres on silica (which reflect the vast majority of existing colloid transport experiments). Even in these simple systems, the need to account for influences such as roughness in addition to charge heterogeneity is well noted and warrants further research. Furthermore, experiments looking at nonsilica surfaces and nonideal colloids, as well as size-distributed porous media present major opportunities to address environmental conditions in a more comprehensive manner.

Together, the above listed challenges represent a significant opportunity for advances that will undoubtedly lead to more informed decisions and design regarding colloids in the environment for the protection of human and ecological health.

Appendix A

Overview of the geometries and equations of select CFT models (Tables A1–A6).

Table A1. Overview of the Geometries and Equations Governing Selected Mechanistic Happel Sphere Models

Model Name	*Rajagopalan and Tien [1976]*	*Tufenkji and Elimelech [2004]*	*Nelson and Ginn [2011]*
Model type	Lagrangian[a]	Eulerian	Lagrangian
Model Geometry[f]		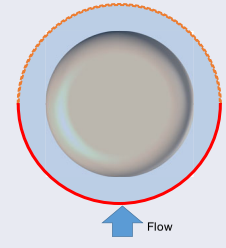	
Particle boundary conditions		Entry boundary(Lagrangian only)[e] Constant concentration (C = C_o) (Eulerian only) Free exit boundary (Lagrangian only) Constant Concentration (C = C_o) (Eulerian only) Perfect sink (C = 0)	
Fluid flow equation		Stokes (creeping) flow[b]: $\nabla p = \mu \nabla^2 v$ Continuity: $\nabla v = 0$	
Governing colloid transport equation[c]	$F_G + F_{LO} + F_{DL} + F_D + F_I = 0$ $t_G + t_{LO} + t_{DL} + t_D + t_I = 0$	$\nabla(uC) = \nabla(D'_{BM} \cdot \nabla C) - \nabla\left(\frac{D'_{BM} \cdot F}{k_B T}\right) C$	$m\frac{du}{dt} = F_H + F_e + F_B$
η correlation[d]	$\eta \approx \gamma^2[4A_s^{1/3}N_{Pe}^{-2/3} + A_s N_{LO}^{1/8} N_R^{15/8} +$ $0.00338 A_s N_G^{1.2} N_R^{-0.4}]$	$\eta \approx 2.4 A_s^{1/3} N_R^{-0.081} N_{Pe}^{-0.715} N_{vdW}^{0.052} +$ $0.55 A_s N_R^{1.675} N_A^{0.125} +$ $0.22 N_R^{-0.24} N_G^{1.11} N_{vdW}^{0.053}$	$\eta \approx \gamma^2[2.4 A_s^{\frac{1}{3}} \left(\frac{N_{Pe}}{N_{Pe}+16}\right)^{0.75} N_{Pe}^{-0.68} N_{LO}^{0.015} N_{Gi}^{0.8} +$ $A_s N_{LO}^{1/8} N_R^{15/8} + 0.7\left(\frac{N_{Gi}}{N_{Gi}+0.9}\right) N_G N_R^{-0.05}]$
Kinetic retention rate equation	$k = \frac{3}{2}\frac{(1-n)^{1/3}U}{d_c n}\eta\alpha$	$k = \frac{3}{2}\frac{(1-n)U}{d_c n}\eta\alpha$	$k = \frac{3}{2}\frac{(1-n)^{1/3}U}{d_c n}\eta\alpha$

[a]Rajagopalan and Tien [1976] only employed a Lagrangian model for colloid interception and sedimentation. An analytical solution (not shown here) was employed for diffusion.
[b]Assumes steady-state conditions (i.e., $\frac{\partial v}{\partial t} = 0$) and negligible external forces. Subject to boundary conditions outlined in each model.
[c]The force/torque equations for each model arc listed below in their respective tables.
[d]The η correlation equation originally presented in Rajagopalan and Tien [1976] is incorrect. Here we are presenting the Logan *et al.* [1995] corrected version.
[e]Trajectory simulations employ random starting locations at upstream (labelled 'injection') collector boundary.
[f]The illustrated models typically considered downwards flow (with gravity).

AGU Water Resources Research

10.1002/2015WR017318

Table A2. Overview of the Geometries and Equations Governing Selected Mechanistic Non-Happel Sphere Models

Model Name	*Yao et al [1971]*	*Hemisphere-in-Cell [Ma et al., 2013]*[a]	*Long and Hilpert [2009]*
Model type	Eulerian	Lagrangian	Eulerian
Model Geometry[g]	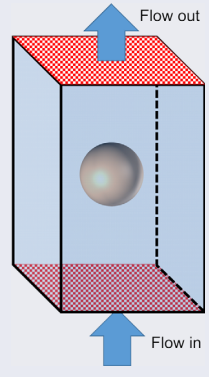	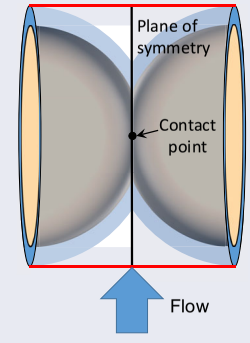	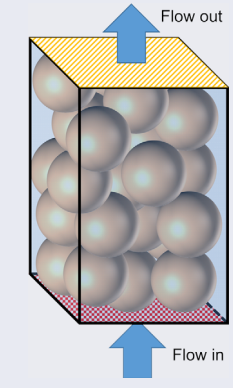
Particle boundary conditions	Constant concentration (C = C_o) Perfect sink (C = 0)	Injection boundary[f] Free exit boundary Perfect sink (C = 0) Perfect sink is replaced with surface friction in Ma *et al.* [2011]	*dC/dz*=0 Constant concentration (C = C_o) Perfect sink (C = 0)
Governing colloid transport equation[c]	$\frac{\partial C}{\partial t}+v\nabla C=D_{BM}\nabla^2 C+\left(1-\frac{\rho_f}{\rho_p}\right)\frac{mg}{3\pi\mu d_p}\frac{\partial C}{\partial Z}$	$(m+m^*)\frac{du}{dt}=F_D+F_G+F_L+F_{EDL}+F_{vdW}+F_B$	$\nabla(vC)=\nabla(D_{BM}\cdot\nabla C)-\nabla\left(\frac{D_{BM}\cdot F}{k_B T}\right)C$
η correlation[d]	$\eta\approx\frac{3}{2}\left(\frac{d_p}{d_c}\right)^2+\frac{(\rho_p-\rho_f)gd_p^2}{18\mu v}+0.9\left(\frac{k_B T}{\mu d_p d_c v}\right)$	$\eta\approx\gamma^2\left[\frac{8+4(1-\gamma)A_s^{1/3}N_{Pe}^{1/3}}{8+(1-\gamma)N_{Pe}^{0.97}}N_{LO}^{0.015}N_{Gi}^{0.8}N_R^{0.028}+A_s N_R^{15/8}N_{LO}^{1/8}+0.7N_R^{-0.05}N_G\frac{N_{Gi}}{N_{Gi}+0.9}\right]$[e]	$\eta\approx(15.56\pm0.21)\frac{(1-n)^3}{n^2}N_{Pe}^{-0.65\pm0.023}N_R^{0.19\pm0.03}+0.55A_s N_R^{0.1675}N_A^{0.125}+0.22N_R^{-0.24}N_G^{1.11}N_{vdW}^{0.053}$
Kinetic retention rate equation	$k=\frac{3}{2}\frac{(1-n)U}{d_c n}\eta\alpha$	$k=\frac{3(1-n)}{2d_c}\eta v\left[\frac{3-n}{3-3n}-\frac{2(3-n)}{\pi(3-3n)}\cos^{-1}\left(\frac{3-3n}{3-n}\right)^{\frac{1}{2}}+\frac{2}{\pi}\sqrt{2\left(\frac{3-n}{3-3n}\right)^{0.5}-1}\right]$	$k=\frac{3}{2}\frac{(1-n)U}{d_c n}\eta\alpha$

[a]There are a number of iterations of the Hemisphere-in-Cell model [*Ma et al.*, 2009; *Ma and Johnson.*, 2010; *Ma et al.*, 2011; *Ma et al.*, 2013]. Here we are specifically presenting the η correlation for Ma *et al.* [2013]. Many of the model details relevant to these tables remain the same between the iterations and, unless noted otherwise, it is not necessary to differentiate between the specific iterations.

[b]Assumes steady-state conditions (i.e., $\frac{\partial v}{\partial t}=0$) and negligible external forces. Subject to boundary conditions outlined in each model.

[c]The force/torque equations for each model are listed below in their respective tables. Yao 1971 does not include forces or torques therefore none are reported here.

[d]Long and Hilpert [2009] adopts the governing equations (in addition to the force balance) from Elimelech [1994] but without van der Waals, anisotropic diffusion or lubrication. The reader is referred to the Tufenkji and Elimelech [2004] table below for further information on the Long and Hilpert [2009] force/torque balance.

[e]In regimes of either pure diffusion or sedimentation mass transfer use the asymptotes described in Ma *et al.* [2013].

[f]Trajectory simulations employ random starting locations at upstream (labelled 'injection') collector boundary.

[g]The illustrated models typically considered downwards flow (with gravity).

AGU Water Resources Research

10.1002/2015WR017318

Table A3. Force/Torque Equations for *Rajagopalan and Tien* [1976]

	Force	Torque
Inertia	$F_I = m\left(\frac{du}{dt} + u \cdot \nabla u\right)$	$t_I = 0$
Gravity	$F_G = \frac{4}{3}\pi a_p{}^3 \left(\rho_p - \rho_f\right) g\left[-\cos(\theta) e_r + \sin(\theta) e_\theta\right]$	$t_G = 0$
London	$F_{LO} = \left[\frac{-2H\pi_{ntd} a_p^3}{3\delta^2\left(2a_p + \delta\right)^2}\right] e_r$	$t_{LO} = 0$
Electrostatic double layer	$F_{DL} = \left\{\left[\frac{\varepsilon a_p \kappa\left(\zeta_c^2 + \zeta_p^2\right)}{2}\right] \times \left[\left(\frac{2\zeta_c\zeta_p}{\zeta_c^2 + \zeta_p^2}\right) - e^{-\kappa\delta}\right]\left[\frac{e^{-\kappa\delta}}{\left(1 - e^{-2\kappa\delta}\right)}\right]\right\} e_r$	$t_{DL} = 0$
Hydrodynamic drag (t = translation, r = rotation, m = movement of fluid around particle)	$(F_D)^t = -6\pi\mu a_p\left[u_r f_r^t e_r + u_\theta f_\theta^t e_\theta\right]$ $(F_D)^r = 6\pi\mu a_p^2 \omega f_\theta^t e_\theta$ $(F_D)^m = 6\pi\mu a_p\left\{-A y_r{}^2 f_r^m e_r + \left[B y_r f_{1\theta}^m + D y_r{}^2 f_{2\theta}^m\right] e_\theta\right\}$	$(t_D)^t = 8\pi\mu a_p{}^2 u_\theta g_\phi^t e_\phi$ $(t_D)^r = -8\pi\mu a_p{}^3 \omega g_\phi^r e_\phi$ $(t_D)^m = 8\pi\mu a_p^3\left(B g_{1\phi}^m + D y_r g_{2\phi}^m\right) e_\phi$

Table A4. Force/Torque Equations for *Tufenkji and Elimelech* [2004b][a]

	Force
External force in governing equation	$F = F_{col} + F_G$
Colloidal forces	$F_{col} = -\nabla\varphi_T$
Gravity	$F_G = \frac{4}{3}\pi a_p^3\left(\rho_p - \rho_f\right) g$
Hydrodynamic drag[b,c]	$u_r = f_1\left(\delta^+\right) f_2\left(\delta^+\right) v_r$
	$u_\theta = f_3\left(\delta^+\right) v_\theta$
	$D_r = f_1\left(\delta^+\right) D_{BM}$
	$D_\theta = f_4\left(\delta^+\right) D_{BM}$

[a]The model equations are presented in *Elimelech* [1994], not *Tufenkji and Elimelech* [2004b].
[b]*Elimelech* [1994] does not present hydrodynamic force equations. We have reproduced the particle velocity equations instead.
[c]D_r and D_θ are referred to more generally as D'_{BM} in the governing colloid transport equation in Table A1.

Table A5. Force/Torque Equations for *Nelson and Ginn* [2011][a,b]

	Equation for θ and r Component Particle Velocities
Particle velocity from streamline	$u_\theta = \left[B^+\left(1+\delta^+\right) + D^+\left(1+\delta^+\right)^2\right]\left(\frac{U}{r}\right)$ $u_r = -A^+\left(1+\delta^+\right)^2 U$
Particle velocity with London van der Waals forces	n.a. to u_θ $u_r = \left[-\frac{\alpha_{ntd} N_{LO}}{\left(\delta^+\right)^2\left(2+\delta^+\right)^2}\right] U$
Particle velocity with sedimentation	$u_\theta = \left[N_G \sin(\theta)\right]\left(\frac{U}{r}\right)$ $u_r = \left[-N_G \cos(\theta)\right] U$
Particle velocity with hydrodynamic retardation	$u_\theta = \frac{1}{s_1}\left[B^+ s_2 + D^+\left(1+\delta^+\right) s_3\right]\left(\frac{U}{r}\right)$ $u_r = \frac{1}{f_r^m}\left[-A^+\left(1+\delta^+\right)^2 f_r^m\right] U$
Total expression for particle velocity	$u_\theta = \frac{1}{s_1}\left[B^+ s_2 + D^+\left(1+\delta^+\right) s_3 + N_G \sin(\theta)\right]\left(\frac{U}{r}\right)$ $u_r = \frac{1}{f_r^m}\left[-A^+\left(1+\delta^+\right)^2 f_r^m - N_G \cos(\theta) - \frac{\alpha_{ntd} N_{LO}}{\left(\delta^+\right)^2\left(2+\delta^+\right)^2}\right] U$
Particle displacement due to Brownian force vector (F_b) (Cartesian)[c]	$\tilde{R}_x = n_x\sqrt{2D_{BM}\Delta t}$ $\tilde{R}_y = n_y\sqrt{2D_{BM}\Delta t}$ $\tilde{R}_z = n_z\sqrt{2D_{BM}\Delta t}$

[a]Many of these equations are not presented in *Nelson and Ginn* [2011] but appear instead in *Nelson and Ginn* [2005].
[b]The *Nelson and Ginn* [2005, 2011] papers do not present their force/torque equations. Instead, they present the contributions to particle velocity from the individual components. We have reproduced these velocity expressions here along with the final, complete equations for particle velocity.
[c]D_{BM} in this table is a function of both δ^+ and the classic Stokes-Einstein equation, please see *Nelson and Ginn* [2011] for full details.

Table A6. List of Force Equations for the Hemisphere-In-Cell Model [*Ma et al.*, 2009; *Ma and Johnson*, 2010; *Ma et al.*, 2011, 2013][a,b]

	Force
Hydrodynamic drag[c]	$F_D^N = \frac{6\pi\mu a_p u_N}{f_1} + 6\pi\mu a_p v_N f_2$
	$F_D^t = -\frac{6\pi\mu a_p u_t}{f_4} + \frac{f_3}{f_4} 6\pi\mu a_p v_t$
Gravity	$F_G = \frac{4}{3}\pi a_p^3 (\rho_p - \rho_f) g$
Shear lift	$F_L = \frac{6.46\mu a_p^3 \left(\frac{\partial u}{\partial r}\right)^{\frac{3}{2}}}{\left(\frac{\mu}{\rho_f}\right)^{0.5}}$
Electrostatic double layer	$F_{EDL} = 4\pi\varepsilon_r\varepsilon_o\kappa\xi_p\xi_c \times \left[\frac{\exp(-\kappa\delta)}{1+\exp(-\kappa\delta)} - \frac{\left(\xi_p-\xi_c\right)^2}{2\xi_p\xi_c}\frac{\exp(-2\kappa\delta)}{1-\exp(-2\kappa\delta)}\right]$
van der Waals	$F_{vdW} = -\frac{Ha_p}{6\delta^2}\frac{\lambda(\lambda+22.232\delta)}{(\lambda+11.116\delta)^2}$
Brownian force	$F_B = \mathcal{R}\sqrt{\frac{2\zeta k_B T}{\Delta t}}$

[a]The hemisphere-in-cell model employs torques that are equivalent to the *Rajagopalan and Tien* [1976] model. The result of this is that, for colloids in contact with the collector surface, all torque-induced rolling is assumed yield translation along the collector surface (i.e., no slipping or friction) in unfavorable conditions. The only difference is an additional surface friction torque that appears in the *Ma et al.* [2011] iteration of the hemisphere-in-cell model.

[b]Many of the terms in the hemisphere-in-cell model and the *Rajagopalan and Tien* [1976] model are similar, however, the hemisphere-in-cell flow field has to be solved numerically, this results in references to velocity (v) in the force equations as opposed to the A, B, and D coefficients employed by *Rajagopalan and Tien* [1976] from their analytical solution of the flow field.

[c]Superscripts and subscripts N and t refer to directions normal and tangential to collector surface respectively.

Notation for Appendix

A brief note on notation: The authors of these mechanistic model studies often use different symbols to represent the same parameter. Wherever possible, we have consolidated the symbols representing each parameter into a single consistent symbol. For instance, the separation distance between colloid and collector surface has been variously referred to as δ, h, and H. In this notation, we use the symbol δ from the *Rajagopalan and Tien* [1976] paper.

Symbol	Definition	Dimensions (L = length, t = time, m = mass, K = temperature, V = electric potential difference, A = current, N.A. = dimensionless)
a_p	= radius of colloid	L
a_s	= radius of collector	L
A_s	=porosity dependent parameter = $2(1-\gamma^5)/(2-3\gamma+3\gamma^5-2\gamma^6)$	N.A.
A, B, D	= coefficients to correct fluid velocity. Refer to the individual papers for their exact values	A:$L^{-1}t^{-1}$, B: t^{-1}, D:$L^{-1}t^{-1}$
A^+, B^+, D^+	= dimensionless versions of the A,B,D coefficients	N.A.
C	= concentration of colloids	m/L^3
C_{in}	= concentration of colloids entering the domain	m/L^3
D_{BM}	= Brownian diffusion coefficient for a sphere in an infinite fluid (from Stokes-Einstein equation: $D_{BM} = \frac{k_B T}{3\pi\mu d_p}$	L^2/t
D_{BM}^r	= diffusion tensor (from D_r, D_θ)	L^2/t
D_r, D_θ	= diffusion coefficient in the radial and angular directions	L^2/t
d_c	= diameter of collector	L
d_p	= diameter of colloid	L
e_r, e_θ, e_ϕ	= unit vectors in the radial and angular directions	N.A.
F	= force vector (subscripts refer to the specific force of interest)	$m{\cdot}L/t^2$
$f_r^t, f_\theta^t, f_\theta^r, f_r^m, f_{1\theta}^m, f_{2\theta}^m$	= drag correction factors in RT 1976 and NG 2011. Refer to individual papers for exact values.	N.A.
f_1, f_2, f_3, f_4	= corrections for hydrodynamic interactions in TE 2004 and MPFJ. Refer to individual papers for exact values.	N.A.
g	= gravitational acceleration, 9.81 m/s^2	L/t^2
$g_\phi^t, g_\phi^r, g_{1\phi}^m, g_{2\phi}^m$	= torque correction factors in RT 1976	N.A.
H	= Hamaker coefficient	$m{\cdot}L^2/t^2$
k_B	= Boltzmann constant ($\sim 1.38 \times 10^{-23}$ $m^2{\cdot}kg{\cdot}s^{-2}{\cdot}K^{-1}$)	$L^2{\cdot}m/(t^2{\cdot}K)$

(Continued)

Symbol	Definition	Dimensions (L = length, t = time, m = mass, K = temperature, V = electric potential difference, A = current, N.A. = dimensionless)
k	= kinetic retention rate coefficient (also commonly denoted as k_{att}, k_f)	1/t
m	= particle mass (m^* refers to virtual particle mass)	m
N_A	= attraction number = $H/(12\pi\mu a_p^2 U)$	N.A.
N_G	= gravity number = $2a_p^2(\rho_p-\rho_f)g/(9\mu U)$	N.A.
N_{Gi}	= $1/(N_G+1)$	N.A.
N_{LO}	= London number = $H/(9\pi\mu a_p^2 U)$	N.A.
N_{Pe}	= Peclet number = Ud_c/D_{BM}	N.A.
N_R	= aspect ratio = a_p/a_s	N.A.
N_{vdW}	= van der Waals number = $H/(k_bT)$	N.A.
n	= porosity	N.A.
n_x, n_y, n_z	= random numbers for Brownian force vector	N.A.
p	= fluid pressure	m/(L·t^2)
$\tilde{R}_x, \tilde{R}_y, \tilde{R}_z$	= random displacement for Brownian motion	L
$\mathscr{R}$	= Gaussian random number	N.A.
r	= radial coordinate	L
s_1, s_2, s_3	= drag correction factors in NG 2011	N.A.
T	= temperature	K
t	= time	T
$t_G, t_{LO}, t_{DL}, t_D, t_I$	= torques	(m·L/t^2)·L
u	= particle velocity (subscripts r and θ refer to its polar components)	L/t
U	= approach (or darcy) velocity = $v\times n$	L/t
v	= fluid velocity (subscripts refer to its directional components)	L/t
y_r	= $(r-a_s)$	L
x, y, z	= Cartesian coordinates	L

Greek Letters

α	= sticking (or collision) efficiency	N.A.
α_{rtd}	= retardation correction for London force	L^{-4}
δ	= surface to surface separation between colloid and collector	L
δ^+	= δ/a_p	N.A.
ε	= dielectric constant of the medium	N.A.
$\varepsilon_r\varepsilon_o$	= permittivity of water	t^4·A^2/(L^2·m)/L
η	= collector contact efficiency	N.A.
ζ	= friction coefficient	m/t
κ	= Debye-Hückel reciprocal length	L^{-1}
ρ_f, ρ_p	= density of fluid and particle	m/L^3
μ	= dynamic (absolute) viscosity of fluid	m/(L·t)
ω	= angular velocity	Radians/t
ξ_c, ξ_p	= surface potentials of the collector and particle (it is common practice to use zeta potentials instead of surface potentials)	V
θ	= angle	Radians
ϕ_t	= total interaction energy (i.e., sum of van der Waals and electric double layer forces)	m·L^2/t^2
λ	= characteristic wave length	L
γ	= $(1-n)^{1/3}$	N.A.

Acknowledgment
Data used in this paper can be requested from the corresponding author.

References

Abudalo, R. A., J. N. Ryan, R. W. Harvey, D. W. Metge, and L. Landkamer (2010), Influence of organic matter on the transport of *Cryptosporidium parvum* oocysts in a ferric oxyhydroxide-coated quartz sand saturated porous medium, *Water Res.*, *44*(4), 1104–1113.

Al-Raoush, R. I., and C. S. Willson (2005), A pore-scale investigation of a multiphase porous media system, *J. Contam. Hydrol.*, *77*(1–2), 67–89.

Albinger, O., B. K. Biesemeyer, R. G. Arnold, and B. E. Logan (1994), Effect of bacterial heterogeneity on adhesion to uniform collectors by monoclonal populations, *FEMS Microbiol. Lett.*, *124*(3), 321–326.

Amirbahman, A., and T. M. Olson (1993), Transport of humic matter-coated hematite in packed beds, *Environ. Sci. Technol.*, *27*(13), 2807–2813.

Auset, M., and A. A. Keller (2006), Pore-scale visualization of colloid straining and filtration in saturated porous media using micromodels, *Water Resour. Res.*, *42*, W12S02, doi:10.1029/2005WR004639.
Bahr, J. M., and J. Rubin (1987), Direct comparison of kinetic and local equilibrium formulations for solute transport affected by surface reactions, *Water Resour. Res.*, *23*(3), 438–452.
Bai, C., and Y. Li (2012), Modeling the transport and retention of nC60 nanoparticles in the subsurface under different release scenarios, *J. Contam. Hydrol.*, *136–137*(0), 43–55.
Bai, R., and C. Tien (1996), A new correlation for the initial filter coefficient under unfavorable surface interactions, *J. Colloid Interface Sci.*, *179*(2), 631–634.
Bai, R., and C. Tien (1999), Particle deposition under unfavorable surface interactions, *J. Colloid Interface Sci.*, *218*(2), 488–499.
Bales, R. C., C. P. Gerba, G. H. Grondin, and S. L. Jensen (1989), Bacteriophage transport in sandy soil and fractured tuff, *Appl. Environ. Microbiol.*, *55*(8), 2061–2067.
Baygents, J. C., J. R. Glynn, O. Albinger, B. K. Biesemeyer, K. L. Ogden, and R. G. Arnold (1998), Variation of surface charge density in monoclonal bacterial populations: Implications for transport through porous media, *Environ. Sci. Technol.*, *32*(11), 1596–1603.
Bear, J., and A. H. D. Cheng (2010), *Modeling Groundwater Flow and Contaminant Transport*, Springer, Netherlands.
Bendersky, M., and J. M. Davis (2011), DLVO interaction of colloidal particles with topographically and chemically heterogeneous surfaces, *J. Colloid Interface Sci.*, *353*(1), 87–97.
Bennett, P., F. He, D. Zhao, B. Aiken, and L. Feldman (2010), In situ testing of metallic iron nanoparticle mobility and reactivity in a shallow granular aquifer, *J. Contam. Hydrol.*, *116*(1–4), 35–46.
Berge, N. D., and C. A. Ramsburg (2009), Oil-in-water emulsions for encapsulated delivery of reactive iron particles, *Environ. Sci. Technol.*, *43*(13), 5060–5066.
Bergendahl, J., and D. Grasso (2000), Prediction of colloid detachment in a model porous media: Hydrodynamics, *Chem. Eng. Sci.*, *55*(9), 1523–1532.
Berkowitz, B., A. Cortis, M. Dentz, and H. Scher (2006), Modeling non-Fickian transport in geological formations as a continuous time random walk, *Rev. Geophys.*, *44*, RG2003, doi:10.1029/2005RG000178.
Bhattacharjee, S., C.-H. Ko, and M. Elimelech (1998), DLVO Interaction between rough surfaces, *Langmuir*, *14*(12), 3365–3375.
Bhattacharjee, S., J. Y. Chen, and M. Elimelech (2000), DLVO interaction energy between spheroidal particles and a flat surface, *Colloids Surf. A*, *165*(1–3), 143–156.
Bhattad, P., C. S. Willson, and K. E. Thompson (2011), Effect of network structure on characterization and flow modeling using X-ray microtomography images of granular and fibrous porous media, *Transp. Porous Media*, *90*(2), 363–391.
Bitton, G., and R. W. Harvey (1992), Transport of pathogens through soil, in *Environmental Microbiology*, edited by R. Mitchell, pp. 103–124, John Wiley, N. Y.
Blanford, W. J., M. L. Brusseau, T. C. Jim Yeh, C. P. Gerba, and R. Harvey (2005), Influence of water chemistry and travel distance on bacteriophage PRD-1 transport in a sandy aquifer, *Water Res.*, *39*(11), 2345–2357.
Boccardo, G., D. L. Marchisio, and R. Sethi (2014), Microscale simulation of particle deposition in porous media, *J. Colloid Interface Sci.*, *417*(0), 227–237.
Bolster, C. H., A. L. Mills, G. M. Hornberger, and J. S. Herman (1999), Spatial distribution of deposited bacteria following miscible displacement experiments in intact cores, *Water Resour. Res.*, *35*(6), 1797–1807.
Bolster, C. H., A. L. Mills, G. Hornberger, and J. Herman (2000), Effect of intra-population variability on the long-distance transport of bacteria, *Ground Water*, *38*(3), 370–375.
Bradford, S. A., and M. Bettahar (2006), Concentration dependent transport of colloids in saturated porous media, *J. Contam. Hydrol.*, *82*(1–2), 99–117.
Bradford, S. A., S. R. Yates, M. Bettahar, and J. Simunek (2002), Physical factors affecting the transport and fate of colloids in saturated porous media, *Water Resour. Res.*, *38*(12), 1327, doi:10.1029/2002WR001340.
Bradford, S. A., J. Simunek, M. Bettahar, M. T. van Genuchten, and S. R. Yates (2003), Modeling colloid attachment, straining, and exclusion in saturated porous media, *Environ. Sci. Technol.*, *37*(10), 2242–2250.
Bradford, S. A., M. Bettahar, J. Simunek, and M. T. van Genuchten (2004), Straining and attachment of colloids in physically heterogeneous porous media, *Vadose Zone J.*, *3*(2), 384–394.
Bradford, S. A., J. Simunek, M. Bettahar, Y. F. Tadassa, M. T. van Genuchten, and S. R. Yates (2005), Straining of colloids at textural interfaces, *Water Resour. Res.*, *41*, W10404, doi:10.1029/2004WR003675.
Bradford, S. A., J. Simunek, M. Bettahar, M. T. van Genuchten, and S. R. Yates (2006a), Significance of straining in colloid deposition: Evidence and implications, *Water Resour. Res.*, *42*, W12S15, doi:10.1029/2005WR004791.
Bradford, S. A., J. Simunek, and S. L. Walker (2006b), Transport and straining of *E. coli* O157:H7 in saturated porous media, *Water Resour. Res.*, *42*, W12S12, doi:10.1029/2005WR004805.
Bradford, S. A., S. Torkzaban, F. Leij, J. Šimůnek, and M. T. van Genuchten (2009), Modeling the coupled effects of pore space geometry and velocity on colloid transport and retention, *Water Resour. Res.*, *45*, W02414, doi:10.1029/2008WR007096.
Bradford, S. A., S. Torkzaban, and A. Wiegmann (2011a), Pore-scale simulations to determine the applied hydrodynamic torque and colloid immobilization, *Vadose Zone J.*, *10*(1), 252–261.
Bradford, S. A., S. Torkzaban, and J. Simunek (2011b), Modeling colloid transport and retention in saturated porous media under unfavorable attachment conditions, *Water Resour. Res.*, *47*, W10503, doi:10.1029/2011WR010812.
Bradford, S. A., S. Torkzaban, and A. Shapiro (2013), A theoretical analysis of colloid attachment and straining in chemically heterogeneous porous media, *Langmuir*, *29*(23), 6944–6952.
Burganos, V. N., C. A. Paraskeva, and A. C. Payatakes (1992), Three-dimensional trajectory analysis and network simulation of deep bed filtration, *J. Colloid Interface Sci.*, *148*(1), 167–181.
Burganos, V. N., C. A. Paraskeva, P. D. Christofides, and A. C. Payatakes (1994), Motion and deposition of non-Brownian particles in upflow collectors, *Sep. Technol.*, *4*(1), 47–54.
Camesano, T. A., K. M. Unice, and B. E. Logan (1999), Blocking and ripening of colloids in porous media and their implications for bacterial transport, *Colloids Surf. A*, *160*(3), 291–307.
Cardenas, M. B. (2008), Three-dimensional vortices in single pores and their effects on transport, *Geophys. Res. Lett.*, *35*, L18402, doi:10.1029/2008GL035343.
Chang, Y.-I., W.-Y. Cheng, and H.-C. Chan (2009), A proposed correlation equation for predicting filter coefficient under unfavorable deposition conditions, *Sep. Purif. Technol.*, *65*(3), 248–250.

Chatterjee, J., S. Pratap, and S. Abdulkareem (2011), Dual-deposition rates in colloid filtration caused by coupled heterogeneities in a colloidal population, *J. Colloid Interface Sci.*, *356*(1), 362–368.
Chen, C., A. I. Packman, and J.-F. Gaillard (2008), Pore-scale analysis of permeability reduction resulting from colloid deposition, *Geophys. Res. Lett.*, *35*, L07404, doi:10.1029/2007GL033077.
Chen, J. Y., C. H. Ko, S. Bhattacharjee, and M. Elimelech (2001), Role of spatial distribution of porous medium surface charge heterogeneity in colloid transport, *Colloid Surf. A*, *191*(1–2), 3–15.
Chowdhury, I., Y. Hong, R. J. Honda, and S. L. Walker (2011), Mechanisms of TiO_2 nanoparticle transport in porous media: Role of solution chemistry, nanoparticle concentration, and flowrate, *J. Colloid Interface Sci.*, *360*(2), 548–555.
Christian, P., F. Von der Kammer, M. Baalousha, and T. Hofmann (2008), Nanoparticles: Structure, properties, preparation and behaviour in environmental media, *Ecotoxicology*, *17*(5), 326–343.
Chrysikopoulos, C. V., and V. I. Syngouna (2014), Effect of gravity on colloid transport through water-saturated columns packed with glass beads: Modeling and experiments, *Environ. Sci. Technol.*, *48*(12), 6805–6813.
Cookson, J. T. (1970), Removal of submicron particles in packed beds, *Environ. Sci. Technol.*, *4*(2), 128–134.
Corapcioglu, M. Y., and S. Jiang (1993), Colloid-facilitated groundwater contaminant transport, *Water Resour. Res.*, *29*(7), 2215–2226.
Crist, J. T., J. F. McCarthy, Y. Zevi, P. Baveye, J. A. Throop, and T. S. Steenhuis (2004), Pore-scale visualization of colloid transport and retention in partly saturated porous media, *Vadose Zone J.*, *3*(2), 444–450.
Cullen, E., D. M. O'Carroll, E. K. Yanful, and B. Sleep (2010), Simulation of the subsurface mobility of carbon nanoparticles at the field scale, *Adv. Water Resour.*, *33*(4), 361–371.
Cushing, R. S., and D. F. Lawler (1998), Depth filtration: Fundamental investigation through three-dimensional trajectory analysis, *Environ. Sci. Technol.*, *32*(23), 3793–3801.
Cvetkovic, V., and G. Dagan (1994), Transport of kinetically sorbing solute by steady random velocity in heterogeneous porous formations, *J. Fluid Mech.*, *265*, 189–215.
de Jonge, H., O. H. Jacobsen, L. W. de Jonge, and P. Moldrup (1998), Particle-facilitated transport of prochloraz in undisturbed sandy loam soil columns, *J. Environ. Qual.*, *27*(6), 1495–1503.
de Jonge, L. W., C. Kjaergaard, and P. Moldrup (2004), Colloids and colloid-facilitated transport of contaminants in soils, *Vadose Zone J.*, *3*(2), 321–325.
DeBorde, D. C., W. W. Woessner, Q. T. Kiley, and P. Ball (1999), Rapid transport of viruses in a floodplain aquifer, *Water Res.*, *33*(10), 2229–2238.
Derjaguin, B., and L. Landau (1941), Theory of the stability of strongly charged lyophobic sols and the adhesion of strongly charged particles in solutions of electrolytes, *Acta Physicochim. USSR*, *14*, 633–662.
DiCarlo, D. A., L. D. Seale, K. Ham, and C. S. Willson (2010), Tomographic measurements of pore filling at infiltration fronts, *Adv. Water Resour.*, *33*(4), 485–492.
Drelich, J., and Y. U. Wang (2011), Charge heterogeneity of surfaces: Mapping and effects on surface forces, *Adv. Colloid Interface Sci.*, *165*(2), 91–101.
Du, Y. C., C. Y. Shen, H. Y. Zhang, and Y. F. Huang (2013), Effects of flow velocity and nonionic surfactant on colloid straining in saturated porous media under unfavorable conditions, *Transp. Porous Media*, *98*(1), 193–208.
Duffadar, R., and J. M. Davis (2007), Interaction of micrometer-scale particles with nanotextured surfaces in shear flow, *J. Colloid Interface Sci.*, *308*(1), 20–29.
Duffadar, R., S. Kalasin, J. M. Davis, and M. M. Santore (2009), The impact of nanoscale chemical features on micron-scale adhesion: Crossover from heterogeneity-dominated to mean-field behavior, *J. Colloid Interface Sci.*, *337*(2), 396–407.
Dunphy Guzman, K. A., M. P. Finnegan, and J. F. Banfield (2006), Influence of surface potential on aggregation and transport of titania nanoparticles, *Environ. Sci. Technol.*, *40*(24), 7688–7693.
Dusek, J., M. Dohnal, M. Snehota, M. Sobotkova, C. Ray, and T. Vogel (2015), Transport of bromide and pesticides through an undisturbed soil column: A modeling study with global optimization analysis, *J. Contam. Hydrol.*, *175–176*(0), 1–16.
Elimelech, M. (1991), Kinetics of capture of colloidal particles in packed beds under attractive double layer interactions, *J. Colloid Interface Sci.*, *146*(2), 337–352.
Elimelech, M. (1992), Predicting collision efficiencies of colloidal particles in porous media, *Water Res.*, *26*(1), 1–8.
Elimelech, M. (1994), Particle deposition on ideal collectors from dilute flowing suspensions—Mathematical formulation, numerical-solution, and simulations, *Sep. Technol.*, *4*(4), 186–212.
Elimelech, M., and C. R. O'Melia (1990a), Effect of particle-size on collision efficiency in the deposition of Brownian particles with electrostatic energy barriers, *Langmuir*, *6*(6), 1153–1163.
Elimelech, M., and C. R. O'Melia (1990b), Kinetics of deposition of colloidal particles in porous-media, *Environ. Sci. Technol.*, *24*(10), 1528–1536.
Elimelech, M., M. Nagai, C.-H. Ko, and J. N. Ryan (2000), Relative insignificance of mineral grain zeta potential to colloid transport in geochemically heterogeneous porous media, *Environ. Sci. Technol.*, *34*(11), 2143–2148.
Eral, H. B., J. M. Oh, D. van den Ende, F. Mugele, and M. H. G. Duits (2010), Anisotropic and hindered diffusion of colloidal particles in a closed cylinder, *Langmuir*, *26*(22), 16,722–16,729.
Espinoza, C., and A. J. Valocchi (1997), Stochastic analysis of one-dimensional transport of kinetically adsorbing solutes in chemically heterogeneous aquifers, *Water Resour. Res.*, *33*(11), 2429–2445.
Faure, B., G. Salazar-Alvarez, and L. Bergström (2011), Hamaker constants of iron oxide nanoparticles, *Langmuir*, *27*(14), 8659–8664.
Flury, M., and H. Qiu (2008), Modeling colloid-facilitated contaminant transport in the vadose zone, *Vadose Zone J.*, *7*(2), 682–697.
Fontes, D. E., A. L. Mills, G. M. Hornberger, and J. S. Herman (1991), Physical and chemical factors influencing transport of microorganisms through porous media, *Appl. Environ. Microbiol.*, *57*(9), 2473–2481.
Foppen, J. W., and J. F. Schijven (2006), Evaluation of data from the literature on the transport and survival of *Escherichia coli* and thermotolerant coliforms in aquifers under saturated conditions, *Water Res.*, *40*(3), 401–426.
Foppen, J. W., A. Mporokoso, and J. F. Schijven (2005), Determining straining of *Escherichia coli* from breakthrough curves, *J. Contam. Hydrol.*, *76*(3–4), 191–210.
Foppen, J. W., M. van Herwerden, and J. Schijven (2007), Transport of *Escherichia coli* in saturated porous media: Dual mode deposition and intra-population heterogeneity, *Water Res.*, *41*(8), 1743–1753.
Foppen, J. W., Y. Liem, and J. Schijven (2008), Effect of humic acid on the attachment of *Escherichia coli* in columns of goethite-coated sand, *Water Res.*, *42*(1–2), 211–219.

Franchi, A., and C. R. O'Melia (2003), Effects of natural organic matter and solution chemistry on the deposition and reentrainment of colloids in porous media, *Environ. Sci. Technol.*, *37*(6), 1122–1129.
Fujikawa, Y., and M. Fukui (1991), Analysis of radioactive cesium and cobalt adsorption to rocks using the two-site kinetic model equations, *J. Contam. Hydrol.*, *8*(1), 43–69.
Gaillard, J.-F., C. Chen, S. H. Stonedahl, B. L. T. Lau, D. T. Keane, and A. I. Packman (2007), Imaging of colloidal deposits in granular porous media by X-ray difference micro-tomography, *Geophys. Res. Lett.*, *34*, L18404, doi:10.1029/2007GL030514.
Gao, Y., Z. Luo, N. He, and M. Wang (2013), Metallic nanoparticle production and consumption in China between 2000 and 2010 and associative aquatic environmental risk assessment, *J. Nanopart. Res.*, *15*(6), 1–9.
Gastone, F., T. Tosco, and R. Sethi (2014), Guar gum solutions for improved delivery of iron particles in porous media (Part 1): Porous medium rheology and guar gum-induced clogging, *J. Contam. Hydrol.*, *166*(0), 23–33.
Golab, A., R. Romeyn, H. Averdunk, M. Knackstedt, and T. J. Senden (2012), 3D characterisation of potential CO_2 reservoir and seal rocks, *Aust. J. Earth Sci.*, *60*(1), 111–123.
Gu, B., J. Schmitt, Z. Chen, L. Liang, and J. F. McCarthy (1995), Adsorption and desorption of different organic matter fractions on iron oxide, *Geochim. Cosmochim. Acta*, *59*(2), 219–229.
Haggerty, R., and S. M. Gorelick (1995), Multiple-rate mass transfer for modeling diffusion and surface reactions in media with pore-scale heterogeneity, *Water Resour. Res.*, *31*(10), 2383–2400.
Haggerty, R., S. A. McKenna, and L. C. Meigs (2000), On the late-time behavior of tracer test breakthrough curves, *Water Resour. Res.*, *36*(12), 3467–3479.
Hahn, M. W., and C. R. O'Melia (2004), Deposition and reentrainment of Brownian particles in porous media under unfavorable chemical conditions: Some concepts and applications, *Environ. Sci. Technol.*, *38*(1), 210–220.
Hahn, M. W., D. Abadzic, and C. R. O'Melia (2004), Aquasols: On the role of secondary minima, *Environ. Sci. Technol.*, *38*(22), 5915–5924.
Han, J., Y. Jin, and C. S. Willson (2006), Virus retention and transport in chemically heterogeneous porous media under saturated and unsaturated flow conditions, *Environ. Sci. Technol.*, *40*(5), 1547–1555.
Han, P., X. Wang, L. Cai, M. Tong, and H. Kim (2014), Transport and retention behaviors of titanium dioxide nanoparticles in iron oxide-coated quartz sand: Effects of pH, ionic strength, and humic acid, *Colloids Surf. A*, *454*(0), 119–127.
Happel, J. (1958), Viscous flow in multiparticle systems—Slow motion of fluids relative to beds of spherical particles, *AIChE J.*, *4*(2), 197–201.
Harter, T., S. Wagner, and E. R. Atwill (2000), Colloid transport and filtration of *Cryptosporidium parvum* in sandy soils and aquifer sediments, *Environ. Sci. Technol.*, *34*(1), 62–70.
Harvey, R. W. (1997), Microorganisms as tracers in groundwater injection and recovery experiments: A review, *FEMS Microbiol. Rev.*, *20*(3–4), 461–472.
Harvey, R. W., and S. P. Garabedian (1991), Use of colloid filtration theory in modeling movement of bacteria through a contaminated sandy aquifer, *Environ. Sci. Technol.*, *25*(1), 178–185.
Harvey, R. W., N. E. Kinner, A. Bunn, D. Macdonald, and D. Metge (1995), Transport behavior of groundwater protozoa and protozoan-sized microspheres in sandy aquifer sediments, *Appl. Environ. Microbiol.*, *61*(1), 209–217.
He, F., and D. Zhao (2008), Hydrodechlorination of trichloroethene using stabilized Fe-Pd nanoparticles: Reaction mechanism and effects of stabilizers, catalysts and reaction conditions, *Appl. Catal. B: Environ.*, *84*(3–4), 533–540.
Hendry, M. J., J. R. Lawrence, and P. Maloszewski (1997), The role of sorption in the transport of *Klebsiella oxytoca* through saturated silica sand, *Ground Water*, *35*(4), 574–584.
Hendry, M. J., J. R. Lawrence, and P. Maloszewski (1999), Effects of velocity on the transport of two bacteria through saturated sand, *Ground Water*, *37*(1), 103–112.
Herring, A. L., L. Andersson, S. Schlüter, A. Sheppard, and D. Wildenschild (2015), Efficiently engineering pore-scale processes: The role of force dominance and topology during nonwetting phase trapping in porous media, *Adv. Water Resour.*, *79*(0), 91–102.
Herzig, J. P., D. M. Leclerc, and P. L. Goff (1970), Flow of suspensions through porous media—Application to deep filtration, *Ind. Eng. Chem.*, *62*(5), 8–35.
Hoek, E. M. V., and G. K. Agarwal (2006), Extended DLVO interactions between spherical particles and rough surfaces, *J. Colloid Interface Sci.*, *298*(1), 50–58.
Hornberger, G. M., A. L. Mills, and J. S. Herman (1992), Bacterial transport in porous media: Evaluation of a model using laboratory observations, *Water Resour. Res.*, *28*(3), 915–923.
Hotze, E. M., T. Phenrat, and G. V. Lowry (2010), Nanoparticle aggregation: Challenges to understanding transport and reactivity in the environment, *J. Environ. Qual.*, *39*(6), 1909–1924.
Iltis, G. C., R. T. Armstrong, D. P. Jansik, B. D. Wood, and D. Wildenschild (2011), Imaging biofilm architecture within porous media using synchrotron-based X-ray computed microtomography, *Water Resour. Res.*, *47*, W02601, doi:10.1029/2010WR009410.
Israelachvili, J. N. (2011), Solvation, structural, and hydration forces, in *Intermolecular and Surface Forces*, 3rd ed., edited by J. N. Israelachvili, chap. 5, pp. 341–380, Academic, San Diego, Calif.
Jaisi, D. P., and M. Elimelech (2009), Single-walled carbon nanotubes exhibit limited transport in soil columns, *Environ. Sci. Technol.*, *43*(24), 9161–9166.
Jiang, X., M. Tong, R. Lu, and H. Kim (2012a), Transport and deposition of ZnO nanoparticles in saturated porous media, *Colloids Surf. A*, *401*(0), 29–37.
Jiang, X., M. Tong, and H. Kim (2012b), Influence of natural organic matter on the transport and deposition of zinc oxide nanoparticles in saturated porous media, *J. Colloid Interface Sci.*, *386*(1), 34–43.
Jin, Y., and M. Flury (2002), Fate and transport of viruses in porous media, *Adv. Agron.*, *77*, 39–102.
Johnson, K. L., K. Kendall, and A. D. Roberts (1971), Surface energy and the contact of elastic solids, *Proc. R. Soc. London, Ser. A*, *324*(1558), 301–313.
Johnson, P. R., and M. Elimelech (1995), Dynamics of colloid deposition in porous-media—Blocking based on random sequential adsorption, *Langmuir*, *11*(3), 801–812.
Johnson, P. R., N. Sun, and M. Elimelech (1996), Colloid transport in geochemically heterogeneous porous media: Modeling and measurements, *Environ. Sci. Technol.*, *30*(11), 3284–3293.
Johnson, R. L., J. T. Nurmi, G. S. O'Brien Johnson, D. Fan, R. L. O'Brien Johnson, Z. Shi, A. J. Salter-Blanc, P. G. Tratnyek, and G. V. Lowry (2013), Field-scale transport and transformation of carboxymethylcellulose-stabilized nano zero-valent iron, *Environ. Sci. Technol.*, *47*(3), 1573–1580.

Johnson, W. P., and M. Hilpert (2013), Upscaling colloid transport and retention under unfavorable conditions: Linking mass transfer to pore and grain topology, *Water Resour. Res.*, *49*, 5328–5341, doi:10.1002/wrcr.20433.
Johnson, W. P., and X. Li (2005), Comment on breakdown of colloid filtration theory: Role of the secondary energy minimum and surface charge heterogeneities, *Langmuir*, *21*(23), 10,895–10,895.
Johnson, W. P., and B. E. Logan (1996), Enhanced transport of bacteria in porous media by sediment-phase and aqueous-phase natural organic matter, *Water Res.*, *30*(4), 923–931.
Johnson, W. P., G. L. Amy, and S. C. Chapra (1995a), Modeling of NOM-facilitated PAH transport through low-f_{oc} sediment, *J. Environ. Eng.*, *121*(6), 438–446.
Johnson, W. P., K. A. Blue, B. E. Logan, and R. G. Arnold (1995b), Modeling bacterial detachment during transport through porous media as a residence-time-dependent process, *Water Resour. Res.*, *31*(11), 2649–2658.
Johnson, W. P., X. Li, and G. Yal (2007a), Colloid retention in porous media: Mechanistic confirmation of wedging and retention in zones of flow stagnation, *Environ. Sci. Technol.*, *41*(4), 1279–1287.
Johnson, W. P., X. Li, and S. Assemi (2007b), Deposition and re-entrainment dynamics of microbes and non-biological colloids during non-perturbed transport in porous media in the presence of an energy barrier to deposition, *Adv. Water Resour.*, *30*(6–7), 1432–1454.
Johnson, W. P., X. Li, M. Tong, and H. Ma (2009), Comment on ''Transport and fate of bacteria in porous media: Coupled effects of chemical conditions and pore space geometry'' by Saeed Torkzaban et al., *Water Resour. Res.*, *45*, W09603, doi:10.1029/2008WR007389.
Johnson, W. P., E. Pazmino, and H. L. Ma (2010), Direct observations of colloid retention in granular media in the presence of energy barriers, and implications for inferred mechanisms from indirect observations, *Water Res.*, *44*(4), 1158–1169.
Johnson, W. P., H. Ma, and E. Pazmino (2011), Straining credibility: A general comment regarding common arguments used to infer straining as the mechanism of colloid retention in porous media, *Environ. Sci. Technol.*, *45*(9), 3831–3832.
Katzourakis, V. E., and C. V. Chrysikopoulos (2014), Mathematical modeling of colloid and virus cotransport in porous media: Application to experimental data, *Adv. Water Resour.*, *68*(0), 62–73.
Keller, A. A., S. Sirivithayapakorn, and C. V. Chrysikopoulos (2004), Early breakthrough of colloids and bacteriophage MS2 in a water-saturated sand column, *Water Resour. Res.*, *40*, W08304, doi:10.1029/2003WR002676.
Kersting, A. B., D. W. Efurd, D. L. Finnegan, D. J. Rokop, D. K. Smith, and J. L. Thompson (1999), Migration of plutonium in ground water at the Nevada Test Site, *Nature*, *397*(6714), 56–59.
Ketcham, R. A., and W. D. Carlson (2001), Acquisition, optimization and interpretation of X-ray computed tomographic imagery: Applications to the geosciences, *Comput. Geosci.*, *27*(4), 381–400.
Kocur, C. M., D. M. O'Carroll, and B. E. Sleep (2013), Impact of nZVI stability on mobility in porous media, *J. Contam. Hydrol.*, *145*(0), 17–25.
Kocur, C. M., et al. (2014), Characterization of nZVI mobility in a field scale test, *Environ. Sci. Technol.*, *48*(5), 2862–2869.
Köhne, J. M., S. Köhne, and J. Šimůnek (2009a), A review of model applications for structured soils: a) Water flow and tracer transport, *J. Contam. Hydrol.*, *104*(1–4), 4–35.
Köhne, J. M., S. Köhne, and J. Šimůnek (2009b), A review of model applications for structured soils: b) Pesticide transport, *J. Contam. Hydrol.*, *104*(1–4), 36–60.
Krol, M. M., A. J. Oleniuk, C. M. Kocur, B. E. Sleep, P. Bennett, Z. Xiong, and D. M. O'Carroll (2013), A field-validated model for in situ transport of polymer-stabilized nZVI and implications for subsurface injection, *Environ. Sci. Technol.*, *47*(13), 7332–7340.
Kuznar, Z. A., and M. Elimelech (2007), Direct microscopic observation of particle deposition in porous media: Role of the secondary energy minimum, *Colloid Surf. A*, *294*(1–3), 156–162.
Kyle, J. R., and R. A. Ketcham (2015), Application of high resolution X-ray computed tomography to mineral deposit origin, evaluation, and processing, *Ore Geol. Rev.*, *65*(Part 4), 821–839.
Landkamer, L. L., R. W. Harvey, T. D. Scheibe, and J. N. Ryan (2013), Colloid transport in saturated porous media: Elimination of attachment efficiency in a new colloid transport model, *Water Resour. Res.*, *49*, 2952–2965, doi:10.1002/wrcr.20195.
Lecoanet, H. F., and M. R. Wiesner (2004), Velocity effects on fullerene and oxide nanoparticle deposition in porous media, *Environ. Sci. Technol.*, *38*(16), 4377–4382.
Lecoanet, H. F., J.-Y. Bottero, and M. R. Wiesner (2004), Laboratory assessment of the mobility of nanomaterials in porous media, *Environ. Sci. Technol.*, *38*(19), 5164–5169.
Leij, F. J., and S. A. Bradford (2013), Colloid transport in dual-permeability media, *J. Contam. Hydrol.*, *150*(0), 65–76.
Levich, V. G. (1962), *Physicochemical Hydrodynamics*, Prentice Hall, Englewood Cliffs, N. J.
Li, X. Q., and W. P. Johnson (2005), Nonmonotonic variations in deposition rate coefficients of microspheres in porous media under unfavorable deposition conditions, *Environ. Sci. Technol.*, *39*(6), 1658–1665.
Li, X. Q., T. D. Scheibe, and W. P. Johnson (2004), Apparent decreases in colloid deposition rate coefficients with distance of transport under unfavorable deposition conditions: A general phenomenon, *Environ. Sci. Technol.*, *38*(21), 5616–5625.
Li, X. Q., P. F. Zhang, C. L. Lin, and W. P. Johnson (2005), Role of hydrodynamic drag on microsphere deposition and re-entrainment in porous media under unfavorable conditions, *Environ. Sci. Technol.*, *39*(11), 4012–4020.
Li, X. Q., Z. L. Li, and D. X. Zhang (2010), Role of low flow and backward flow zones on colloid transport in pore structures derived from real porous media, *Environ. Sci. Technol.*, *44*(13), 4936–4942.
Li, Z., D. X. Zhang, and X. Li (2010), Tracking colloid transport in porous media using discrete flow fields and sensitivity of simulated colloid deposition to space discretization, *Environ. Sci. Technol.*, *44*(4), 1274–1280.
Li, Z., D. X. Zhang, and X. Li (2012), Tracking colloid transport in real pore structures: Comparisons with correlation equations and experimental observations, *Water Resour. Res.*, *48*, W05533, doi:10.1029/2012WR011847.
Liang, Y., S. A. Bradford, J. Simunek, H. Vereecken, and E. Klumpp (2013), Sensitivity of the transport and retention of stabilized silver nanoparticles to physicochemical factors, *Water Res.*, *47*(7), 2572–2582.
Lin, S. H., Y. W. Cheng, Y. Bobcombe, K. L. Jones, J. Liu, and M. R. Wiesner (2011), Deposition of silver nanoparticles in geochemically heterogeneous porous media: Predicting affinity from surface composition analysis, *Environ. Sci. Technol.*, *45*(12), 5209–5215.
Lindquist, W. B., S. M. Lee, D. A. Coker, K. W. Jones, and P. Spanne (1996), Medial axis analysis of void structure in three-dimensional tomographic images of porous media, *J. Geophys. Res.*, *101*(B4), 8297–8310.
Lindqvist, R., J. S. Cho, and C. G. Enfield (1994), A kinetic model for cell density dependent bacterial transport in porous media, *Water Resour. Res.*, *30*(12), 3291–3299.
Lipp, E. K., S. A. Farrah, and J. B. Rose (2001), Assessment and impact of microbial fecal pollution and human enteric pathogens in a coastal community, *Mar. Pollut. Bull.*, *42*(4), 286–293.

Litton, G. M., and T. M. Olson (1993), Colloid deposition rates on silica bed media and artifacts related to collector surface preparation methods, *Environ. Sci. Technol.*, *27*(1), 185–193.
Liu, X. Y., D. M. O'Carroll, E. J. Petersen, Q. G. Huang, and C. L. Anderson (2009), Mobility of multiwalled carbon nanotubes in porous media, *Environ. Sci. Technol.*, *43*(21), 8153–8158.
Liu, Y., D. Janjaroen, M. S. Kuhlenschmidt, T. B. Kuhlenschmidt, and T. H. Nguyen (2009), Deposition of *Cryptosporidium parvum* oocysts on natural organic matter surfaces: Microscopic evidence for secondary minimum deposition in a radial stagnation point flow cell, *Langmuir*, *25*(3), 1594–1605.
Logan, B., D. Jewett, R. Arnold, E. Bouwer, and C. O'Melia (1995), Clarification of clean-bed filtration models, *J. Environ. Eng.*, *121*(12), 869–873.
Long, W., and M. Hilpert (2009), A correlation for the collector efficiency of Brownian particles in clean-bed filtration in sphere packings by a Lattice-Boltzmann method, *Environ. Sci. Technol.*, *43*(12), 4419–4424.
Long, W., H. Huang, J. Serlemitsos, E. Liu, A. H. Reed, and M. Hilpert (2010), Pore-scale study of the collector efficiency of nanoparticles in packings of nonspherical collectors, *Colloids Surf. A*, *358*(1–3), 163–171.
Loveland, J. P., S. Bhattacharjee, J. N. Ryan, and M. Elimelech (2003), Colloid transport in a geochemically heterogeneous porous medium: aquifer tank experiment and modeling, *J. Contam. Hydrol.*, *65*(3–4), 161–182.
Ma, H., and W. P. Johnson (2009), Colloid retention in porous media of various porosities: Predictions by the hemispheres-in-cell model, *Langmuir*, *26*(3), 1680–1687.
Ma, H., and W. P. Johnson (2010), Colloid retention in porous media of various porosities: Predictions by the hemispheres-in-cell model, *Langmuir*, *26*(3), 1680–1687.
Ma, H., J. Pedel, P. Fife, and W. P. Johnson (2009), Hemispheres-in-cell geometry to predict colloid deposition in porous media, *Environ. Sci. Technol.*, *43*(22), 8573–8579.
Ma, H., E. Pazmino, and W. P. Johnson (2011), Surface heterogeneity on hemispheres-in-cell model yields all experimentally-observed non-straining colloid retention mechanisms in porous media in the presence of energy barriers, *Langmuir*, *27*(24), 14,982–14,994.
Ma, H., M. Hradisky, and W. P. Johnson (2013), Extending applicability of correlation equations to predict colloidal retention in porous media at low fluid velocity, *Environ. Sci. Technol.*, *47*(5), 2272–2278.
Majestic, B., G. Erdakos, M. Lewandowski, K. Oliver, R. Willis, T. Kleindienst, and P. Bhave (2010), A review of selected engineered nanoparticles in the atmosphere: Sources, transformations, and techniques for sampling and analysis, *Int. J. Occupational Environ. Health*, *16*(4), 488–507.
Marambio-Jones, C., and E. M. V. Hoek (2010), A review of the antibacterial effects of silver nanomaterials and potential implications for human health and the environment, *J. Nanopart. Res.*, *12*(5), 1531–1551.
Matthess, G., and A. Pekdeger (1985), Survival and transport of pathogenic bacteria and viruses in groundwater, *in Ground Water Quality*, edited by C. H. Ward, W. Giger, and P. McCarty, pp. 472–482, John Wiley, N. Y.
Mattison, N. T., D. M. O'Carroll, R. Kerry Rowe, and E. J. Petersen (2011), Impact of porous media grain size on the transport of multi-walled carbon nanotubes, *Environ. Sci. Technol.*, *45*(22), 9765–9775.
May, R., and Y. S. Li (2013), The effects of particle size on the deposition of fluorescent nanoparticles in porous media: Direct observation using laser scanning cytometry, *Colloid Surf. A*, *418*, 84–91.
May, R., S. Akbariyeh, and Y. Li (2012), Pore-scale investigation of nanoparticle transport in saturated porous media using laser scanning cytometry, *Environ. Sci. Technol.*, *46*(18), 9980–9986.
McCarthy, J. F., and J. M. Zachara (1989), Subsurface transport of contaminants, *Environ. Sci. Technol.*, *23*(5), 496–502.
McCaulou, D. R., R. C. Bales, and J. F. McCarthy (1994), Use of short-pulse experiments to study bacteria transport through porous media, *J. Contam. Hydrol.*, *15*(1–2), 1–14.
McCaulou, D. R., R. C. Bales, and R. G. Arnold (1995), Effect of temperature-controlled motility on transport of bacteria and microspheres through saturated sediment, *Water Resour. Res.*, *31*(2), 271–280.
McClaine, J. W., and R. M. Ford (2002), Reversal of flagellar rotation is important in initial attachment of *Escherichia coli* to glass in a dynamic system with high- and low-ionic-strength buffers, *Appl. Environ. Microbiol.*, *68*(3), 1280–1289.
McDowell-Boyer, L. M., J. R. Hunt, and N. Sitar (1986), Particle transport through porous media, *Water Resour. Res.*, *22*(13), 1901–1921.
Molnar, I. L., D. M. O'Carroll, and J. I. Gerhard (2011), Impact of surfactant-induced wettability alterations on DNAPL invasion in quartz and iron oxide-coated sand systems, *J. Contam. Hydrol.*, *119*(1–4), 1–12.
Molnar, I. L., C. S. Willson, D. M. O'Carroll, M. L. Rivers, and J. I. Gerhard (2014), Method for obtaining silver nanoparticle concentrations within a porous medium via synchrotron X-ray computed microtomography, *Environ. Sci. Technol.*, *48*(2), 1114–1122.
Mondal, P. K., and B. E. Sleep (2013), Virus and virus-sized microsphere transport in a dolomite rock fracture, *Water Resour. Res.*, *49*, 808–824, doi:10.1002/wrcr.20086.
Morales, V. L., W. Zhang, B. Gao, L. W. Lion, J. J. Bisogni Jr, B. A. McDonough, and T. S. Steenhuis (2011), Impact of dissolved organic matter on colloid transport in the vadose zone: Deterministic approximation of transport deposition coefficients from polymeric coating characteristics, *Water Res.*, *45*(4), 1691–1701.
Moreno-Atanasio, R., R. A. Williams, and X. Jia (2010), Combining X-ray microtomography with computer simulation for analysis of granular and porous materials, *Particuology*, *8*(2), 81–99.
Mosley, L. M., K. A. Hunter, and W. A. Ducker (2003), Forces between colloid particles in natural waters, *Environ. Sci. Technol.*, *37*(15), 3303–3308.
Mueller, N. C., and B. Nowack (2008), Exposure modeling of engineered nanoparticles in the environment, *Environ. Sci. Technol.*, *42*(12), 4447–4453.
Mylon, S. E., K. L. Chen, and M. Elimelech (2004), Influence of natural organic matter and ionic composition on the kinetics and structure of hematite colloid aggregation: Implications to iron depletion in estuaries, *Langmuir*, *20*(21), 9000–9006.
Nelson, K. E., and T. R. Ginn (2005), Colloid filtration theory and the Happel sphere-in-cell model revisited with direct numerical simulation of colloids, *Langmuir*, *21*(6), 2173–2184.
Nelson, K. E., and T. R. Ginn (2011), New collector efficiency equation for colloid filtration in both natural and engineered flow conditions, *Water Resour. Res.*, *47*, W05543, doi:10.1029/2010WR009587.
Neukum, C., A. Braun, and R. Azzam (2014), Transport of stabilized engineered silver (Ag) nanoparticles through porous sandstones, *J. Contam. Hydrol.*, *158*(0), 1–13.
Novikov, A. P., S. N. Kalmykov, S. Utsunomiya, R. C. Ewing, F. Horreard, A. Merkulov, S. B. Clark, V. V. Tkachev, and B. F. Myasoedov (2006), Colloid transport of plutonium in the far-field of the Mayak Production Association, Russia, *Science*, *314*(5799), 638–641.
Nowack, B., and T. D. Bucheli (2007), Occurrence, behavior and effects of nanoparticles in the environment, *Environ. Pollut.*, *150*(1), 5–22.

O'Carroll, D., B. Sleep, M. Krol, H. Boparai, and C. Kocur (2013), Nanoscale zero valent iron and bimetallic particles for contaminated site remediation, *Adv. Water Resour.*, *51*(0), 104–122.
O'Connor, D. R. (2002), *Part One: A Summary. Report of the Walkerton Inquiry: The Events of May 2000 and Related Issues*. Ont. Minist. of the Attorney Gen., Toronto, 2002.
Ouyang, Y., D. Shinde, R. S. Mansell, and W. Harris (1996), Colloid-enhanced transport of chemicals in subsurface environments: A review, *Crit. Rev. Environ. Sci. Technol.*, *26*(2), 189–204.
Paraskeva, C. A., V. N. Burganos, and A. C. Payatakes (1991), Three-dimensional trajectory analysis of particle deposition in constricted tubes, *Chem. Eng. Commun.*, *108*(1), 23–48.
Payatakes, A. C., R. Rajagopalan, and C. Tien (1974a), On the use of Happel's model for filtration studies, *J. Colloid Interface Sci.*, *49*(2), 321–325.
Payatakes, A. C., C. Tien, and R. M. Turian (1974b), Trajectory calculation of particle deposition in deep bed filtration: Part I. Model formulation, *AIChE J.*, *20*(5), 889–900.
Pazmino, E. F., J. Trauscht, and W. P. Johnson (2014a), Release of colloids from primary minimum contact under unfavorable conditions by perturbations in ionic strength and flow rate, *Environ. Sci. Technol.*, *48*(16), 9227–9235.
Pazmino, E. F., J. Trauscht, B. Dame, and W. P. Johnson (2014b), Power law size-distributed heterogeneity explains colloid retention on soda lime glass in the presence of energy barriers, *Langmuir*, *30*(19), 5412–5421.
Pelley, A. J., and N. Tufenkji (2008), Effect of particle size and natural organic matter on the migration of nano- and microscale latex particles in saturated porous media, *J. Colloid Interface Sci.*, *321*(1), 74–83.
Petersen, E. J., et al. (2011), Potential release pathways, environmental fate, and ecological risks of carbon nanotubes, *Environ. Sci. Technol.*, *45*(23), 9837–9856.
Petosa, A. R., D. P. Jaisi, I. R. Quevedo, M. Elimelech, and N. Tufenkji (2010), Aggregation and deposition of engineered nanomaterials in aquatic environments: Role of physicochemical interactions, *Environ. Sci. Technol.*, *44*(17), 6532–6549.
Phenrat, T., N. Saleh, K. Sirk, R. D. Tilton, and G. V. Lowry (2007), Aggregation and sedimentation of aqueous nanoscale zerovalent iron dispersions, *Environ. Sci. Technol.*, *41*(1), 284–290.
Phenrat, T., H.-J. Kim, F. Fagerlund, T. Illangasekare, R. D. Tilton, and G. V. Lowry (2009), Particle size distribution, concentration, and magnetic attraction affect transport of polymer-modified Fe0 nanoparticles in sand columns, *Environ. Sci. Technol.*, *43*(13), 5079–5085.
Phenrat, T., J. E. Song, C. M. Cisneros, D. P. Schoenfelder, R. D. Tilton, and G. V. Lowry (2010a), Estimating attachment of nano- and submicrometer-particles coated with organic macromolecules in porous media: Development of an empirical model, *Environ. Sci. Technol.*, *44*(12), 4531–4538.
Phenrat, T., A. Cihan, H. J. Kim, M. Mital, T. Illangasekare, and G. V. Lowry (2010b), Transport and deposition of polymer-modified Fe-0 nanoparticles in 2-D heterogeneous porous media: Effects of particle concentration, Fe-0 content, and coatings, *Environ. Sci. Technol.*, *44*(23), 9086–9093.
Phenrat, T., H. J. Kim, F. Fagerlund, T. Illangasekare, and G. V. Lowry (2010c), Empirical correlations to estimate agglomerate size and deposition during injection of a polyelectrolyte-modified Fe-0 nanoparticle at high particle concentration in saturated sand, *J. Contam. Hydrol.*, *118*(3–4), 152–164.
Pieper, A. P., J. N. Ryan, R. W. Harvey, G. L. Amy, T. H. Illangasekare, and D. W. Metge (1997), Transport and recovery of bacteriophage PRD1 in a sand and gravel aquifer: Effect of sewage-derived organic matter, *Environ. Sci. Technol.*, *31*(4), 1163–1170.
Pinchuk, A. O. (2012), Size-dependent Hamaker constant for silver nanoparticles, *J. Phys. Chem. C*, *116*(37), 20,099–20,102.
Porter, M. L., and D. Wildenschild (2010), Image analysis algorithms for estimating porous media multiphase flow variables from computed microtomography data: A validation study, *Comput. Geosci.*, *14*(1), 15–30.
Porter, M. L., D. Wildenschild, G. Grant, and J. I. Gerhard (2010), Measurement and prediction of the relationship between capillary pressure, saturation, and interfacial area in a NAPL-water-glass bead system, *Water Resour. Res.*, *46*, W08512, doi:10.1029/2009WR007786.
Porubcan, A. A., and S. Xu (2011), Colloid straining within saturated heterogeneous porous media, *Water Res.*, *45*(4), 1796–1806.
Potter, M. C., and D. C. Wiggert (2002), *Mechanics of Fluids*, Brooks Cole, Pacific Grove, calif.
Powelson, D. K., C. P. Gerba, and M. T. Yahya (1993), Virus transport and removal in wastewater during aquifer recharge, *Water Res.*, *27*(4), 583–590.
Prodanović, M., W. B. Lindquist, and R. S. Seright (2007), 3D image-based characterization of fluid displacement in a Berea core, *Adv. Water Resour.*, *30*(2), 214–226.
Qi, Z., L. Hou, D. Zhu, R. Ji, and W. Chen (2014), Enhanced transport of phenanthrene and 1-naphthol by colloidal graphene oxide nanoparticles in saturated soil, *Environ. Sci. Technol.*, *48*(17), 10,136–10,144.
Quinn, J., et al. (2005), Field demonstration of DNAPL dehalogenation using emulsified zero-valent iron, *Environ. Sci. Technol.*, *39*(5), 1309–1318.
Rajagopalan, R., and C. Tien (1976), Trajectory analysis of deep-bed filtration with sphere-in-cell porous-media model, *AIChE J.*, *22*(3), 523–533.
Raychoudhury, T., G. Naja, and S. Ghoshal (2010), Assessment of transport of two polyelectrolyte-stabilized zero-valent iron nanoparticles in porous media, *J. Contam. Hydrol.*, *118*(3–4), 143–151.
Raychoudhury, T., N. Tufenkji, and S. Ghoshal (2014), Straining of polyelectrolyte-stabilized nanoscale zero valent iron particles during transport through granular porous media, *Water Res.*, *50*(0), 80–89.
Ren, D., and J. A. Smith (2013), Proteinate-capped silver nanoparticle transport in water-saturated sand, *J. Environ. Eng.*, *139*(6), 781–787.
Ross, S., and I. D. Morrison (1988), *Colloidal Systems and Interfaces*, John Wiley, N. Y.
Rotter, B. E., D. A. Barry, J. I. Gerhard, and J. S. Small (2008), Modeling U(VI) biomineralization in single- and dual-porosity porous media, *Water Resour. Res.*, *44*, W08437, doi:10.1029/2007WR006301.
Ruckenstein, E., and D. C. Prieve (1976), Adsorption and desorption of particles and their chromatographic separation, *AIChE J.*, *22*(2), 276–283.
Ruohola, A.-M. J., R. F. Considine, D. R. Dixon, C. Fong, and C. J. Drummond (2012), Mapping the nano-scale interaction between bio-colloidal *Giardia lamblia* cysts and silica, *Soft Matter*, *8*(22), 6083–6091.
Russell, T. L., K. M. Yamahara, and A. B. Boehm (2012), Mobilization and transport of naturally occurring enterococci in beach sands subject to transient infiltration of seawater, *Environ. Sci. Technol.*, *46*(11), 5988–5996.
Ryan, J. N., and M. Elimelech (1996), Colloid mobilization and transport in groundwater, *Colloids Surf. A*, *107*(0), 1–56.
Ryan, J. N., M. Elimelech, R. A. Ard, R. W. Harvey, and P. R. Johnson (1999), Bacteriophage PRD1 and silica colloid transport and recovery in an iron oxide-coated sand aquifer, *Environ. Sci. Technol.*, *33*(1), 63–73.

Ryan, J. N., R. W. Harvey, D. Metge, M. Elimelech, T. Navigato, and A. P. Pieper (2002), Field and laboratory investigations of inactivation of viruses (PRD1 and MS2) attached to iron oxide-coated quartz sand, *Environ. Sci. Technol.*, *36*(11), 2403–2413.
Sagee, O., I. Dror, and B. Berkowitz (2012), Transport of silver nanoparticles (AgNPs) in soil, *Chemosphere*, *88*(5), 670–675.
Sakthivadivel, R. (1966), *Theory and Mechanism of Filtration of Non-Colloidal Fines Through a Porous Medium, Rep. HEL 15-5*, Hydraulic Eng. Lab., Univ. of Calif., Berkeley.
Sakthivadivel, R. (1969), *Clogging of a Granular Porous Medium by Sediment, Rep. HEL 15-7*, Hydraulic Eng. Lab., Coll. of Eng., Univ. of Calif, Berkeley.
Sakulchaicharoen, N., D. M. O'Carroll, and J. E. Herrera (2010), Enhanced stability and dechlorination activity of pre-synthesis stabilized nanoscale FePd particles, *J. Contam. Hydrol.*, *118*(3–4), 117–127.
Sang, W., V. L. Morales, W. Zhang, C. R. Stoof, B. Gao, A. L. Schatz, Y. Zhang, and T. S. Steenhuis (2013), Quantification of colloid retention and release by straining and energy minima in variably saturated porous media, *Environ. Sci. Technol.*, *47*(15), 8256–8264.
Scheibe, T. D., S. S. Hubbard, T. C. Onstott, and M. F. DeFlaun (2011), Lessons learned from bacterial transport research at the south oyster site, *Ground Water*, *49*(5), 745–763.
Scheibe, T. D., Z. S. Hou, B. J. Palmer, and A. M. Tartakovsky (2013), Pore-scale simulation of intragranular diffusion: Effects of incomplete mixing on macroscopic manifestations, *Water Resour. Res.*, *49*, 4277–4294, doi:10.1002/wrcr.20333.
Schijven, J. F., and S. M. Hassanizadeh (2000), Removal of viruses by soil passage: Overview of modeling, processes, and parameters, *Crit. Rev. Environ. Sci. Technol.*, *30*(1), 49–127.
Schijven, J. F., and S. M. Hassanizadeh (2002), Virus removal by soil passage at field scale and groundwater protection of sandy aquifers (vol 46, pg 123, 2002), *Water Sci. Technol.*, *46*(6–7), 411–411.
Schijven, J. F., and J. Šimůnek (2002), Kinetic modeling of virus transport at the field scale, *J. Contam. Hydrol.*, *55*(1–2), 113–135.
Schijven, J. F., W. Hoogenboezem, M. Hassanizadeh, and J. H. Peters (1999), Modeling removal of bacteriophages MS2 and PRD1 by dune recharge at Castricum, Netherlands, *Water Resour. Res.*, *35*(4), 1101–1111.
Schnaar, G., and M. L. Brusseau (2005), Pore-scale characterization of organic immiscible-liquid morphology in natural porous media using synchrotron X-ray microtomography, *Environ. Sci. Technol.*, *39*(21), 8403–8410.
Scholl, M. A., and R. W. Harvey (1992), Laboratory investigations on the role of sediment surface and groundwater chemistry in transport of bacteria through a contaminated sandy aquifer, *Environ. Sci. Technol.*, *26*(7), 1410–1417.
Sen, T. K. (2011), Processes in pathogenic biocolloidal contaminants transport in saturated and unsaturated porous media: A review, *Water Air Soil Pollut.*, *216*(1–4), 239–256.
Sen, T. K., and K. C. Khilar (2006), Review on subsurface colloids and colloid-associated contaminant transport in saturated porous media, *Adv. Colloid Interface Sci.*, *119*(2–3), 71–96.
Shang, J., M. Flury, G. Chen, and J. Zhuang (2008), Impact of flow rate, water content, and capillary forces on in situ colloid mobilization during infiltration in unsaturated sediments, *Water Resour. Res.*, *44*, W06411, doi:10.1029/2007WR006516.
Shellenberger, K., and B. E. Logan (2002), Effect of molecular scale roughness of glass beads on colloidal and bacterial deposition, *Environ. Sci. Technol.*, *36*(2), 184–189.
Shen, C., B. Li, Y. Huang, and Y. Jin (2007), Kinetics of coupled primary- and secondary-minimum deposition of colloids under unfavorable chemical conditions, *Environ. Sci. Technol.*, *41*(20), 6976–6982.
Shen, C., Y. Huang, B. Li, and Y. Jin (2008), Effects of solution chemistry on straining of colloids in porous media under unfavorable conditions, *Water Resour. Res.*, *44*, W05419, doi:10.1029/2007WR006580.
Shen, C., V. Lazouskaya, Y. Jin, B. Li, Z. Ma, W. Zheng, and Y. Huang (2012), Coupled factors influencing detachment of nano- and micro-sized particles from primary minima, *J. Contam. Hydrol.*, *134–135*(0), 1–11.
Shen, C., V. Lazouskaya, H. Zhang, B. Li, Y. Jin, and Y. Huang (2013), Influence of surface chemical heterogeneity on attachment and detachment of microparticles, *Colloids Surf. A*, *433*(0), 14–29.
Sheppard, A., et al. (2014), Techniques in helical scanning, dynamic imaging and image segmentation for improved quantitative analysis with X-ray micro-CT, *Nucl. Instrum. Methods Phys. Res., Sect. B*, *324*(0), 49–56.
Simoni, S. F., H. Harms, T. N. P. Bosma, and A. J. B. Zehnder (1998), Population heterogeneity affects transport of bacteria through sand columns at low flow rates, *Environ. Sci. Technol.*, *32*(14), 2100–2105.
Šimůnek, J., and M. T. van Genuchten (2008), Modeling nonequilibrium flow and transport processes using HYDRUS, *Vadose Zone J.*, *7*(2), 782–797.
Šimůnek, J., N. J. Jarvis, M. T. van Genuchten, and A. Gärdenäs (2003), Review and comparison of models for describing non-equilibrium and preferential flow and transport in the vadose zone, *J. Hydrol.*, *272*(1), 14–35.
Song, L., and M. Elimelech (1992), Deposition of Brownian particles in porous media: Modified boundary conditions for the sphere-in-cell model, *J. Colloid Interface Sci.*, *153*(1), 294–297.
Song, L., P. R. Johnson, and M. Elimelech (1994), Kinetics of colloid deposition onto heterogeneously charged surfaces in porous media, *Environ. Sci. Technol.*, *28*(6), 1164–1171.
Sprague, L. A., J. S. Herman, G. M. Hornberger, and A. L. Mills (2000), Atrazine adsorption and colloid-facilitated transport through the unsaturated zone, *J. Environ. Qual.*, *29*(5), 1632–1641.
Subramanian, S. K., Y. Li, and L. M. Cathles (2013), Assessing preferential flow by simultaneously injecting nanoparticle and chemical tracers, *Water Resour. Res.*, *49*, 29–42, doi:10.1029/2012WR012148.
Taboada-Serrano, P., V. Vithayaveroj, S. Yiacoumi, and C. Tsouris (2005), Surface charge heterogeneities measured by atomic force microscopy, *Environ. Sci. Technol.*, *39*(17), 6352–6360.
Taghavy, A., A. Mittelman, Y. Wang, K. D. Pennell, and L. M. Abriola (2013), Mathematical modeling of the transport and dissolution of citrate-stabilized silver nanoparticles in porous media, *Environ. Sci. Technol.*, *47*(15), 8499–8507.
Taylor, R., A. Cronin, S. Pedley, J. Barker, and T. Atkinson (2004), The implications of groundwater velocity variations on microbial transport and wellhead protection—Review of field evidence, *FEMS Microbiol. Ecol.*, *49*(1), 17–26.
Thompson, K. E., C. S. Willson, and W. L. Zhang (2006), Quantitative computer reconstruction of particulate materials from microtomography images, *Powder Technol.*, *163*(3), 169–182.
Tong, M., and W. P. Johnson (2006), Excess colloid retention in porous media as a function of colloid size, fluid velocity, and grain angularity, *Environ. Sci. Technol.*, *40*(24), 7725–7731.
Tong, M., and W. P. Johnson (2007), Colloid population heterogeneity drives hyperexponential deviation from classic filtration theory, *Environ. Sci. Technol.*, *41*(2), 493–499.
Tong, M., X. Li, C. N. Brow, and W. P. Johnson (2005), Detachment-influenced transport of an adhesion-deficient bacterial strain within water-reactive porous media, *Environ. Sci. Technol.*, *39*(8), 2500–2508.

Tong, M., H. Ma, and W. P. Johnson (2008), Funneling of flow into grain-to-grain contacts drives colloid−colloid aggregation in the presence of an energy barrier, *Environ. Sci. Technol.*, *42*(8), 2826–2832.
Torkzaban, S., S. A. Bradford, and S. L. Walker (2007), Resolving the coupled effects of hydrodynamics and DLVO forces on colloid attachment in porous media, *Langmuir*, *23*(19), 9652–9660.
Torkzaban, S., S. S. Tazehkand, S. L. Walker, and S. A. Bradford (2008), Transport and fate of bacteria in porous media: Coupled effects of chemical conditions and pore space geometry, *Water Resour. Res.*, *44*, W04403, doi:10.1029/2007WR006541.
Torkzaban, S., Y. Kim, M. Mulvihill, J. M. Wan, and T. K. Tokunaga (2010), Transport and deposition of functionalized CdTe nanoparticles in saturated porous media, *J. Contam. Hydrol.*, *118*(3–4), 208–217.
Tosco, T., and R. Sethi (2010), Transport of non-Newtonian suspensions of highly concentrated micro- and nanoscale iron particles in porous media: A modeling approach, *Environ. Sci. Technol.*, *44*(23), 9062–9068.
Tosco, T., A. Tiraferri, and R. Sethi (2009), Ionic strength dependent transport of microparticles in saturated porous media: Modeling mobilization and immobilization phenomena under transient chemical conditions, *Environ. Sci. Technol.*, *43*(12), 4425–4431.
Tosco, T., M. Petrangeli Papini, C. Cruz Viggi, and R. Sethi (2014a), Nanoscale zerovalent iron particles for groundwater remediation: a review, *J. Cleaner Prod.*, *77*(0), 10–21.
Tosco, T., F. Gastone, and R. Sethi (2014b), Guar gum solutions for improved delivery of iron particles in porous media (Part 2): Iron transport tests and modeling in radial geometry, *J. Contam. Hydrol.*, *166*(0), 34–51.
Tufenkji, N. (2007), Modeling microbial transport in porous media: Traditional approaches and recent developments, *Adv. Water Resour.*, *30*(6–7), 1455–1469.
Tufenkji, N., and M. Elimelech (2004a), Deviation from the classical colloid filtration theory in the presence of repulsive DLVO interactions, *Langmuir*, *20*(25), 10,818–10,828.
Tufenkji, N., and M. Elimelech (2004b), Correlation equation for predicting single-collector efficiency in physicochemical filtration in saturated porous media, *Environ. Sci. Technol.*, *38*(2), 529–536.
Tufenkji, N., and M. Elimelech (2005a), Spatial distributions of cryptosporidium oocysts in porous media: Evidence for dual mode deposition, *Environ. Sci. Technol.*, *39*(10), 3620–3629.
Tufenkji, N., and M. Elimelech (2005b), Breakdown of colloid filtration theory: Role of the secondary energy minimum and surface charge heterogeneities, *Langmuir*, *21*(3), 841–852.
Tufenkji, N., J. A. Redman, and M. Elimelech (2003), Interpreting deposition patterns of microbial particles in laboratory-scale column experiments, *Environ. Sci. Technol.*, *37*(3), 616–623.
Tufenkji, N., G. F. Miller, J. N. Ryan, R. W. Harvey, and M. Elimelech (2004), Transport of cryptosporidium oocysts in porous media: role of straining and physicochemical filtration, *Environ. Sci. Technol.*, *38*(22), 5932–5938.
Uyusur, B., C. J. G. Darnault, P. T. Snee, E. Koken, A. R. Jacobson, and R. R. Wells (2010), Coupled effects of solution chemistry and hydrodynamics on the mobility and transport of quantum dot nanomaterials in the vadose zone, *J. Contam. Hydrol.*, *118*(3–4), 184–198.
van der Wielen, P. W. J. J., W. J. M. K. Senden, and G. Medema (2008), Removal of bacteriophages MS2 and ΦX174 during transport in a sandy anoxic aquifer, *Environ. Sci. Technol.*, *42*(12), 4589–4594.
van Kooten, J. J. A. (1996), A method to solve the advection-dispersion equation with a kinetic adsorption isotherm, *Adv. Water Resour.*, *19*(4), 193–206.
Verwey, E. J. W., and J. T. G. Overbeek (1948), *Theory of the Stability of Lyophobic Colloids*, Elsevier, Amsterdam, Netherlands.
Vogel, H. J., and K. Roth (2001), Quantitative morphology and network representation of soil pore structure, *Adv. Water Resour.*, *24*(3–4), 233–242.
Wang, C., A. D. Bobba, R. Attinti, C. Shen, V. Lazouskaya, L.-P. Wang, and Y. Jin (2012), Retention and transport of silica nanoparticles in saturated porous media: Effect of concentration and particle size, *Environ. Sci. Technol.*, *46*(13), 7151–7158.
Wang, D., S. A. Bradford, R. W. Harvey, B. Gao, L. Cang, and D. Zhou (2012), Humic acid facilitates the transport of ARS-labeled hydroxyapatite nanoparticles in iron oxyhydroxide-coated sand, *Environ. Sci. Technol.*, *46*(5), 2738–2745.
Wang, D., L. Ge, J. He, W. Zhang, D. P. Jaisi, and D. Zhou (2014), Hyperexponential and nonmonotonic retention of polyvinylpyrrolidone-coated silver nanoparticles in an Ultisol, *J. Contam. Hydrol.*, *164*(0), 35–48.
Wang, Y., Y. Li, J. D. Fortner, J. B. Hughes, L. M. Abriola, and K. D. Pennell (2008), Transport and Retention of nanoscale C60 aggregates in water-saturated porous media, *Environ. Sci. Technol.*, *42*(10), 3588–3594.
Wang, Y., S. A. Bradford, and J. Šimůnek (2014a), Physicochemical factors influencing the preferential transport of *Escherichia coli* in soils, *Vadose Zone J.*, *13*(1).
Wang, Y., S. A. Bradford, and J. Šimůnek (2014b), Estimation and upscaling of dual-permeability model parameters for the transport of *E. coli* D21g in soils with preferential flow, *J. Contam. Hydrol.*, *159*(0), 57–66.
Wiesner, M. R., G. V. Lowry, P. Alvarez, D. Dionysiou, and P. Biswas (2006), Assessing the risks of manufactured nanomaterials, *Environ. Sci. Technol.*, *40*(14), 4336–4345.
Wildenschild, D., and A. P. Sheppard (2013), X-ray imaging and analysis techniques for quantifying pore-scale structure and processes in subsurface porous medium systems, *Adv. Water Resour.*, *51*(0), 217–246.
Wildenschild, D., C. M. P. Vaz, M. L. Rivers, D. Rikard, and B. S. B. Christensen (2002), Using X-ray computed tomography in hydrology: systems, resolutions, and limitations, *J. Hydrol.*, *267*(3–4), 285–297.
Xu, S., and J. E. Saiers (2009), Colloid straining within water-saturated porous media: Effects of colloid size nonuniformity, *Water Resour. Res.*, *45*, W05501, doi:10.1029/2008WR007258.
Xu, S., B. Gao, and J. E. Saiers (2006), Straining of colloidal particles in saturated porous media, *Water Resour. Res.*, *42*, W12S16, doi:10.1029/2006WR004948.
Xu, S., Q. Liao, and J. E. Saiers (2008), Straining of nonspherical colloids in saturated porous media, *Environ. Sci. Technol.*, *42*(3), 771–778.
Xu, W., S. C. Ayirala, and D. N. Rao (2006), Wettability alterations due to crude oil composition and an anionic surfactant in petroleum reservoirs, *J. Adhesion Sci. Technol.*, *20*(7), 693–704.
Yao, K.-M., M. T. Habibian, and C. R. O'Melia (1971), Water and waste water filtration. Concepts and applications, *Environ. Sci. Technol.*, *5*(11), 1105–1112.
Yates, M. V., C. P. Gerba, and L. M. Kelley (1985), Virus persistence in groundwater, *Appl. Environ. Microbiol.*, *49*(4), 778–781.
Zhang, H., and H. M. Selim (2006), Modeling the transport and retention of arsenic (V) in soils, *Soil Sci. Soc. Am. J.*, *70*(5), 1677–1687.
Zhang, L., L. Hou, L. Wang, A. T. Kan, W. Chen, and M. B. Tomson (2012), Transport of fullerene nanoparticles (nC60) in saturated sand and sandy soil: Controlling factors and modeling, *Environ. Sci. Technol.*, *46*(13), 7230–7238.

Zhang, P., W. P. Johnson, T. D. Scheibe, K.-H. Choi, F. C. Dobbs, and B. J. Mailloux (2001a), Extended tailing of bacteria following breakthrough at the Narrow Channel Focus Area, Oyster, Virginia, *Water Resour. Res.*, *37*(11), 2687–2698.

Zhang, P., W. P. Johnson, M. J. Piana, C. C. Fuller, and D. L. Naftz (2001b), Potential artifacts in interpretation of differential breakthrough of colloids and dissolved tracers in the context of transport in a zero-valent iron permeable reactive barrier, *Ground Water*, *39*(6), 831–840.

Zheng, C., and S. M. Gorelick (2003), Analysis of solute transport in flow fields influenced by preferential flowpaths at the decimeter scale, *Ground Water*, *41*(2), 142–155.